2019

ENGINEERING THE ALVEOLAR GAS EXCHANGE BARRIER WITH EXTRACELLULAR MATRIX COATINGS FOR BIOENGINEERED LUNGS

Bethany M. Young
VCU

ENGINEERING THE ALVEOLAR GAS EXCHANGE BARRIER WITH EXTRACELLULAR MATRIX COATINGS FOR BIOENGINEERED LUNGS

A dissertation submitted in partial fulfillment of the requirements for the degree of Doctor of Philosophy at Virginia Commonwealth University

By

Bethany Marie Young
B.S. in Biology, University of Richmond, 2014
M.S. in Biomedical Engineering, Virginia Commonwealth University, 2016

Director: Rebecca L. Heise, Ph.D.
Associate Professor, Department of Biomedical Engineering

ACKNOWLEDGMENTS

I would first like to thank Dr. Rebecca Heise for all your guidance and encouragement. You were one of my biggest advocates, and I am grateful that you never let me give up on research even during the hardest of times. My doctorate education would never have happened if you hadn't shown me my full potential.

I would also like to extend my appreciation to Dr. Daniel Weiss, Dr. Daniel Conway, Dr. Jenifer Puetzer, and Dr. MaryPeace McRae for being a part of my committee and giving valuable feedback to this work. Each member of my committee was an active mentor throughout my graduate research experience, whether it be with grant sponsorship and reviewing, figure legend format debates, antibody donations, career advice, or troubleshooting ECIS equipment. I was lucky to have had this committee to shape my doctoral experience.

To the other members of the Heise Laboratory, Brittaney Ritchie, Keerthana Shankar, Mike Valentine, Patrick Link, Franck Kamaga Gninzeko, Sahil Chindal, Krista Powell, Cindy Tho, and Gabrielle Cotman, I am forever grateful for all your support and friendship over the years.

Microscopy was performed at the VCU Microscopy Facility, supported, in part, by funding from NIH-NCI Cancer Center Support Grant P30 CA016059, and the VCU Nanomaterials Core Characterization Facility. Histology services in support of the research project were generated by the Virginia Commonwealth University Cancer Mouse Models Core Laboratory, supported, in part, with funding from NIH-NCI Cancer Center Support Grant P30 CA016059. Funding for this research was provided in part by NSF CAREER CMMI 135162 and NIH RO1AG041823.

Lastly, but most importantly, I would like to express my sincere appreciation to my family and boyfriend Benjamin Fowler, who have both been my rock throughout graduate school. I am

so lucky to have grown up in such a loving household that showed me the importance of education. Ben, I am incredibly grateful that you have been endlessly supportive and made sure that I have smiled every day that I have known you. I can't wait to see what the future holds.

TABLE OF CONTENTS

LIST OF FIGURES

LIST OF TABLES

GLOSSARY

Keywords

Lung Recellularization, Epithelial Barrier, Extracellular Matrix, Laminin

Abbreviations

AJ	Adherens Junction
TJ	Tight Junction
JAM	Junctional Adhesion Molecule
ZO	Zonula Occluden
ECM	Extracellular Matrix
dECM	Decellularized Extracellular Matrix
ARDS	Acute Respiratory Distress Syndrome
COPD	Chronic Obstructive Pulmonary Disease
IPF	Idiopathic Pulmonary Fibrosis
CF	Cystic Fibrosis
TEER	Transepithelial Electrical Resistance
ECIS	Electric Cell-Substrate Impedance Sensing
AF-6	Afadin
MSC	Mesenchymal Stem Cell
BESC	Basal Epithelial Stem Cell
H & E	Hematoxylin and Eosin
BM	Basement membrane
EMT	Epitheilial to mesenchymal transition

ABSTRACT

ENGINEERING THE ALVEOLAR GAS EXCHANGE BARRIER WITH EXTRACELLULAR MATRIX COATINGS FOR BIOENGINEERED LUNGS

By

Bethany Marie Young
B.S. in Biology, University of Richmond, 2014
M.S. in Biomedical Engineering, Virginia Commonwealth University, 2016

A dissertation submitted in partial fulfillment of the requirements for the degree of Doctor of Philosophy at Virginia Commonwealth University

Director: Rebecca L. Heise, Ph.D.
Associate Professor, Department of Biomedical Engineering

Lower respiratory diseases are currently the third leading cause of death worldwide. For many end-stage patients with these diseases, there is no cure and a shortage of donor organs available for transplant. A promising solution is to design regenerative scaffolds or complete bioengineered lungs, using decellularized lung tissues as a template for regeneration. Recent advances in the field have made significant strides towards developing a transplantable lung. However, the current technology has not produced a functional lung for *in vivo* transplant due to immature gas exchange barriers. The mechanisms driving alveolar barrier maturation and role that extracellular matrix (ECM) plays within the strengthening of each type of junction are not fully understood. This research has characterized and tailored a decellularized ECM (dECM) coating for the *in vitro* study of dECM component depletion and potential effects on cell barrier function, attachment, and survival. Adjustments to dECM digestion duration drastically changed the resulting structural and biochemical properties for each cellular microenvironment. Shorter digestion time resulted in a dense branching of the ECM architecture and biomimetic mechanical properties needed for epithelial culture. Also, through systematic supplementation of essential

basement membrane (BM) proteins to dECM, we have found that supplementation with laminin enhanced barrier strength by ZO-1 junction stabilization. This indicates that dECM can promote barrier formation but may have lost vital proteins that need to be replenished. Laminin-mediated barrier function was determined to be caused by the upregulation of the Epac/Rap1 pathway. This pathway has previously been implicated in lung endothelial barriers but not alveolar epithelial junction strengthening. Finally, to establish the translatability of these findings to whole lung recellularization, the dECM coating was used to pre-treat the airways of decellularized lungs for recellularization. Culture of MLE12 mouse epithelial cells into dECM-coated lungs increased cell survival and distribution. In combination with dECM coatings, rotational cell seeding improved cell dispersal and viability. Altogether, these techniques, devised to promote healthy alveolar barriers, are vital to enhancing current lung recellularization strategies and the treatment of many edema-associated pulmonary diseases.

CHAPTER 1: INTRODUCTION

1.2 Rationale

The lung is susceptible to many incurable diseases, such as chronic obstructive pulmonary disease (COPD), idiopathic pulmonary fibrosis (IPF), and cystic fibrosis (CF), that combined have become the third leading cause of death in the United States and worldwide. For many patients with these end-stage diseases, the only option is lung transplantation. With a shortage of donor's lungs, a promising alternative is recellularization of decellularized lungs. Decellularized lungs offer the complex native architecture of the lung with minimal immune response. Research to date has been able to create highly recellularized organs, but the current technology is not yet able to develop viable, long-lasting, functional tissue [1]–[3]. After implantation, bioengineered lungs often suffer from severe edema, indicative of loss of alveolar-capillary barrier integrity. By understanding how the extracellular matrix (ECM) that is left behind interacts with the alveolar epithelium, this technology can be modified to encourage the formation of a functional gas-exchange barrier.

Within decellularized ECM (dECM), many matrix proteins are preserved, including collagens, elastin, laminins, fibronectin, and glycosaminoglycans (GAG)s, but there are reports of up to a 50% loss of most of these components compared to native ECM [3]–[7]. We hypothesize that by identifying ECM components that are highly integral to the maturing gas exchange barrier and by increasing the concentration those components at the airway and alveolar surfaces, we can promote attachment and barrier function within the bioengineered lung.

dECM has been incorporated into a wide range of lung biomaterials including hydrogels, bioinks, scaffolds, and coatings; however, there has been little done to thoroughly characterize the

effect that functionality and composition of the ECM after decellularization have on cell response, and specifically barrier function. ECM hydrogels and coatings are widely used because they offer an *in vitro* tool to study cell-ECM interactions. Current methods use pepsin to increase the solubility of ECM proteins but do not consider the effect that further digestion has on dECM composition. We have chosen to utilize the dECM hydrogel and coating technology to replenish lost ECM components at the decellularized lung alveolar surface but to do that we must first identify the proper digestion duration and ECM supplementation to elicit the desired alveolar epithelial barrier formation.

With the use of our tailored ECM coating, this research aims to better recapitulate the necessary microenvironment required for maturation of the epithelial air-liquid interface and proper gas exchange, which has not previously been investigated comprehensively. This approach utilizes the natural ECM structure of the decellularized lung as a blueprint for lung regeneration and replenishes valuable ECM components that can be lost during removal of donor cells. We will then evaluate cell attachment and barrier integrity through the maturation of cell-cell junctions *in vitro* and *ex vivo*.

1.2 Objectives

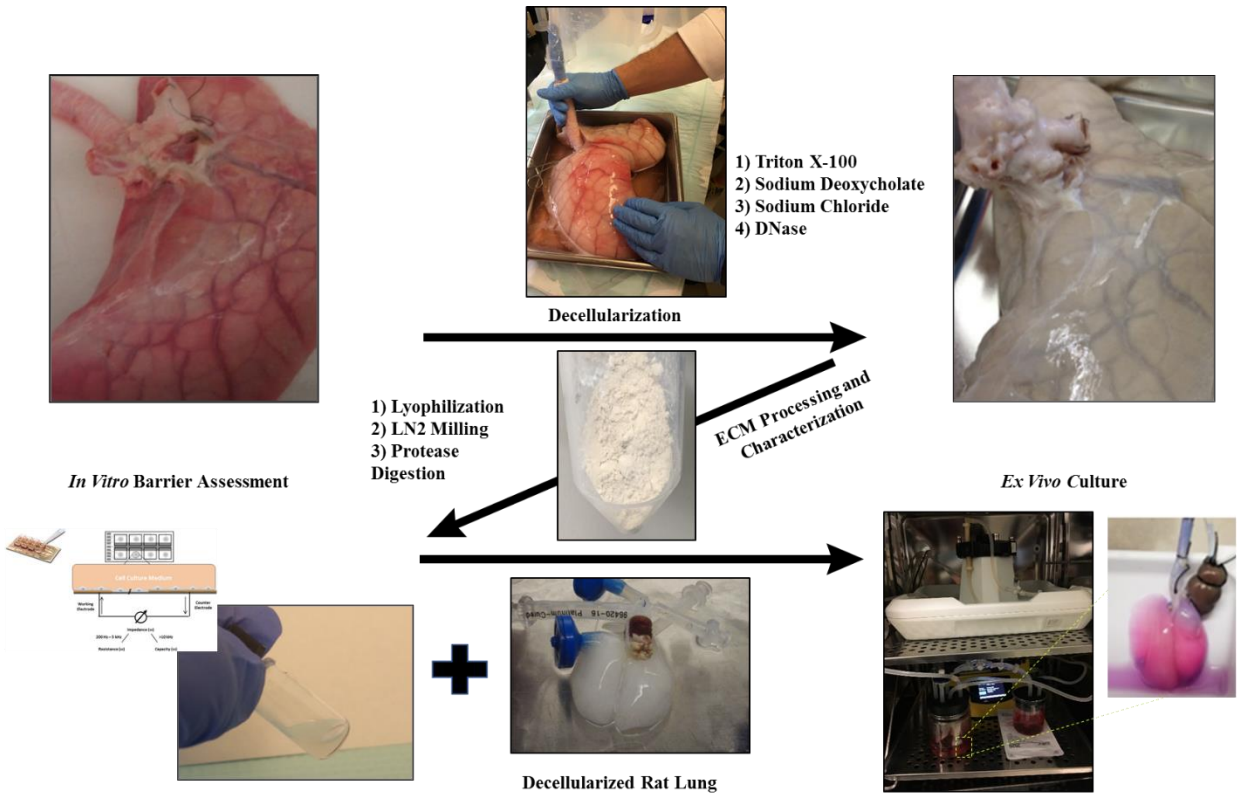

Figure 1.1. Overview of dECM characterization, processing, and utilization for engineering the gas-exchange barrier within recellularized lungs. This schematic shows the porcine lung decellularization process that will produce the ECM powder used to form dECM coatings and hydrogels. The coating can then be perfused into a decellularized rat lung before repopulating with epithelial cells and conditioned within a bioreactor of long-term culture.

Characterizing lung dECM and identifying the optimal ECM coating for natural alveolar epithelial barrier formation.

Previous studies found that minor variations in ECM composition greatly affects epithelial differentiation. Collagen and fibronectin rich matrices support initial epithelial attachment but ultimately promote migration, while laminin enhances long-term barrier strength [8], [9]. Nevertheless, the effect of ECM composition after decellularization on both tight junction (TJ)

and adherens junction (AJ) protein modulation has not yet been investigated. *Hypothesis 1: dECM structure and composition will facilitate attachment and maturation of alveolar epithelial cells by increasing cell-cell adhesion and therefore, barrier function.* To control the fragmentation of coated proteins, protease digestion of dECM coatings will be tailored based on protein cleavage, collagen organization, gel storage modulus, and cellular interactions. dECM protein loss during decellularization and hydrogel processing are characterized by mass spectrometry, SDS-PAGE, and western blotting to compare to native tissue. Through the measurement of transepithelial electrical resistance (TEER) and fluorescently-labeled dextran membrane permeability assays, we have also determined if barrier strengthening is dependent on ECM coating compositions.

Investigate the role of the Epac/Rap1/AF-6 pathway in barrier strengthening and junctional protein expression with respect to ECM substrate.

Epac has been implicated in ECM-mediated signaling and strengthening of endothelial and epithelial barriers. Epac's role in alveolar barrier strengthening by ECM interactions, however, is far less understood. *Hypothesis 2: dECM causes upregulation and maturation of AJ and TJ proteins, mediated by integrin binding of ECM and modulation of Epac activation.* Junctional protein staining and mRNA expression of cells cultured on various ECM coatings can shed light on which aspect of the cell-cell junction is causing barrier strengthening and how it can be manipulated. We have quantified expression of Rap1 and other associated genes with Epac inhibition and activation to confirm the mechanism of barrier modulation.

Development of a rotational cell seeding bioreactor to improve dispersal and attachment of epithelial cells in 3D tissue engineering scaffolds.

Two main bioreactor designs are currently used for decellularized lung culture: a perfusion ventilation system [10] and a rotating wall (RWV) bioreactor [11]. Both systems offer delivery of nutrient-rich media and dynamic culture capabilities, yet, either sedimentation of cells or decreased attachment can occur. *Hypothesis 3: By rotating the lung scaffold periodically during the first hours of culture, at a rate determined by cell type-specific attachment, overall cell surface coverage of the airways and alveoli structures will be improved.* Resting intervals allow for cell focal adhesion formation, followed by the movement of unattached cells to a new region for adherence or unattached cells. With repetition of these movements and varying degrees of rotation, a defined percentage of cells will attach at each plane of the lung. Metabolic function and cell attachment have been assessed through resazurin staining, Picogreen dsDNA quantification, and histology of multiple regions throughout the re-epithelialized lung.

Barrier assessment in e*x vivo* whole lung recellularization of dECM coated lung scaffolds.

Whole lung recellularization has been geared towards improving attachment and differentiation of epithelial cells within a decellularized airway [11]–[13] but has yet to produce a functional transplant option due to lack of cell coverage and edema. Utilizing mechanisms uncovered through this research to improve the integrity of the epithelial barrier in combination the latest advancements in the field may bridge the gap within lung recellularization. *Hypothesis 4: Pre-treatment with concentrated dECM coatings to decellularized scaffolds prior to epithelial reseeding will increase attachment and decrease barrier permeability compared to recellularization without coatings.* The previously mentioned rotational seeding unit for initial attachment and a traditional perfusion bioreactor for long term culture has been utilized for *ex vivo* epithelial lung culture of dECM coated rat lungs. Metabolic function and cell attachment were

assessed through resazurin staining, Picogreen dsDNA quantification, and histology. Alveolar barrier protein integrity was evaluated by junctional gene expression and a dextran permeability assay.

Together, the completion of these objectives would offer tools to improve tissue engineering with dECM and engineering of functional lung gas exchange barriers in hopes of bringing transplant alternatives closer to the clinic.

CHAPTER 2: LITERATURE REVIEW

2.1 The Role of ECM in Lung Homeostasis

ECM not only provides the macrolevel structural and mechanical support to tissues; it also offers biochemical cues that can guide cell morphology, function, and differentiation. There are two main classes of ECM proteins focused on in this research: 1) structural components such as collagens, which dictate most of the mechanical properties of the lung, and 2) basement membrane (BM) ECM, which creates the meshwork by which epithelial monolayers are formed.

The lung-specific matrix is primarily comprised of collagens (types I, III, IV, V) and elastin that provide structural support and the elastic recoil of the lung. Large structural ECM fibers are predominantly found within the submucosal layer of the lung, creating a porous matrix for fibroblasts and smooth muscle cells. Directly above the submucosa is the BM that is composed mostly of collagen type IV, laminin, entactin/nidogen, and heparan sulfate [14], [15]. These proteins arrange themselves in a dense mesh to form a flat surface for epithelial cells. Other essential components are dispersed within both regions, including fibronectin, decorin, hyaluronan, tenascin-X/C, and many other glycosaminoglycans [6]. Within both regions, any dysregulation of ECM crosslinking, degradation, or production can be catastrophic to lung function and propagate lung sever pathologies [16] as seen in Figure 2.1. A delicate balance between ECM production and matrix metalloprotease (MMP) degradation continually regulate the subtle differences in ECM structure and composition that differentiate the properties and cells of each tissue. Excessive cleavage is necessary for natural renewal of ECM; however, over-degradation of the ECM can release unnecessary growth factors and compromise structural

integrity. Disproportionate production of any ECM component, primarily collagen, can lead to many pathologies, including fibrosis and cancer [17].

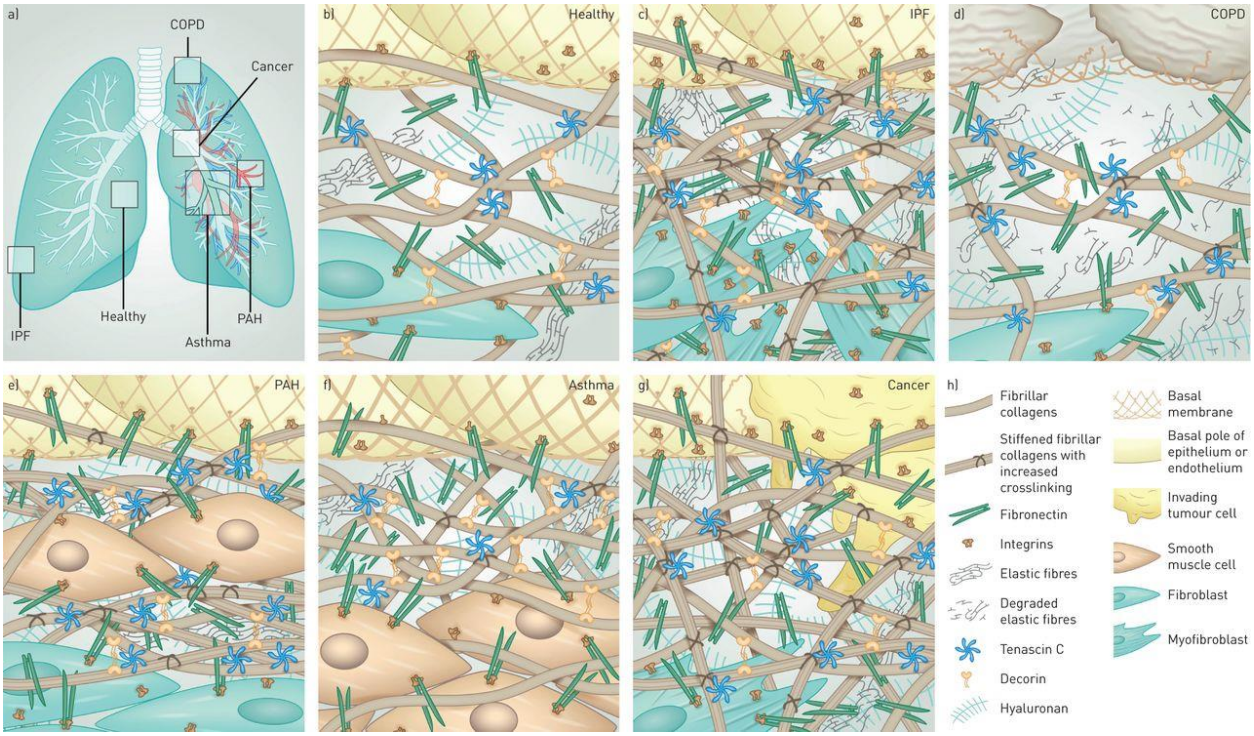

Figure 2.1. Lung ECM structure and changes in lung pathologies. Healthy lung ECM is arranged into the mucosa and submucosa regions that provide both structural support and cellular biochemical cues. Reprinted from [16].

Collagens are the most abundant protein within the human body and have a significant effect on tissue mechanical properties [18]. 45 collagen genes encode for 28 collagen protein variations that all are comprised of a trimeric protein structure. Variations in monomer isotypes form homotrimers or heterotrimers that ultimately dictate collagen type. Each collagen peptide has a repeating Gly-C-Y sequence that allows for the highly conserved and organized arrangement of

the triple helix structure. Some collagens have interruptions in this repetitive sequence causing variations in collagen isoform structures. The fibrillar collagens are collagen I, II, III, V, and XI and make up 80 to 90 percent of collagen within the body [19]. Other collagens (IV, VI, VII, VIII, X) are either anchoring fibrils or form the basement membrane [20].

Collagens are produced by cells in a procollagen form that is modified to form the monomer structure. Depending on mechanical requirements of the tissue, collagen monomers undergo fibrillogenesis to increase fiber size, as depicted in Figure 2.2. Resulting fiber diameter can be altered by several different factors: collagen sequence variations, post-transcriptional glycosylation levels [21], and nucleator presence [22]. Collagens also binds other molecules such as integrins, growth factors, other matrix proteins, MMPs and even water [23]–[25] that can enhance the triple helix conformation and can drastically change inherent properties of collagen. Without disruptions in collagen monomer sequences, ECM nucleators are essential to modulation of collagen structure, and the type of nucleator controls the resulting fibrillar structure. For these reasons, alterations in both fibrillar collagens and nucleators could disrupt fibrillogenesis *in vivo* and within dECM based biomaterials.

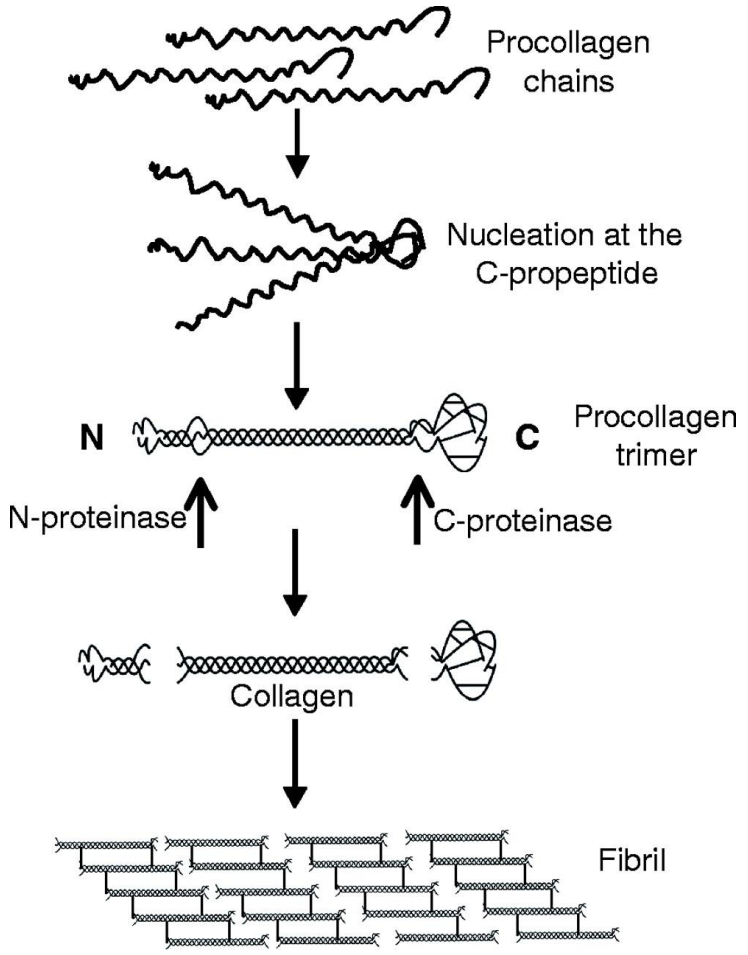

Figure 2.2. Collagen fibrillogenesis from cell-secreted procollagen. Post-translational modifications and removal of the N and C-propeptides take place before hydrogen bonding of monomer chains into the triple-helix structure. This image was reprinted with permission from [26].

Conversely, BM ECM is comprised of fewer load-bearing collagens and creates a dense network of laminins, fibronectin, nidogens, proteoglycans, and collagen IV. The ratio and isoform of each ECM component within the BM are tissue-specific and provides direct signals to epithelial cells for differentiation and homeostasis [27], [28]. When an injury has occurred, and cells are

displaced, the BM is left behind to guide regeneration [29]. This phenomenon is widely seen in neuromuscular junctions where, after injury, the BM separates the muscle and neuron spaces so that there is neuron-specific basal lamina to guide elongation [30]. For cells to distinguish the makeup of the BM and its structure, they must interact directly with ECM components via specific integrins.

Integrins are primarily ECM adhesion receptors that also provide feedback to the cell from the extracellular environment [31]. Airway epithelium has a specific repertoire of 8 integrins to interact with environmental mediators at the airway lumen and to interact with the BM. The integrins that specifically bind ECM proteins including, α2β1 specific to collagen, α3β1 and α6β4 specific to laminins and matrix proteins in the BM, α9β1 specific to tenascin, α5β1 specific to fibronectin, and αvβ6 that binds both fibronectin and tenascin [31]–[33]. Integrins are not independent initiators of downstream signaling cascades, but instead are anchoring proteins for kinases and scaffolding proteins upon conformational changes caused by ligand binding (Figure 2.3, [34]).

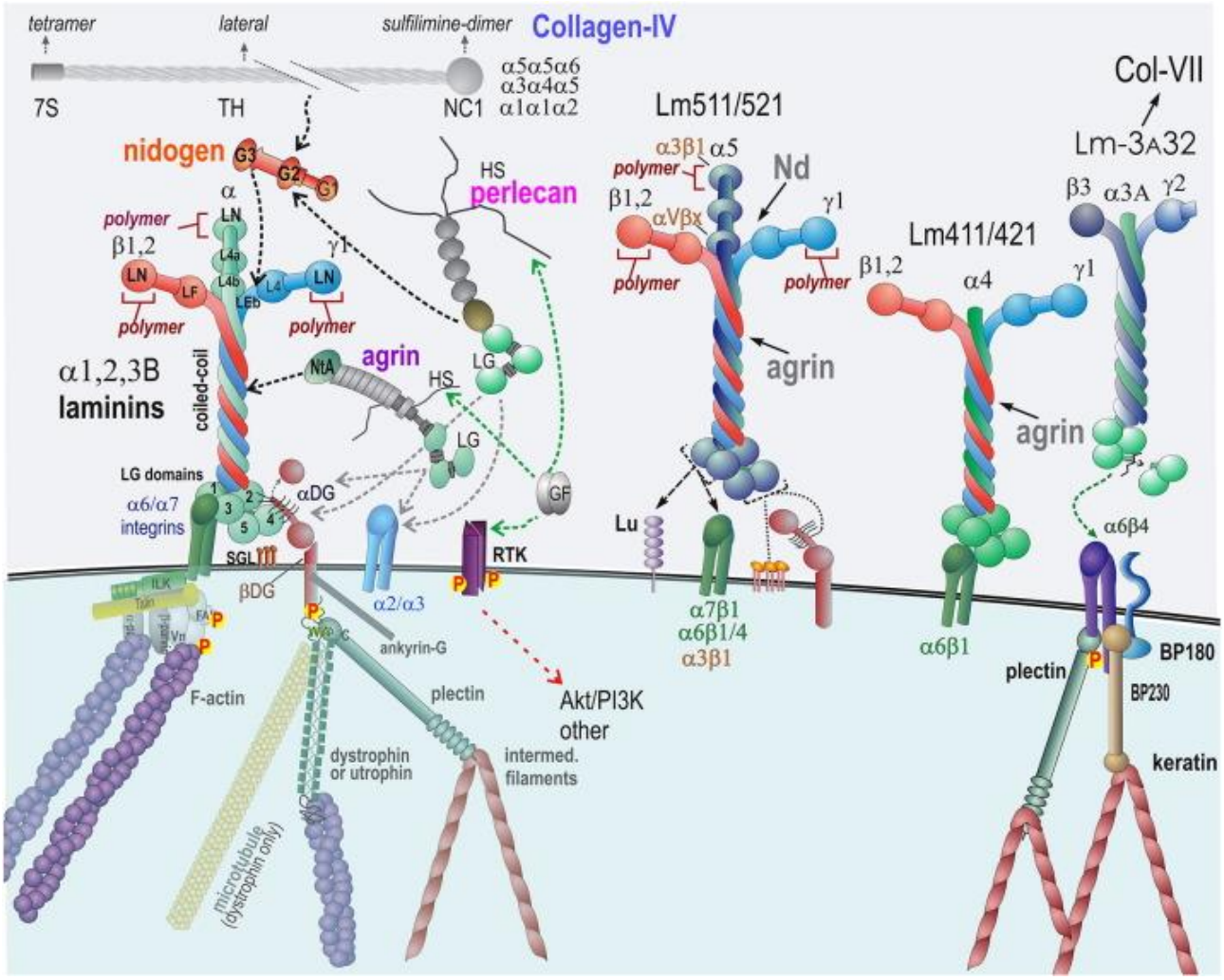

Figure 2.3. Basement membrane assembly largely organized by laminin interaction with integrins and other BM proteins to form a dense mesh. Variations in laminin isoform determine the integrins ECM that will bind. Reprinted with permissions from [15].

Laminin directs assembly of the BM by binding cells, other matrix proteins like collagen IV and nidogen, and itself to form the backbone of the BM. The interaction of collagen IV, nidogen, and laminin form a net-like sheet below the epithelial layer. Laminin is a glycoprotein composed of an α, β, and γ peptide chain that combine to make up to 16 mammalian isoforms [29].

During development, elevated levels of laminin are found in the BM compared to collagen IV, and with age, the ratio of laminin and collagen IV will become equal [35]. The adult lung alveoli contain mostly laminin- α3, α4, and α5 isoforms [36], [37]. Studies have shown that laminin is a primary driver of barrier maturation within the lungs [35], [38], [39], and regulates epithelial to mesenchymal transition (EMT) [40]. Laminin is a critical regulator in epithelial differentiation, and its direct interaction with cells at the basal lamina make it an attractive option for alveolar barrier stabilization.

Also of importance in the maintenance of cell phenotype is the regulation of fibronectin concentration within the extracellular environment. Fibronectin aids in cellular adhesion to the matrix with Arg-Gly-Asp (RGD), collagen, and heparin binding sites exposed under tension [29]. During initial attachment, cells preferentially adhere to areas with high fibronectin, laminin, collagen I, and collagen IV, but over time, cells do not proliferate or generate high resistance barriers on fibronectin [9], [41], [42]. This would suggest that fibronectin promotes initial attachment after injury, but growth and post-adherence interactions are less dependent on fibronectin [6]. After an injury or during cancer migration, an overabundance of fibronectin can drive EMT through TGF-B sequestration or fibrosis [43], [44]. These pathological consequences illustrate the importance of regulation of fibronectin and other ECM protein concentration in lung homeostasis.

2.2 3D Decellularized ECM Culture Systems

Decellularization of tissues was first pioneered in the late 1970s [45] to isolate the tissue-specific basement membrane for cell culture. Over the years, several core groups, such as the

Badylak and Ott laboratories, have made great strides in the development of decellularization methods, extending to xenograft or allograft scaffolds of many different organs. This tissue-specific scaffold would promote cell growth and differentiation of a patient's cells as an option for transplant. Removal of cellular material is achieved with repetitive rinses of detergents, enzymes, or acidic solutions. Once cells are removed, the extracellular matrix that is left behind can be used as a scaffold for tissue engineering by providing the architecture of the native organ. The properties of the tissue determine the techniques and solutions that need to be used for the decellularization process, which includes, degree of cellularity, tissue density, lipid content, and architecture.

Removal of cellular material to produce a decellularized tissue can be done by chemical reagents, mechanical abrasion, or freeze-thaw procedures. The most common method includes perfusion of chemical reagents such as acids and bases, hypertonic or hypotonic solutions, non-ionic detergents such as Triton X-100, ionic detergents such as sodium dodecyl sulfate (SDS) or sodium deoxycholate, Zwitterionic detergents such as CHAPS, or enzymatic solutions such as nucleases, trypsin, or dispase through both the trachea and vasculature. Some of the physical methods include pressure, electroporation, or agitation. Most protocols use a combination of various chemicals and mechanical processes to ensure removal of all cellular remnants within the tissue [2], [46], [47]. A gold standard for this procedure has not definitively been established because there are disadvantages to some reagents over others. Some reagents are more effective at removing cellular material such as SDS and sodium deoxycholate, but they can also cause damage to the ECM. Less harsh chemicals such as Triton X-100, Trypsin, or CHAPS do not disrupt the ECM composition but are inefficient at cellular removal.

Each tissue requires tailoring of the decellularization protocol based on the tissue's density or lipid content [48]. Lungs have a low lipid content, and the airway and vasculature arrangement

allows for efficient distributing of the reagents to all parts of the tissue, making it a great candidate for decellularization research. Quality control for removal of DNA, proteins, or α-galactosidase in cases of xenogeneic tissues, is essential to eliminate immunological reactions or other adverse effects. To be considered a fully decellularized scaffold, the lung must pass the standard of less than 50 ng dsDNA per mg ECM dry weight and less than 200 base pair DNA fragment length, with lack of visible nuclear staining [49]. These standards are confirmed by histological nuclei staining with DAPI or hematoxylin and eosin (H&E), and dsDNA quantification methods such as Picogreen assay, propidium iodide, or gel electrophoresis [49].

Absence of even one ECM component in the lung profile, such as laminin and fibronectin, can drastically change cell differentiation of barrier formation within tissue engineered scaffolds [9], [50]–[54]. Matrix proteins such as collagen, elastin, laminin, fibronectin, and glycosaminoglycans (GAGs) are preserved through the decellularization process, as shown by immunofluorescent staining of collagen1, laminin, and fibronectin before and after decellularization in Figure 2.4. However, there are reports of up to a 50% loss of most ECM components through the decellularization process compared to native ECM [3], [55]. Directly at the surface of decellularized lung alveoli and airways, there are more alterations to the ECM composition compared to deeper within the tissue because of direct exposure to decellularization detergents. Variations in ECM composition and stiffness can have a profound effect on cell phenotype, as well as cell attachment and barrier function [9], [56]–[58]. High collagen and fibronectin content promote cell attachment at the expense of suboptimal barriers, indicative of metastasis and fibrosis [6], [41], [43], [59]. Laminin is integral to both strong barrier formation and epithelial differentiation [35], [38], [40], [60]–[63].

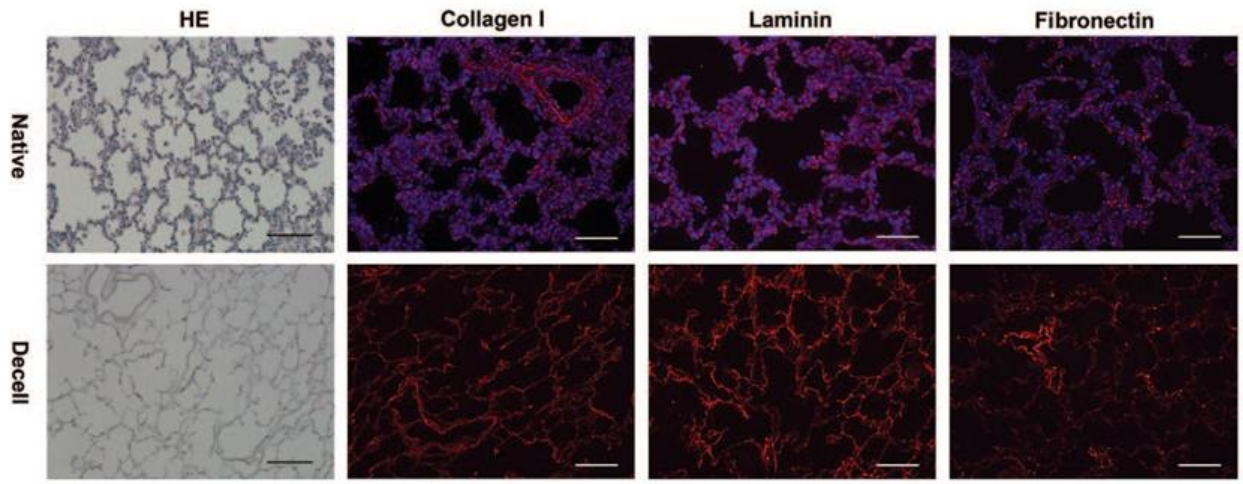

Figure 2.4. Alteration in ECM structure and composition with lung decellularization. Histological sections of decellularized lung matrix show removal of all cells and presence but depletion of collagen I, laminin, and fibronectin. Reprinted with permission from [3].

Decellularization techniques are used to create partial or whole organ scaffolds for in vitro models and tissue engineering. Decellularized tissue is also a source of tissue-specific ECM for more advanced biomaterials including electrospun [64], [65] or lyophilized sheets [66], [67], microparticle powders [68], bioinks[69], [70], and self-assembling ECM hydrogels [71]–[73] from a variety of organs and tissue origins. Hydrogels specifically are a promising tool for translation to the clinic because the cells can be incorporated within the gel easily and it is in liquid form before injection to the site of interest but then will undergo gelation once in the body. I*n vivo* studies with naturally derived ECM hydrogels for myocardial infarction [74], [75], nervous tissue [76], and lung [72], to name a few, show increased tissue function and minimal immune response. Incorporation of ECM into hydrogels or coatings can cause challenges because enzymatic digestion of the proteins is often necessary to achieve full solubilization. The implications of the

additional digestion step on the bioactivity and structure of the final ECM product has not been fully characterized and potentially compromises critical biophysical and biochemical cues. It has been confirmed that even with additional digesting, the resulting matrix retains tissue-specific composition, growth factors, matrikines, and matrix-bound vesicles that can direct tissue-specific cell behavior and differentiation [77].

2.3 Lung Bioengineering

End-stage chronic obstructive pulmonary disease (COPD), idiopathic pulmonary fibrosis (IPF), or cystic fibrosis (CF) is the most common need for lung transplantation. Chronic lower respiratory diseases, such as these, have become the third leading cause of death in the United States, reported by the Center for Disease Control [78], [79]. Without a cure for these diseases, there were nearly 3,000 people added to the lung transplant waiting list each year in the United States; however, viable lung tissue only becomes available for 50% of those on the waitlist [80]. Of those patients that do receive lungs, all will remain on immunosuppressive drugs, and many will have lung failure within 5 years. With a shortage of donor's lungs, there is a critical need for a bioengineered transplant option. Recellularization of decellularized lungs offers a promising solution to this problem.

There are currently two main unanswered questions in the field of lung recellularization. 1) What are the best cell lines for recellularization that will differentiate into all cell types of the adult lung? 2) What are the best cell delivery and culturing methods to produce viable, long-lasting tissues? Both sides of the gas exchange barrier, epithelial and endothelial, need to be recellularized fully to produce functional tissue. Heterogeneous populations of primary lung cell from a human donor can offer multiple cell types with the least amount of effort, but this will not

always result in the full cellular profile. One cell population that must be present within a bioengineered lung transplant is alveolar epithelial cells, which are difficult to culture and have low viability. Another promising option for epithelial recellularization are lung stem cells such as basal progenitor cells (Trp63+, Krt5+)[12], alveolar type 2 cells (sftpc +, sftpb+) [46], club cells (scgb1a1+, Cyp2f2-), induced pluripotent stem cells (IPSCs) [81], or resident mesenchymal stem cells (MSCs) from either a bone marrow or adipose lineage [82]. As for revascularization, similar cell options are available, such as heterogeneous mixture of vascular cells [83], human umbilical vein endothelial cells (HUVECs) [84], iPSCs, endothelial stem cells [85], [86] or MSCs. The ideal recellularization protocol has not been determined but will ultimately include multiple cell types at a perfect concentration, providing a physiological niche like the native lung. Even with an ideal cell type for repopulation, there is still debate regarding the number of cells needed to repopulate a lung. For mouse and rat lung scaffolds a range from 2 to 100 million cells [87]–[90] and 100-500 million cells for human and porcine scaffolds [13], [90], [91] administered to either the trachea or vasculature.

To improve recellularization, researchers have increased cells attachment with pre-treatment of decellularized scaffolds with matrix proteins, immune cells, or native lung microbiome [12], [88], [92], [93], optimizing cell delivery techniques [94]–[96], and long-term culture with multiple cell installations [91], [93]. These improvements to recellularization methods have increase function and maturation but have resulted in only partial function; withstanding a maximum of one month *in vivo* [93], and most other attempts have resulted in much less. Most suffer from airway collapse and occlusion, insufficient cell coverage, and edema that has hindered their ability to perform gas exchange as needed. To overcome this challenge, it is imperative that

research is done to fully understand extensive physiology of the respiratory epithelium and endothelium with emphasis on the gas-exchange barrier.

2.4 Bioreactors and Culture Methods of Lung Bioengineering

A bioreactor is an overarching term to describe systems mimicking *in vivo* conditions, often for cell culture and maturation of bioengineered tissues. For the culture of tissue engineered constructs, bioreactors are used to improve several phases of regeneration: 1) cell seeding and dispersal, 2) delivery of fresh nutrients to enhance cell viability, and 3) application of a biomimetic mechanical stimulus to guide differentiation [97], [98]. Adequate simulation of healthy lung physiology depends on graft species origin and size. For rats specifically, *in vivo*, the maximum arterial flow rate would be between 10 and 20 mL/min and total lung capacity of 10-15 mL [99]. The output parameters of designed bioreactors may not need to be as high as seen in healthy tissue but must resemble similar dynamic conditions. To achieve this, the design specifications for a lung bioreactor include, design of a closed system to reduce contamination, ventilation with negative pressure to administer 0-15 breaths per minute, pulsatile perfusion at 4 mL/min, and constant oxygenation of a medium [100]. While ideal physiological conditions would ventilate the culturing lung with air through the trachea to achieve an air-liquid interface, during the initial stages of cell seeding, prematurely introducing air can cause epithelial detachment, and therefore ventilation with media is advised for the first several weeks of culture [101].

Some of the most simple bioreactor systems are hollow fiber bioreactors that allow for basic perfusion of media or air around the structure for cell culture [102]. More complex and controlled bioreactors are whole lung perfusion systems equipped with artificial silicone pleura and functional monitoring (Fig. 2.5A-B) [103]. Cell distribution onto and within scaffolds is

improved by culturing in a dynamic bioreactor system to simulate the physiological environment and innovative protocols that allow for the most effective seeding of cells [12], [83], [95]. Bioreactors have also been automated for both decellularization and recellularization procedures to ensure reproducibility. With many minor variations, the most common system performs cell seeding and culture with pulsatile or continuous vascular perfusion and negative pressure breathing [10], [84].

Histological sections of recellularized lungs show the regional distribution and lack of complete alveolar or airway cell coverage. This indicates that cell seeding and dispersal techniques still need to be optimized during the first few hours. The most common method is seeding within the perfusion bioreactor system is done without flow for the first 12 hours to 2 days to allow for seeding. With this method, gravity and cell settling can drastically affect cell dispersal. Within the same system, cellular seeding has also been done in the presence of either vascular or airway flow, continuously moving cells and media. This method would increase the dispersal of cells; however, suspension cultures can disrupt cell attachment rates [91], [104].

Another bioreactor designed to increase cell dispersal is the rotating wall vessel (RWV) bioreactor system (Figure 2.5C, [11]). Within this system, scaffolds are perfused with cells, centrifuged to initially disperse cells throughout the lung, then cultured statically for 1 to 4 days before initiating rotation culture [11], [53], [105]. This system mainly increases nutrient flow and creates microgravity throughout the culture; however, since the lungs are statically cultured prior to horizontal rotation, the coating of cells throughout the lung is not possible and still suffer from sedimentation and regional seeding of cells. Even if the rotation began during the time of seeding, constant rotation at 20 RPM would not allow cells to remain stationary for long enough for cells to adhere to the matrix. For these reasons, this research has designed a bioreactor system that

combines some beneficial aspects of all methods, with intermittent rotation tailored to cell attachment rates, a period of static culture to allow adhesions to mature, and finally perfusion and ventilation culture for mechanical conditioning.

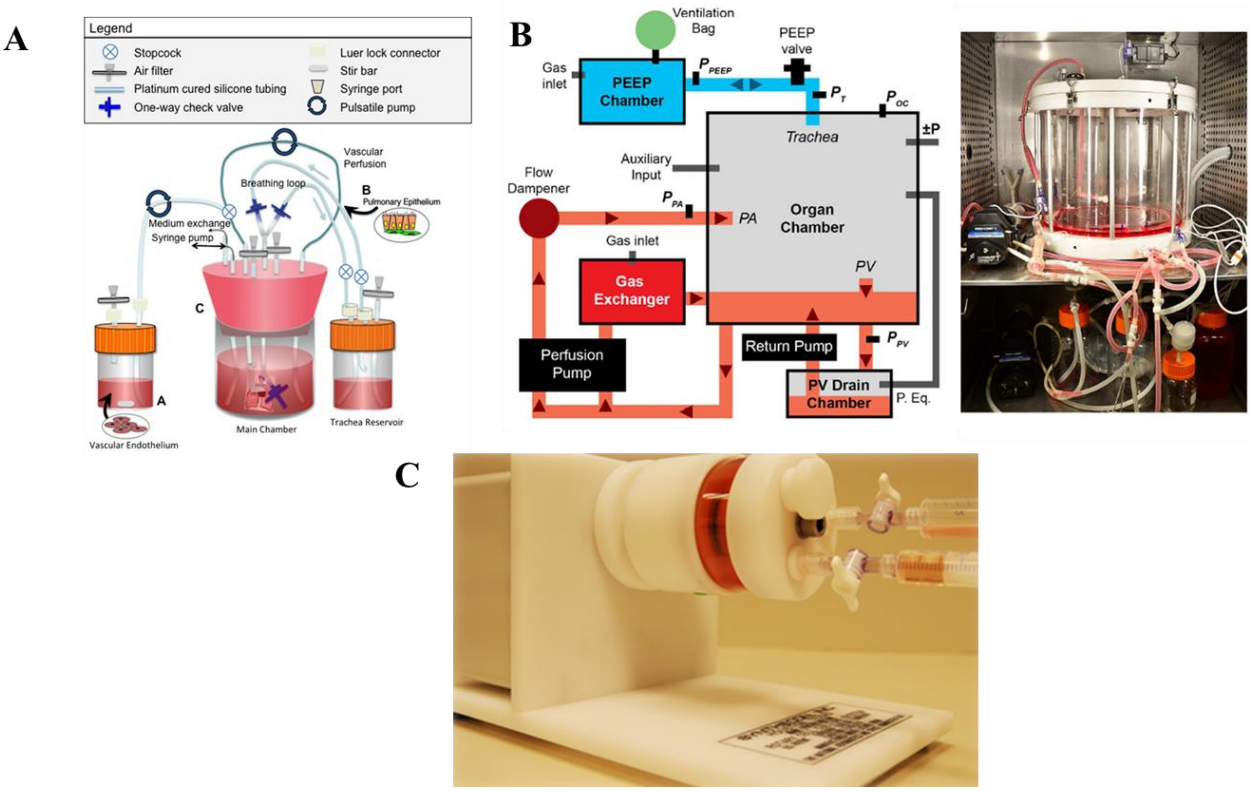

Figure 2.5. Traditional bioreactor designs for whole lung culture. (A) Small rodent bioreactor systems with pulsatile vascular perfusion and negative pressure breathing (reprinted from [106]). (B) Large species (porcine and human) bioreactor design (reprinted with permission from [13]) equipped with silicone artificial pleural membrane and lung mechanics. (C) Rotation wall vessel (RWV) used to create microgravity and decrease cell sedimentation (reprinted from [11]).

2.5 Alveolar Epithelial Junction Formation and Epac Regulation

Molecule selectivity and homeostasis of the alveolar epithelial barrier is maintained by two main structures: tight junctions (TJ) and adherens junctions (AJ). Barrier development begins with

E-cadherin and nectin recruitment to form “primordial AJs” seen in Figure 2.6. Adherens play a crucial role in the maturation of the epithelial junction by then initiating the recruitment of TJ proteins [107]. TJs further reinforce the cell-cell adhesion with transmembrane claudins, occludin, and junctional adhesion molecules (JAMs). During junction maturation, AJ transmembrane proteins associate with afadin (AF-6) and catenins, while TJ transmembrane proteins associate with zonula occludins (ZO) to stabilize the connection from the extracellular environment to cytoskeletal elements [107]–[109]. Once cells have formed mature cell-cell contacts, epithelial cells will exhibit a cobblestone morphology with the cortical arrangement of junction proteins and the actin cytoskeleton. Protein deficiencies within these structures including, claudin-3, claudin-4, claudin-18, JAM-A, occludin, ZO, and E-cadherin have been known to cause barrier disruption and edema specific lung pathologies [107], [110]–[112]. This suggests that AJs and TJs must form sequentially and synergistically for proper barrier regulation.

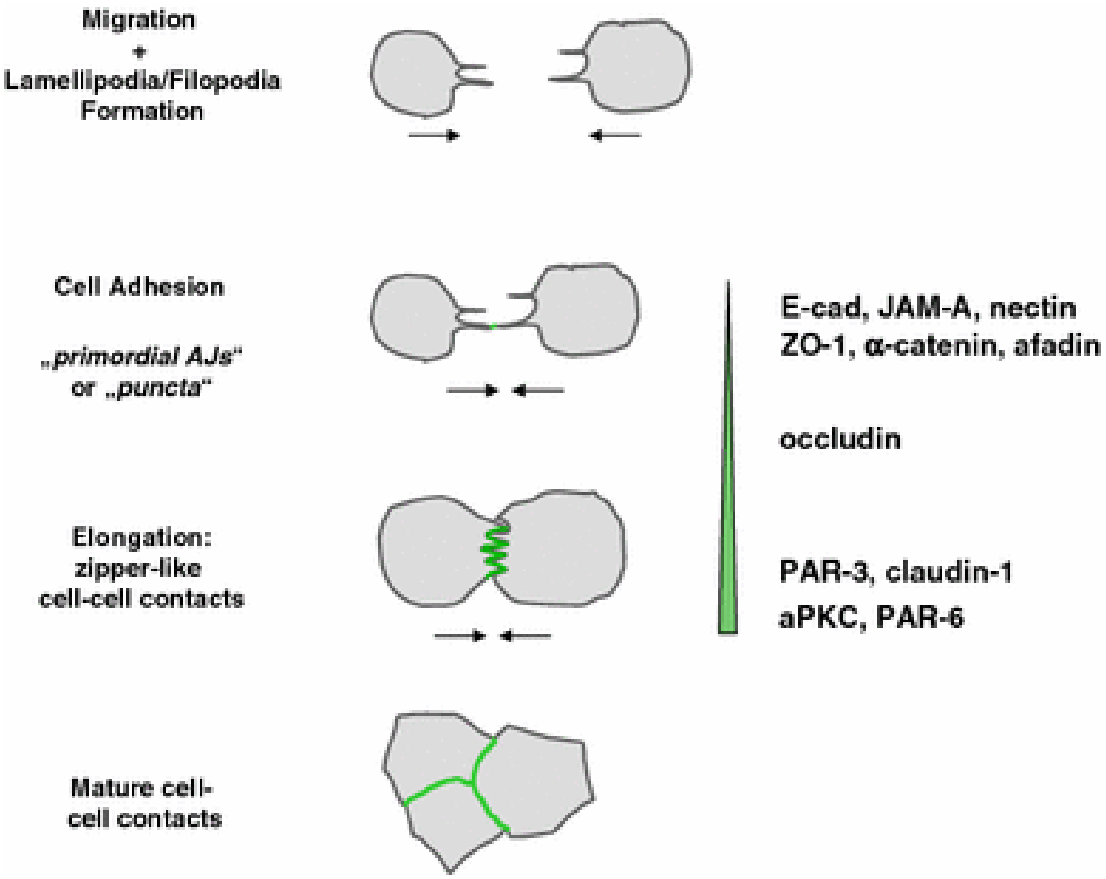

Figure 2.6. Epithelial cell junction formation. Junctions are first composed of AJ structures, but with maturation, TJ structures are recruited, and both are stabilized by scaffolding proteins. During this time, the cell contact transition from a "zipper-like" cell-cell contact arrangement to a cortical organization. Reprinted from [113].

Many aspects of the cellular microenvironment, such as ECM composition and stiffness, can alter barrier formation and junction protein expression [9], [56]. Two main signaling molecules involved in barrier modulation are protein kinase A (PKA) and the exchange factor directly activated by cyclic AMP (Epac). PKA has traditionally been thought of as the primary regulator in cell-cell junctions by inhibiting RhoA/ROCK and stabilizing cell junctions [114]. However, inhibition of PKA does not attenuate cAMP driven barrier strengthening. The Epac/Rap1 pathway

alternatively, was identified as another critical junction regulator [115] that can be dependent on ECM interactions, such as laminin fragments [116], [117] and can affect multiple cell-cell adhesion structures. Epac is widely researched in endothelium and other tight barriers throughout the body; however, there is less information on the role of ECM in the regulation of this pathway within the alveolar epithelium.

Rap1 has been implicated in cellular migration, metastasis, and junction disassembly, but depending on the mode of initiation and downstream activation, Rap1 can play an equally impactful role in actin arrangement, integrin expression, and cell-cell adhesion. Epac can act directly on the AJ formation factor, afadin (AF-6) [111], [118]–[120]. AF-6 interacts with p120-catenin and E-cadherin of AJs to inhibit E-cadherin endocytosis [109], [118], promote dimerization with E-cadherin with neighboring cells, and the overall organization and maturation of AJs. AJ formation is proceeded by TJ formation and can also be controlled by Epac/Rap-1/AF-6 signaling. AF-6 also associates with nectins, zona occludins (ZO), and junctional adhesion molecule A (JAM-A) to stabilize TJs [121], [122]. TJs have been studied at the alveolar barrier and are driven by ECM composition by increasing expression of lung-specific claudins, such as claudin-3, claudin-4, and claudin-18, JAM-A, ZO-1, and occludins [9], [110], [123]. The absence of any essential ECM protein in a scaffold will inhibit healthy TJ maturation, as seen by time-dependent barrier impedances or increased attachment of epithelial cells on different ECM coatings [60], [61]. This suggests a strong correlation between ECM composition, the Epac/Rap1 pathway, and the regulation of junctional proteins. Epac activation of Rap1 promotes junction formation and increased β1 integrin translocation to the membrane for further cell-matrix interactions [124]. Rap1 interacts with AF-6 and E-cadherin to increase attachment to ECM and stabilize AJs and TJs to the actin cytoskeleton [118], [120]. Further understanding of Rap1's

influence on both AJ and TJ structures within alveolar epithelium has not yet been completed in extensive detail. A hypothesized compilation of the many identified roles of Epac and Rap1 within both endothelial and epithelial junctions is shown in Figure 2.7. This research aims to confirm the synergistic roles of Epac and ECM in the regulation of alveolar epithelial junctions that has yet to be demonstrated fully.

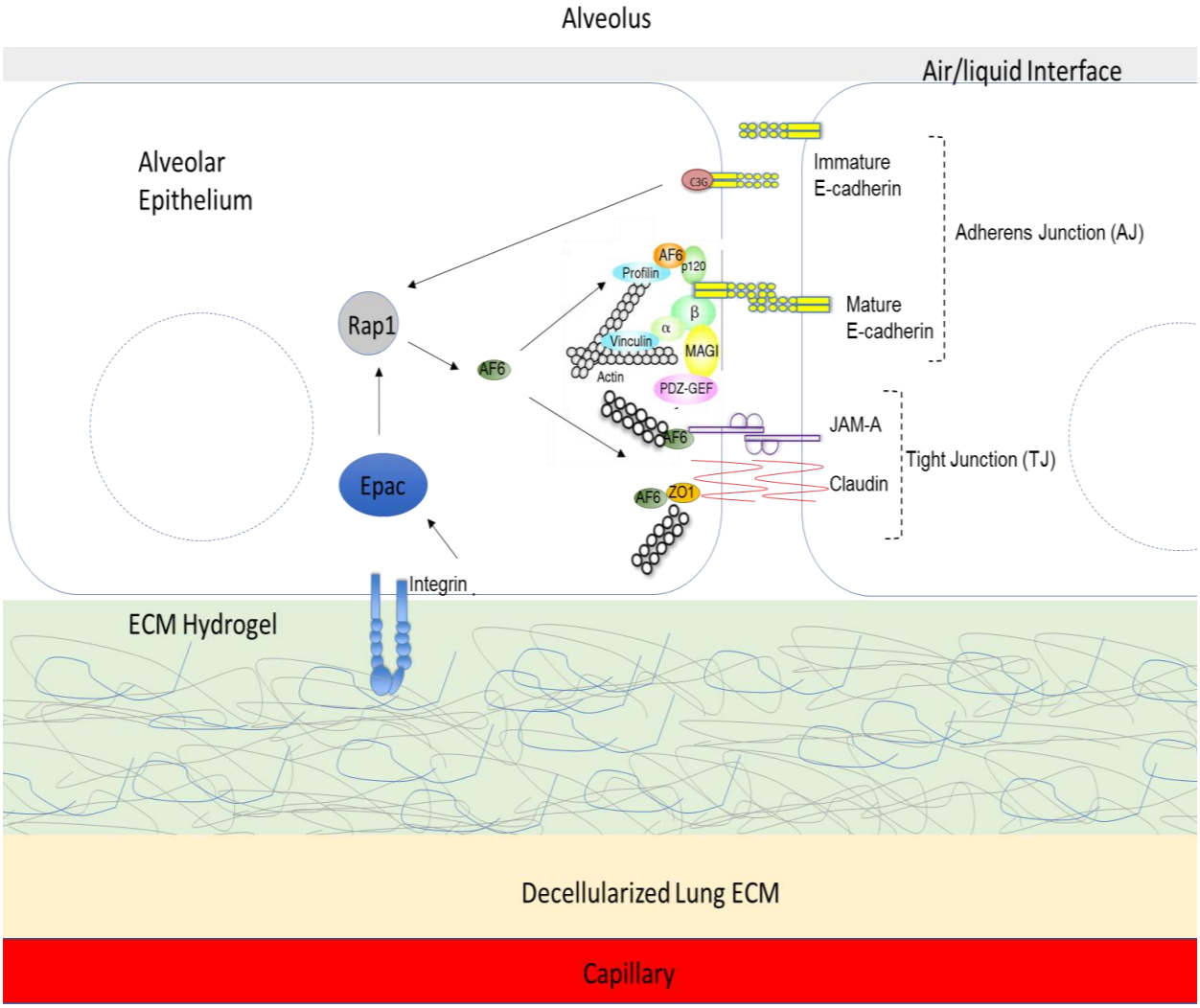

Figure 2.7. Hypothesized regulation of AJ and TJ structures through the ECM-mediated activation of the Epac/Rap1 pathway. α3β1 and α6β4 integrins recognize the laminin-enriched dECM coating composition at the alveolar BM of decellularized lungs. Integrin conformational changes increase cytoplasmic cAMP by G-protein coupled receptors. cAMP influx causes activation of Epac to modulate actin dynamics, gene expression, cytokine response, adhesion, proliferation, and barrier function. Epac then stimulates Rap1 to increase AF-6 stabilization of ZO-1 and other scaffolding proteins at the epithelial junction [120], [125].

CHAPTER 3: dECM CHARACTERIZATION

3.1 Rationale

Decellularization is used to create partial or whole organ scaffolds for a variety of tissue engineering applications. Decellularized tissue is also a source of tissue-specific ECM for more advanced biomaterials including electrospun [64], [65] or lyophilized sheets [66], [67], microparticle powders [68], bioinks[69], [70], and self-assembling ECM hydrogels [72], [73] from a variety of organs and tissue origins. Incorporation of ECM into some applications, such as hydrogels or coatings, requires enzymatic digestion with pepsin, trypsin, or other degradative enzymes to achieve solubilization. However, even with significant digestion, the resulting solubilized material retains tissue-specific composition, growth factors, matrikines, and matrix-bound vesicles that can direct tissue-specific cell behavior and differentiation [77]. The implications of the additional digestion step on the bioactivity and structure of the final ECM product has not been fully characterized and potentially compromises critical biophysical and biochemical cues. For these reasons, this research aims to further characterize hydrogel properties with increasing digestion to minimize adverse effects on the ECM and allow for tailorability for multiple tissue origins and applications.

Current research with ECM hydrogels or coatings utilizes enzymatic digestion of the ECM within an acidic medium for at least 48 hours to achieve solubility [71]. Prior research has characterized several properties of hydrogels produced from a single digestion duration, including resulting scaffold pH, salt ion concentration, mechanics, and ability to be chemically crosslinked [126]. However, variability in these parameters caused by differing lengths of enzymatic digestion

has not been fully understood or optimized. Insoluble ECM proteins are progressively digested into the solution at a rate dependent on pepsin activity and particle surface area. At pepsin's peak digestive pH range of 1.5 – 2.5, pepsin will continuously cleave proteins at relatively unspecific target sites. Digestion slows as the pH of the solution rises to 8 when it is terminally deactivated. As soluble proteins fragment into smaller peptide chains with prolonged digestion, the resulting biomaterial properties change significantly. By varying ECM hydrogel production, we may be able to tailor our preparation to a broader range of applications.

The mechanical properties of ECM hydrogels are known to be an order of magnitude less or more than the tissue they are isolated from [72]. We believe this is caused by a loss of tertiary and quaternary collagen fibril organization, dissociation of tropocollagen, lack of cellular tension, and fragmentation of proteins. Pepsin first disrupts the collagen triple helix structure by cleavage of telopeptide and helical hydrogen crosslinks resulting in drastic weakening [18]. As digestion continues, pepsin will cleave beyond disassembly of the helix structure and can potentially influence binding sites and monomer protein size. If digestion progresses to this extent, hydrogel strength, crosslinking ability, and bioactivity will decrease drastically, potentially causing the exposure of cryptic binding sites [127], [128].

Collagen I is the main component of all mammal tissue and therefore is the main component of lung ECM hydrogels and will dictate overall gel properties. Collagen fibrillogenesis and fiber diameter can alter several different factors: collagen sequence variations, post-transcriptional glycosylation levels [21], and nucleator presence [22]. Collagen also binds other molecules such as integrins, growth factors, other matrix proteins, MMPs and even water [23]–[25] that can enhance the triple helix conformation and can drastically change inherent properties of collagen. Without disruptions in collagen monomer sequences, ECM nucleators are essential to

modulation of collagen structure, and the type of nucleator controls the resulting fibrillar structure. For these reasons, alterations in both fibrillar collagens and nucleators could disrupt fibrillogenesis within ECM hydrogels. Characterization of ECM digestion by pepsin is needed to uncover any changes in resulting changes in hydrogel structure and bioactivity [19], [129].

While collagen I dictates mechanical, structural, and biochemical characteristics of the hydrogel, other less abundant ECM components can also play a crucial role in cell differentiation. The ability of decellularized ECM coatings to influence differentiation as well as promote specific cell morphology without providing a 3D hydrogel structure suggests that there are biochemical cues that are intact and active in these materials. The concern with over-digestion of the ECM is that loss of entire binding motifs and the complex fiber architecture may compromise vital cellular responses. It is currently undefined whether the degree of cellular response changes with ECM digestion and therefore we are interested in characterizing these aspects for further experimentation with epithelial culture. It is hypothesized that longer durations of pepsin digestion will increase ECM fragmentation and decrease collagen assembly. Furthermore, shorter digestion times would create more ideal microenvironments for epithelial culture. This work is more broadly relevant in the field of ECM biomaterials and addresses a significant gap in knowledge and methodology, reducing the effective translation and improvement of these materials.

3.2 Materials and Methods

Decellularization, ECM Solubilization, and Hydrogel Formation

Male and female porcine lungs were obtained from Smithfield-Farmland slaughterhouse or euthanized research pigs to produce dECM powder, as previously published by our laboratory [72], [130]. Quality control of dECM powders from different donors is performed by picogreen dsDNA quantification to ensure each has below 50 ng of dsDNA per mg of dry tissue. 1% (w/v) of decellularized ECM powder and 0.1% (w/v) of pepsin from porcine gastric mucosa (3450 units/mg proteins, Sigma P68875G) was added to 0.01 M HCl. The digestion solution was uniformly agitated for 4, 12, 24, 48, and 72 hours. At each digestion time point, a fraction of the digestion solution was removed and chilled on ice for 2 minutes to avoid gelation upon addition of neutralizing reagents. 10% (w/v) chilled 0.1 M NaOH, and 11.11% chilled 10X PBS were then added to the extracted digest for neutralization. The digests solution is now considered a pre-gel or coating solution and can be stored at 4 ° C and used within 7 days. To produce a hydrogel, 220.5 µl/cm^2 of the pre-gel solution was added to a tissue culture plate and allowed to gel for 30 minutes to 1 hour at 37° C.

Mass Spectrometry

Mass spectrometry was performed according to previously developed protocols with decellularized tissue [3], [89]. Pre-gel solution after 48 hours of digestion was trypsinized for protein identification with MALDI mass spectrometer. Software analysis identified proteins detected with a 99 to 100% probability.

SEM Imaging, Interconnectivity, and Fiber Diameter Analysis

In preparation for SEM imaging hydrogels digested for 4, 12, 24, 48, and 72 hours were fixed in 5% glutaraldehyde and 4% osmium tetroxide, and dehydrated to 100% ethanol. Scaffolds were then critical point dried and plasma sputter coated before visualization with JEOL JSM-5610LV SEM or the Hitachi SU-70 FE SEM SEM. Representative images were taken at 10,000x. ImageJ was used to quantify the amount of branching and fiber diameter with a minimum of 3 images per sample for each digestion time. The total number of interconnections for each image were averaged and divided by the total image area to present the data as network density using interconnections per um^2.

Rheometry

Rheometry was used to assess the mechanical properties of the hydrogels after 4, 12, 24, 48, and 72 hours of digestion. Rheometry was performed according to established protocol with dECM hydrogels [72].

SDS-PAGE Protein Size Distribution Analysis

To determine the resulting molecular weight profile from each length of digestion or laminin and fibronectin protein addition, SDS-PAGE gel size distribution was used. Coating solutions were further solubilized using a 1% SDS, 25 nM Tris, and 4.5 M urea solution and heated to 60 °C for 1 hour. The amount of each protein in each sample was quantified using Peirce BCA protein assay kit and a microplate reader and balanced to the lowest concentration. The protein was loaded into each well of a MiniPROTEAN TGX stain-free gel (BIO-RAD), and 200 V was

applied until the dye front reached the bottom of the gel using a Mini-PROTEAN tetra system (BIO-RAD). Resulting gels were imaged using a BIO-RAD gel imager, and band intensities were quantified using BIORAD ImageLab software. The sum of the band intensities above and below 240 kDa for each experimental replicate was summed and compared at each digestion time.

Western Blotting and Collagen I Helical Structure Analysis

Resulting gels from SDS-PAGE were transferred to polyvinylidene fluoride (PVDF) membranes for western blotting. Fibronectin (Abcam) and collagen IA (Proteintech), and laminin (Abcam) antibodies were used for western blotting according to manufacturer's protocols to determine the amount of each protein within the solution and the degree of degradation. Using BIORAD ImageLab software, intensities of bands at 400 kDa (Trimeric), 270 kDa (Dimeric), and 140 kDa (Monomeric) were determined the percent of each quaternary structure relative to the total collagen I intensity of each digestion time.

Statistical Analysis

All data are presented as mean +/- standard deviation with an $N \geq 3$ unless otherwise stated. Statistical significance was determined by a Two or One-way ANOVA and a Tukey's multiple comparisons tests using GraphPad Prism.

3.3 Results

dECM coating composition

Total protein composition within the dECM powder, pregel/coating solutions, and 3D hydrogels from both porcine and human sources were detected using SDS-PAGE analysis (Figure 3.1A**)**. When comparing porcine to human dECM powder and pregel solution, there are only slight differences in intensity of bands, but there is an overall resemblance in the amount and location of bands. The differences between porcine powder and porcine pregel solutions indicate changes caused by protease digestion. A significant amount of bands remaining after digestion but with a drastic decrease in the amount of high molecular weight bands. Little differences are seen between the porcine pregel and porcine gel lanes, suggesting no change in protein digestion upon gelation. This is also supported by the proteomic analysis of the dECM pregel solution (Figure 3.1B**),** showing that several essential matrix proteins are abundant within the solution, even with digestion.

A

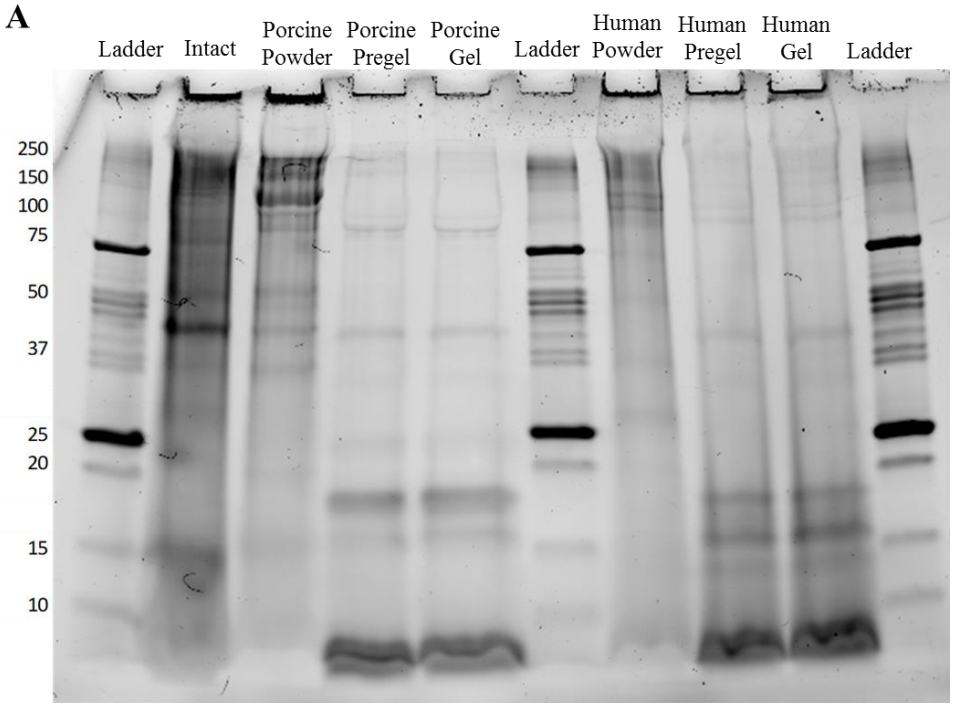

B

Matrix proteins found in dECM pregel solution with a 99-100% probability
Collagen I
Collagen II
Collagen III
Fibrillin
Laminin
Collagen IV
Fibronectin
Collagen VI
Nr-CAM
Nephronectin

Figure 3.1. dECM hydrogel and coating protein characterization. (A) The SDS-PAGE analysis of porcine and human, dECM powder, pregel solution, and gel digested for 48 hours to show the size distribution of remaining proteins. (B) Mass spectrometry results of dECM pregel/coating solution.

SEM Imaging and Calculating Hydrogel Interconnectivity

The hydrogel structure resulting from each digest was investigated using SEM imaging. Images were taken of 4, 12, 24, 48, and 72-hour digests, shown in figure 12A, demonstrates changes in hydrogel network structure. Shorter time digest hydrogels have the most branched, interconnected, structure while longer digestion times leads to a less branched and more porous hydrogel organization. Using Image J analysis, we calculated the number of intersections over the area of the image, to quantify hydrogel interconnectivity. With three technical replicates per sample and three experimental replicates per time point, we were able to demonstrate a significant

reduction in network interconnectivity as the digest progressed, in figure 3.2 B. Rheological properties (Figure 3.2C) of dECM gels with respect to digestion time have decreased storage moduli with increasing digestion and resemble the trend seen with interconnectivity.

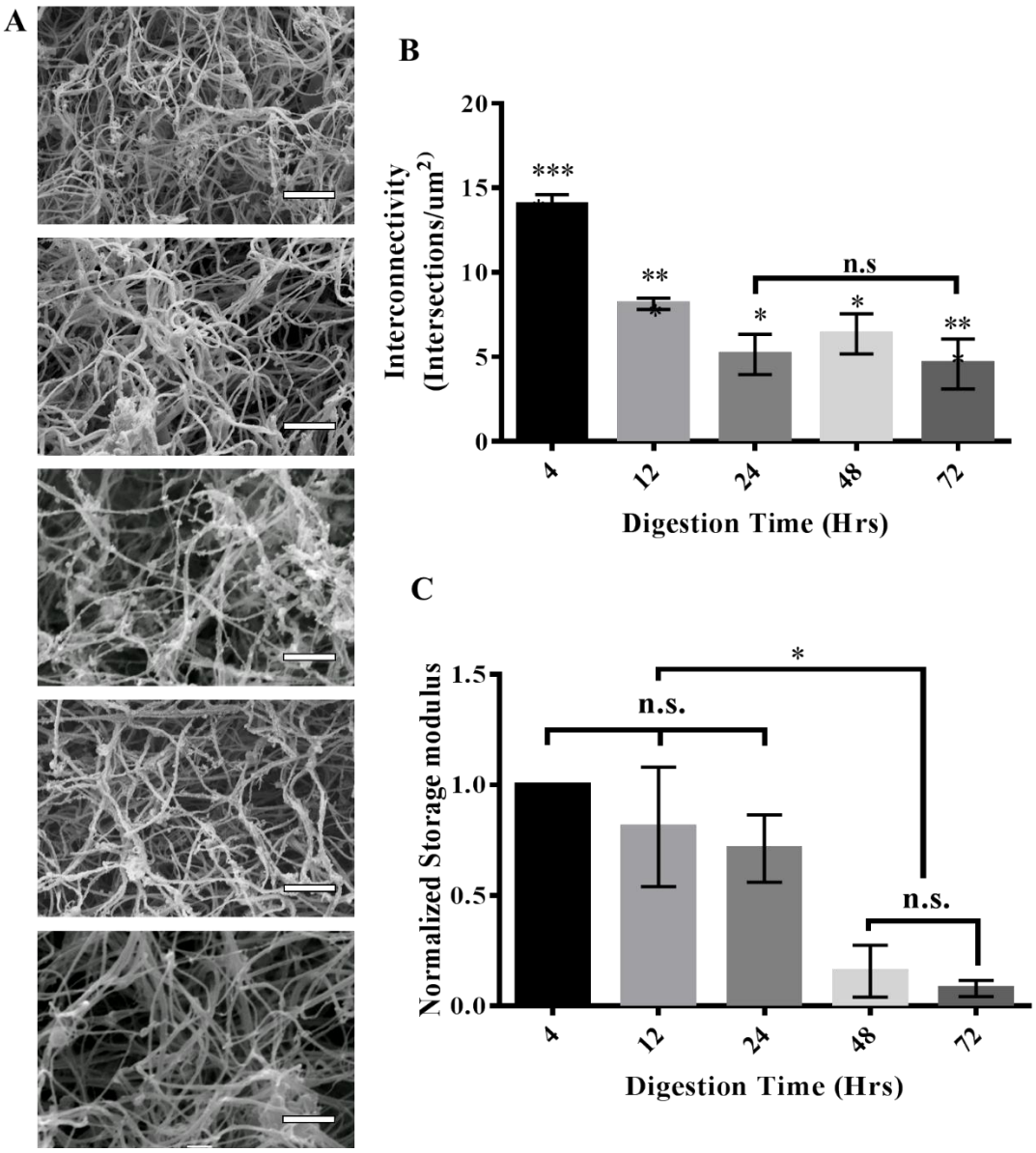

Figure 3.2. **Duration of pepsin digestion alters ECM branching and resulting mechanical properties.** (A) Representative SEM images of hydrogels prepared from 4, 12, 24, 48, and 72-

hour digests, from top to bottom respectively, show enzymatic digestion effects on matrix architecture (scale bar= 1μm). (B) Interconnectivity analysis of hydrogel fibers within SEM images was analyzed using ImageJ and correlate to (C) shear properties determined through gel rheometry of ECM hydrogels with varying digestion times. Data are shown as mean +/- standard deviation. N=3 separate experiments for each condition (n.s. $p > 0.05$, * $p < 0.05$, ** $p < 0.01$, *** $p < 0.001$, and **** $p < 0.0001$).

SDS-PAGE protein size distribution

The SDS-PAGE analysis of the digested ECM protein shown in figure 3.3A to qualitatively demonstrate how higher molecular weight bands are relatively depleted and lower molecular weight band become more pronounced as digestion time increases. Some higher molecular weight bands have become faint or disappeared entirely by 72 hours. Quantitative analysis of the molecular weight distribution seen in the SDS-PAGE gel (Figure 3.3B-C) also shows decreases in molecular weights above 240 kDa and increases in protein sizes below 240 kDa, suggesting larger ECM proteins are being fragmented with longer digestion.

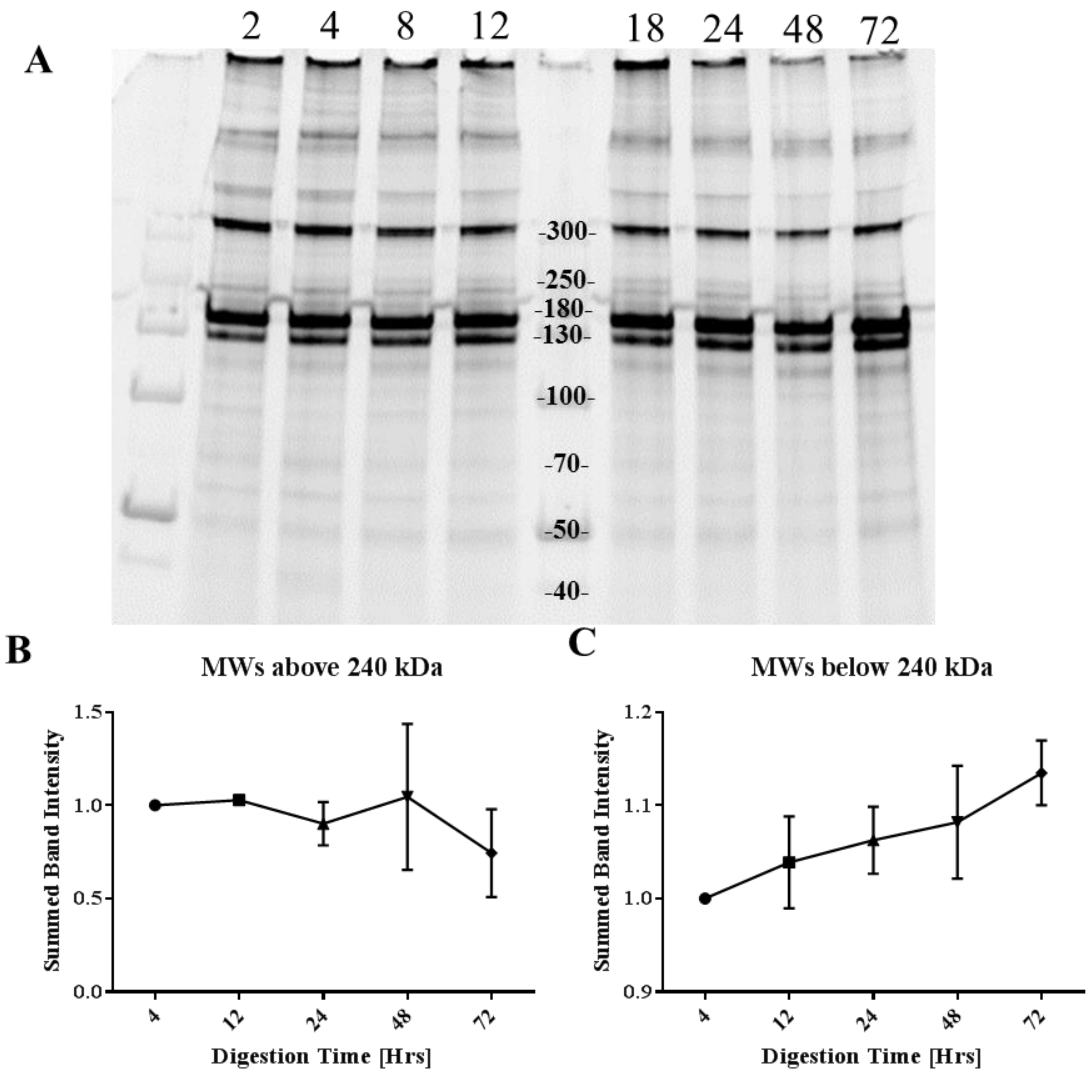

Figure 3.3. Longer pepsin digestion causes ECM fragmentation. (A) The SDS-PAGE analysis of dECM by digestion time (hours). Protein size quantification of band intensities (A) above and (B) below 240 kDa analysis using ImageJ. Data are presented as mean +/- standard deviation. N=2 replicates.

Western Blotting, Quantification, & Analysis

Western blotting of collagen I (Figure 3.4A) confirms that increasing lower molecular weight band intensities seen with longer digestion times are partially due to collagen I trimeric

helical structure disassembly. Band quantification (Figure 3.4B) shows increased monomeric and decreased dimeric and trimeric collagen I after just 12 hours of digestion. Between 48 and 72 hours of digestion, another drastic increase in collagen monomers is seen. Fibronectin western blotting of lower molecular weights also shows increasing fragmentation with longer digestion. Molecular weights for intact fibronectin is not shown (MW=220 kDa) but is assumed to be present at least at shorter digestion times since digestion is not occurring until 48 hours.

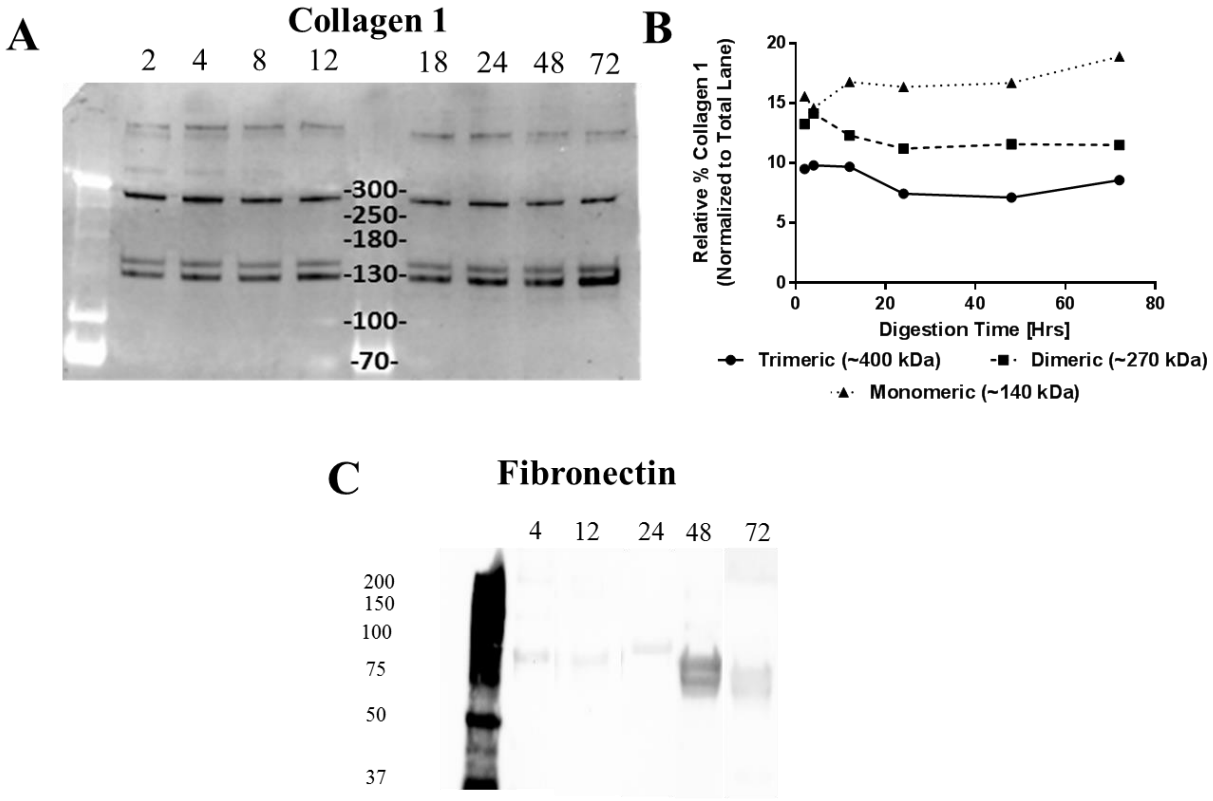

Figure 3.4. Collagen helical disassembly and fibronectin fragmentation with increasing digestion time. (A) Western blotting of collagen I with increasing digestion. Each lane is a different duration of digestion in hours. (B) ImageJ quantification of the 400, 270, and 140 kDa bands correspond to amount of collagen I trimeric, dimeric, and monomeric helical structures

respectively. Graphed band intensities are from one western quantification. (C) Fibronectin western blotting of fragmented molecular weights (below 220 kDa).

4 Hour dECM Coating Composition with Laminin and Fibronectin Supplementation

Digestion duration of 4 hours was chosen for further experimentation based on increased small airway proliferation on ECM hydrogels digested for 4 hours [131] and increased branching, more resembling a dense BM for epithelial culture. SDS-PAGE (Figure 3.5A) analysis shows increasing band intensities at laminin and fibronectin molecular weights with the addition of laminin and fibronectin as expected. This confirms that 0.01 mg/mL addition of each laminin and fibronectin increases gel concentration sufficiently. Western blotting for laminin (Figure 3.5B) and fibronectin (Figure 3.5C) shows that the dECM coating alone has very minute amounts of laminin content and greater amounts of fibronectin content. Addition of laminin and fibronectin to dECM drastically increases both laminin and fibronectin band intensities.

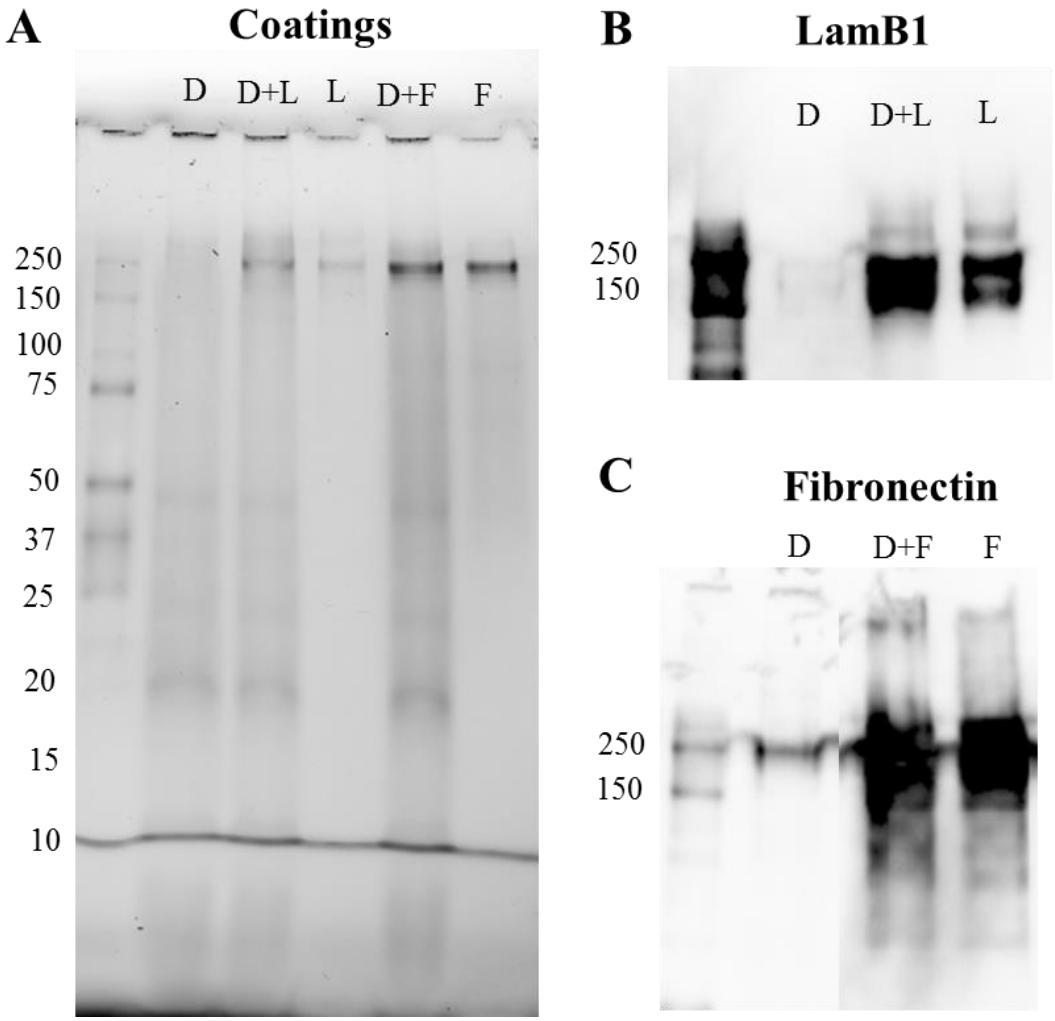

Figure 3.5. Laminin and fibronectin addition to dECM and detection of proteins. (A) SDS-PAGE of the dECM coating alone and with 0.01 mg/mL of either fibronectin or laminin supplementation. (B) LamB1 and (C) Fibronectin immunoblotting to determine the concentration within dECM and how much is replenished.

3.4 Discussion

ECM hydrogels and coatings offer a unique insight into tissue-specific cell-matrix interactions by retaining many vital ECM proteins and creating a porous substrate for cell infiltration and 3D biophysical cues. ECM hydrogels have been developed for more than 15 different tissue applications; however, most characterization has been limited to high-level structural analysis with only one digestion time. Traditionally, pepsin digestion is performed for 48 to 72 hours, chosen for maximum solubility of ECM [71], [130]. We have shown in these data that the duration of digestion affects many of the inherent properties of the ECM hydrogel and may need to be adjusted for each application.

Pepsin is a digestive protease naturally found within the stomach. Pepsin prefers to cleave proteins at sites after phenylalanine and leucine but rarely cleaves after histidine and lysine [132]; otherwise digesting proteins relatively nonspecifically but with consistent degrees of fragmentation [133]. Protease digestion is also affected by pH changes, with its optimal pH range for pepsin of 2.5. We have seen that with increases in digestion time, pH does increase to approximately 3.5 (data not shown), which still allows for pepsin activity but can potentially cause digestion to slow. Future experimentation would need to be conducted to determine if more digestion would occur if the pH was maintained at 2.5 throughout the digestion. With both collagen disassembly and fibronectin fragmentation after just 12 to 24 hours, optimal digestion time concerning protein disruption would be less than 24 hours.

Both porcine and human dECM powder and gel composition were compared by SDS-PAGE analysis. We did not detect drastic differences between the two species, supporting past evidence that ECM protein structure and reactivity is considered mostly homogenous across mammalian species, with only some differences in mechanics and composition [134]. Comparison of pregel to the powder shows that many matrix proteins are preserved through the decellularization and protease digestion process, including high mass proteins. These results are further supported by the proteomic analysis of the dECM solution digested for 48 hours, identifying collagen types

I and II, laminin, fibronectin, GAGs, and other less frequent proteins. We have identified fewer matrix proteins than those identified by other researchers with MS analysis of decellularized lung components and we speculate that this is because some of the fragments are not comparable to the whole protein library available with mass spectrometry. This also indicates that even with 48 hours of pepsin digestion, we can preserve major components of the ECM profile for cellular interactions.

While achieving full solubility of the ECM is ideal, the level of protein fragmentation we have shown by SDS-PAGE and western blotting may cause adverse changes in mechanical and biochemical properties. Increases in protein sizes below 240 kDa were seen with digestion after just 24 hours, leading us to question whether this degree of disassembly or fragmentation may compromise the ability of ECM proteins to participate in gel crosslinking, seen by a decrease in gel interconnectivity with digestion.

Identification of specific proteins within the fragmented matrix can be difficult, however, through western blotting and analysis of molecular weights associated with the collagen helical structures, we have more definitively characterized ECM structure with increasing pepsin digestion. At 12 hours, a drastic disassembly of collagen I into its dimeric and monomeric form occurs. The absence of fibrillar collagen within the gel would explain decreased gel stiffness due to less mechanically functional collagen. Since pepsin-digested collagen requires nucleators for fibral reformation, lack of fibrillogenesis can be due to nucleator or collagen 1 damage. Fibronectin fragmentation increased after 24 hours of digestion with prominent bands at 70 kDa, which would support the latter theory of fibrillogenesis inhibition [135], [136]. Collagen and fibronectin both have binding sites that are only present in their natural triple helix structure or opened by cellular interaction. Fibronectin fragments can destabilize collagen confirmation, allowing fibronectin

binding without confirmation and possibly rendering binding sites inactive for functional ECM proteins [137]. Fragmentation of fibronectin also exposes binding sites for other matrix proteins such as GAGs and can change the binding affinity of fibronectin to specific types of GAGs [138]–[140]. Disassembly or fragmentation of either collagen or fibronectin may enhance or inhibit ECM assembly and fibrillogenesis, potentially disrupting the overall gel structure and bioactivity.

Collagen fiber assembly within pepsin digested hydrogels can also be altered by variations in ECM nucleators other than fibronectin [22], [141], [142]. Previous studies have found that increasing concentrations of dermatan sulfate, heparin, and collagen VI during collagen fibrillogenesis decrease fiber density, delay fibril formation, and increase fiber thickness, while increases in chondroitin sulfate delay fibril formation promoting denser, thinner fibrils [141], [143]–[146]. Our results showing lower fiber interconnectivity with higher digestion times may suggest that digestion of PGs that increase fibrillogenesis, such as chondroitin sulfate, may be occurring after 4 hours, impacting fiber branching. Once branching PGs have been digested, PGs such as chondroitin sulfate could become most prominent, causing increased fiber diameter. Increased pepsin digestion could not only be breaking helical structures and render structural proteins inactive, but it can also be disabling fibrillogenesis nucleators. Differential pepsin digestion of ECM nucleators beyond their functional capacity could explain hydrogel fiber formation and mechanics.

It is widely accepted that ECM elasticity and dynamic mechanical properties can directly affect cell differentiation through cell mechanotransduction [147], [148]. For this reason, when considering hydrogel response, 3D matrix mechanics must be evaluated. However, when assessing ECM coatings that would adopt the bulk mechanical properties of the coated substrate, the biochemical composition may be the primary modulator of cell response. By assessing the

mechanical behavior of the ECM hydrogel by rheometry, we have determined how the gel mechanics are altered by digestion. Properties derived from rheometry provide insight into crosslinking within the ECM structure that is resisting the shearing stresses, which account for the similarities between the trends of gel interconnectivity and storage modulus. The highest storage modulus with 4 hours of ECM digestion showing properties closer to native tissue [149].

From these data, we have observed that mechanical properties and protein structure can change drastically with digestion time. Showing that these properties can be altered by changing digestion time allows ECM hydrogels and coatings to be tailored for each application and cell origin. The structure and storage modulus of hydrogels and coatings produced from digestions shorter than 12 hours more closely resembled that of the BM, compared to longer digestion durations. Also, data evaluating SAEC attachment and proliferation over two days [131] determined that SAEC prefer shorter digestion times. With all of these data considered, for the purpose for further experimentation with ECM pre-gels in this research, we determined that the 4-hour hydrogel would provide the preferred epithelial response and was used for the remainder of the studies.

Further experimentation in this research will include supplementation with laminin and fibronectin. Therefore we also aimed to determine if the addition of 0.01 mg/mL of commercially available fibronectin and laminin would alter the ECM protein profile. Western blotting showed the dECM retained a relatively large amount of fibronectin, yet little laminin was detected. This may indicate that laminin supplementation within the coating solution is likely beneficial. Addition of fibronectin may also be necessary, but since residual levels were detected, there may be enough fibronectin within dECM to elicit cellular attachment and differentiation. Caution must be taken with the addition of fibronectin, as excessive amounts could mimic disease states [60]. Further

experimentation with cell behavior will aid in this determination. After supplementation, distinct bands at the appropriate molecular weights for intact and some fragmented proteins were detected for both laminin and fibronectin. We expect that this concentration of supplementation is appropriate according to similar *in vitro* comparisons [9], [12], [92].

The current digestion duration standard of 48 and 72 hours for ECM solubilization, may be over digesting the ECM. Desired gel properties vary for the chosen cell type and tissue application; however, for most applications' digestion should be reduced to a range between 4 and 24 hours. From a mechanical and structural standpoint, hydrogels produced from pepsin digestion between 4 and 24 hours more ECM-ECM interactions and similar mechanical characteristics as native lung tissue. Also, to minimize protein fragmentation, particularly of collagen and fibronectin, decreased digestion would be beneficial. For the culture of lung epithelial cells specifically, the 4 hour digestion time is ideal based on increased SAEC proliferation and denser fiber architecture.

CHAPTER 4: IMPROVING ALVEOLAR JUNCTIONS ON dECM

4.1 Rationale

Decellularized lung tissue engineering offers a promising regeneration strategy for patients with a variety of incurable pulmonary diseases. This technology can provide the native structure and biochemical cues of the lung to guide healthy maturation of functional tissue. Decellularized lungs are the gold standard scaffold for whole lung bioengineering; however, current approaches do not produce a long-term, functional lung replacement, indicated by severe edema after implantation. Insufficient recellularization and immature barriers keep this technology from the clinic. Most of the research to date has focused on assessments of stem cell differentiation and attachment [92], [94], [150], [151] or mimicking lung development during regeneration [12], [91]. More recently, researchers in this field have examined recellularization on a smaller scale by evaluating endothelial barriers [152]; however, there is little research on epithelial barrier formation with recellularized lungs. This research takes a unique approach to re-epithelialization of whole organ scaffolds by examining alveolar junction formation on a cellular level to then inform future recellularization strategies. Therefore, we are attempting to systematically determine which components are essential to the alveolar barrier function and develop a scaffold coating to replenish these essential matrix proteins.

Homeostatic alveolar epithelial barrier function is maintained by two main structures: tight junctions (TJ) and adherens junctions (AJ). Both junctions provide tension resistance and selective permeability during resting mechanical load. Formation of substantial barriers relies on a highly regulated sequential recruitment of several main junction proteins including cadherins, claudins, zonula occludins (ZO), and junctional adhesion molecules (JAM)s [107], [108], [153]. Protein

kinase A (PKA) and exchange protein directly activated by cAMP (Epac) have both been identified as regulators of barrier function by activation of G-protein-coupled receptor and release of cyclic AMP (cAMP) [39], [118, p. 1], [120], [154], [155]. While PKA has traditionally been studied as the primary mediator of barrier function, inhibition of PKA does not result in substantial barrier disruption [115], [156], [157]. This has led to a recent transition into investigating the role of Epac within endothelial [115], [158]–[162] and less often, epithelial barriers [163]–[165]. After activation, Epac is rapidly translocated to the plasma membrane from the cytoplasm and nuclear membrane to activate Rap1 to regulate afadin (AF-6) stabilization of AJs, TJs, and integrins [166]. Within epithelial cells, Epac signaling has also been implicated in the inhibition of cell migration and EMT, [167] and promoting adhesion to laminin and fibronectin [116], [168], [169]. This suggests that epithelial junction mediation may be a function of Epac in response to specific ECM proteins; however, the direct causes and mechanisms of this within the alveolar epithelium are not fully understood.

Decellularization techniques utilize several harsh detergents to ensure complete removal of cellular debris, but these detergents can drastically alter the ratio of ECM components that are left behind. Matrix proteins such as collagen, elastin, laminin, fibronectin, and glycosaminoglycans (GAGs) are preserved through the decellularization process, but there are reports of up to a 50% loss of most of these components compared to native ECM [3], [55]. Variations in ECM composition and stiffness can have a profound effect on cell phenotype, as well as cell attachment and barrier function [9], [56], [57]. High collagen and fibronectin content promote cell attachment at the expense of suboptimal barriers, indicative of metastasis and fibrosis [6], [41], [43], [59]. Laminin is integral to both strong barrier formation and epithelial differentiation [35], [38], [40], [60]–[63]. We hypothesize that the discrepancy between native

ECM and decellularized airway surface ECM can alter the epithelial cell-cell junction assembly during recellularization through activation of Epac. Understanding how and which ECM components modulate alveolar barriers, specifically TJs and AJs, is integral to producing a whole lung replacement that is functional on the cellular level. This research is the first step to creating a tailorable ECM environment within decellularized lungs by methodically replenishing BM proteins that promote alveolar barrier formation.

4.2 Materials and Methods

Decellularization and Coating Preparation

Male and female porcine lungs were obtained from Smithfield-Farmland slaughterhouse or euthanized research pigs to produce dECM coating solution as previously published by our laboratory [72], [130]. Quality control of dECM powders from different donors is performed by picogreen dsDNA quantification to ensure each has below 50 ng of dsDNA per mg of dry tissue. The dECM hydrogel solution is produced by pepsin digestion of 8 mg/mL dECM powder for 4 hours. The solution was diluted to 0.1 mg/mL for use as a coating. Type I collagen from bovine skin (Sigma) diluted to 0.1 mg/mL in PBS was used as a control coating solution. The collagen and dECM solutions were also supplemented with 0.01 mg/mL laminin (Sigma, L2020) and fibronectin (Sigma, F0895) from human plasma. Collagen and dECM coating concentrations were determined by literature review, and laminin and fibronectin concentrations were determined by literature review and qPCR dosing experiments (data not shown). TCP was coated overnight at 4°C to avoid gelation, then rinsed 3 times with PBS or saline (for TEER experiments) prior to cell culture.

Cell culture and reagents

All cells were cultured at 37 °C with 5% CO_2. Mouse alveolar type II cells (MLE12, ATCC) were cultured with HITES medium containing 2% fetal bovine serum according to the manufacturer's protocols. MLE12s offer rapid doubling times and express lung surfactant proteins B and C. MLE12s were also chosen because primary differentiated human alveolar epithelial cells

are not commercially available, and slow proliferation of isolated cells would not be feasible. Primary human airway basal epithelial stem cells (BESCs, identified by integrin α6, KRT5, and KRT14) from healthy donors, in EpiX medium (Propagenix) were also used to demonstrate translatability to recellularization with stem cell populations [170]. Passages between 2 and 6 were used for experimentation. Longer culture periods were used for BESC experimentation to allow for differentiation and barrier formation to occur. BESCs and MLE12s on hydrogel coatings were treated with either ESI-09 (Sigma), a highly specific Epac inhibitor that does not affect PKA expression, or 8-pCPT-2-O-Me-cAMG-AM (007-AM, TOCRIS), an Epac agonist that does not discriminate between Epac1 or Epac2. 5 nM of each treatment or a DMSO vehicle control was added in media. Concentrations were determined by a dose response assay (data not shown), testing a range determined by a literature review [155], [171] for 8 to 24 hours. Antibodies for immunofluorescent staining included, ZO-1 (Invitrogen), Vinculin (Sigma), AF-6 (B-5, Santa Cruz Biotechnology), JAM-A (J10.4, Santa Cruz Biotechnology), E-cadherin (A42, Cell Signaling Technology), Epac (A-5, Santa Cruz Biotechnology), Rap1 (4C8/1, Santa Cruz Biotechnology), Alexa Fluor 488 Phalloidin (Invitrogen), and Alexa Flour 647 secondary antibody (Invitrogen). Stained cells were mounted using ProLong Gold Antifade with DAPI and dried overnight at 4° C. Images were acquired at 63x magnification on a Zeiss AxioObserver Z1 fluorescence microscope.

Cell adhesion and spreading assay

Cell Counting Kit-8 (CCK8, Dojindo Molecular Technologies) colorimetric assay was used to determine cell viability and proliferation on each coating. 4 and 24 hours after inoculating 3.2 x10^3 MLE12 cells per cm^2, media and unattached cells were aspirated from each well. The CCK8 and media solution was added to each well according to the manufacturer's protocol. A

microplate reader detected the absorbance of each well. Data are shown as normalized absorbance to collagen.

Transepithelial electrical resistance (TEER)

96W10idf PET plates (Applied Biophysics) were coated overnight at 4ºC with each coating type then rinsed with media. BESCs and MLE12s seeded at a density of 200,000 cells/cm^2 to achieve confluence shortly after the start of culture. Cell attachment and cell-cell junction resistances are quantified using electric cell-substrate impedance sensing (ECIS, Applied Biophysics). Wells were coated, and resistances were measured according to manufacturer instructions. Resistance is reported at low frequencies (4000 Hz) and longer time points to highlight cell-cell junction formation and shorter time points to show cell attachment.

Fluorescently-labeled dextran membrane permeability assay

Alveolar epithelial monolayers formed on 0.4 µm Transwells (Corning) coated with each ECM combination as previously stated prior to seeding of 200,000 cells/cm^2. After 1 and 3 days, 2 mg/mL of 4 kDa FITC-dextran in PBS (Sigma) was added to the apical chamber of the Transwell for 24 hours. 100 uL was taken from the bottom chamber of the well to measure fluorescent intensity using a microplate reader with excitation at 490 nm and emission at 520 nm. The intensity of media without FITC-Dextran was subtracted from each value to determine relative amounts of dextran that has passed through the barrier.

Gene expression quantification

mRNA was extracted and purified from MLE12s and BESCs seeded onto each coating for 5 days then treated with a DMSO vehicle control or Epac treatment for 4 hours, using an RNeasy Mini kit (Qiagen) and converted to cDNA using iScript cDNA synthesis kit (Biorad). qPCR was performed with primers designed for the desired target genes shown in Table 1. After the previous examination of multiple housekeepers, 18s will be used to analyze further results.

Target Protein		Mouse Forward Primer Sequence	Human Forward Primer Sequence
E-cadherin	For	AACCCAAGCACGTATCAGGG	--
	Rev	ACTGCTGGTCAGGATCGTTG	--
Rap1A	For	GTCAACCCAAAATTGGCACCA	ATTGTGTCCCCCACCCTTCA
	Rev	GTCAGAGCAGACTTCCCCAC	CCAGGGAACTTGTGCAAACC
AF-6	For	CGCCAAGAGACTCGTCTGG	CAGCCAATCCGAACAGACCT
	Rev	CTGCCCACGCTTCAATAGC	CCATGGGAAACACGCAGAAG
Claudin-18	For	GTGCGATGACGTGATCTG TGA	GGATCATGTCCACCACCACAT
	Rev	GTTTATTGGGACTGGGGGCA	TGGTCTGAACAGTCTGCACC
JAMA	For	CTCTGCTCCTCCTGTTCGAC	GACCAAGGAGACACCACCAG
	Rev	ATGCTCCCCTGGAAGACGAT	AAGGTCACC CGTCCTCATA
Epac1	For	GCA ATATTCCCCATGAACG	TCCGGCAAGATGAG AAAGC
	Rev	GGATGGAGCAGACTGCCTTT	TCCAGATCCAAGGGGAGAGG
18s	For	TCCGGCAAGATCGAGAAAGC	GCAATTATTCCCCATGAACG
	Rev	GGATGGAGCAGACTGCCTTT	GGGACTTAATCAACGCAAGC

Table 4.1. Primer sequences used in the qPCR analysis.

Immunofluorescence and ZO-1 Quantification

MLE12 cells were seeded onto sterilized glass coverslips or Transwell inserts coated with each of the ECM combinations and was cultured until a confluent monolayer was achieved. Cells were treated with either ESI-09, 007-AM, or the DMSO vehicle control for 4 hours. To permeabilize and fix, 0.5% Triton X-100 in 4% paraformaldehyde was applied for 2 min, then replaced with 4% paraformaldehyde for 20 min. After several rinses with PBS, the cells were blocked with 0.1% BSA before labeling with primary antibodies for 30 minutes at 37°C. 0.1% BSA was applied again before labeling with each with their respective secondary antibodies for 30 minutes at 37°C. Images were acquired on a Zeiss LSM 710 confocal microscope using ZEN2011 software.

Quantification of the ZO-1 staining was done using the AngioTool software developed by the NIH Center for Cancer Research. A minimum of 3 images per sample and 3 samples per group were used to create a map of the junction structure and then analyze spatial parameters. The number of cells per image was counted using ImageJ software. Number of junction endpoints or breaks per cell and mean lacunarity were used to characterize junction integrity for each sample. Lacunarity quantifies the degree of spatial order within the junction structure by comparing the variation in both the background and foreground pixel densities [172], [173].

Statistical Analysis

All data are presented as mean +/- standard deviation with an $N \geq 3$ unless otherwise stated. Statistical significance was determined by a Two or One-way ANOVA and a Tukey's multiple comparisons tests using GraphPad Prism.

4.2 Results

ECM coating modulation of attachment and barrier function

Alveolar epithelial cell barrier formation on each dECM combination compared to dECM alone was examined by TEER and transwell permeability of MLE12 cells cultured onto matrix-coated plates (Figure 4.2A-B). The first 12 hours indicates resistance predominately caused by attachment and spreading of the cells on each matrix, showing initially increased resistance by cells cultured on laminin alone, dECM with laminin, and dECM with fibronectin coatings. Cell viability at 4 and 24 hours using CCK8 also shows a significant increase of MLE12 attachment to fibronectin-enhanced matrices compared to all other substrates (Figure 4.1) This trend persisted through 24 hours when the highest resistance monolayer was produced by cells cultured on the combination of dECM and laminin. dECM with laminin has a significantly higher barrier function compared to collagen and fibronectin for the entire 3-day culture.

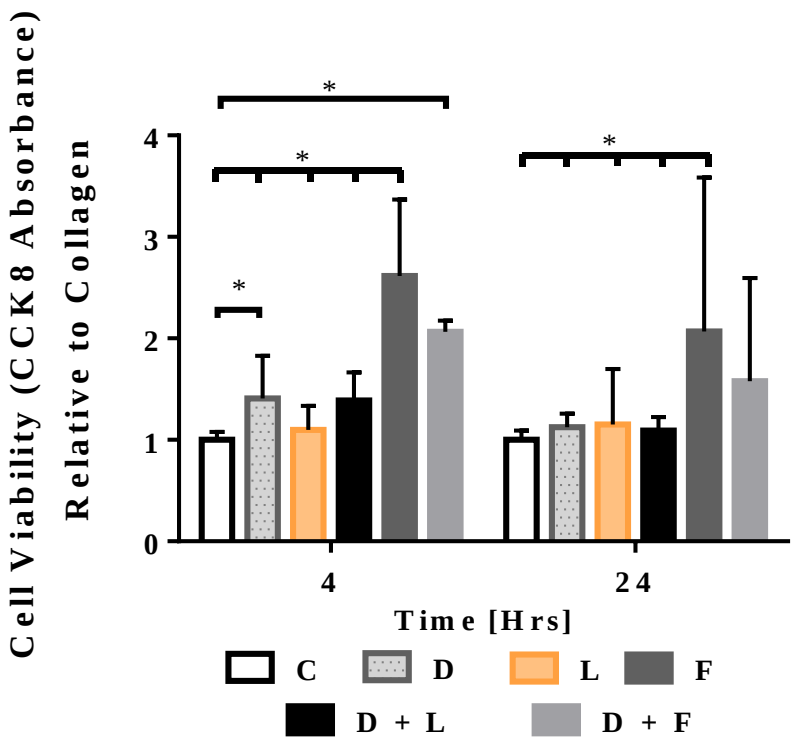

Figure 4.1. Attachment and proliferation of MLE12 cells with respect to ECM coating. Relative cell viability of MLE12 cells cultured on collagen I (C), dECM (D), laminin (L), or fibronectin (F) matrix combinations determined by a cck8 assay at 4 and 24 hours. Data are presented as mean +/- standard deviation. N=3 per group. * indicates $p < 0.05$.

Small molecule permeability with 4 kDa dextran by MLE12 monolayers formed onto matrix-coated transwell supports was also examined. At two days of culture, both dECM with laminin and laminin alone have less permeability compared to collagen, but not significantly

different from dECM (Figure 4.2C). It is only after four days that cells cultured on laminin alone are less permeable compared to cells cultured on both collagen and dECM (Figure 4.2D).

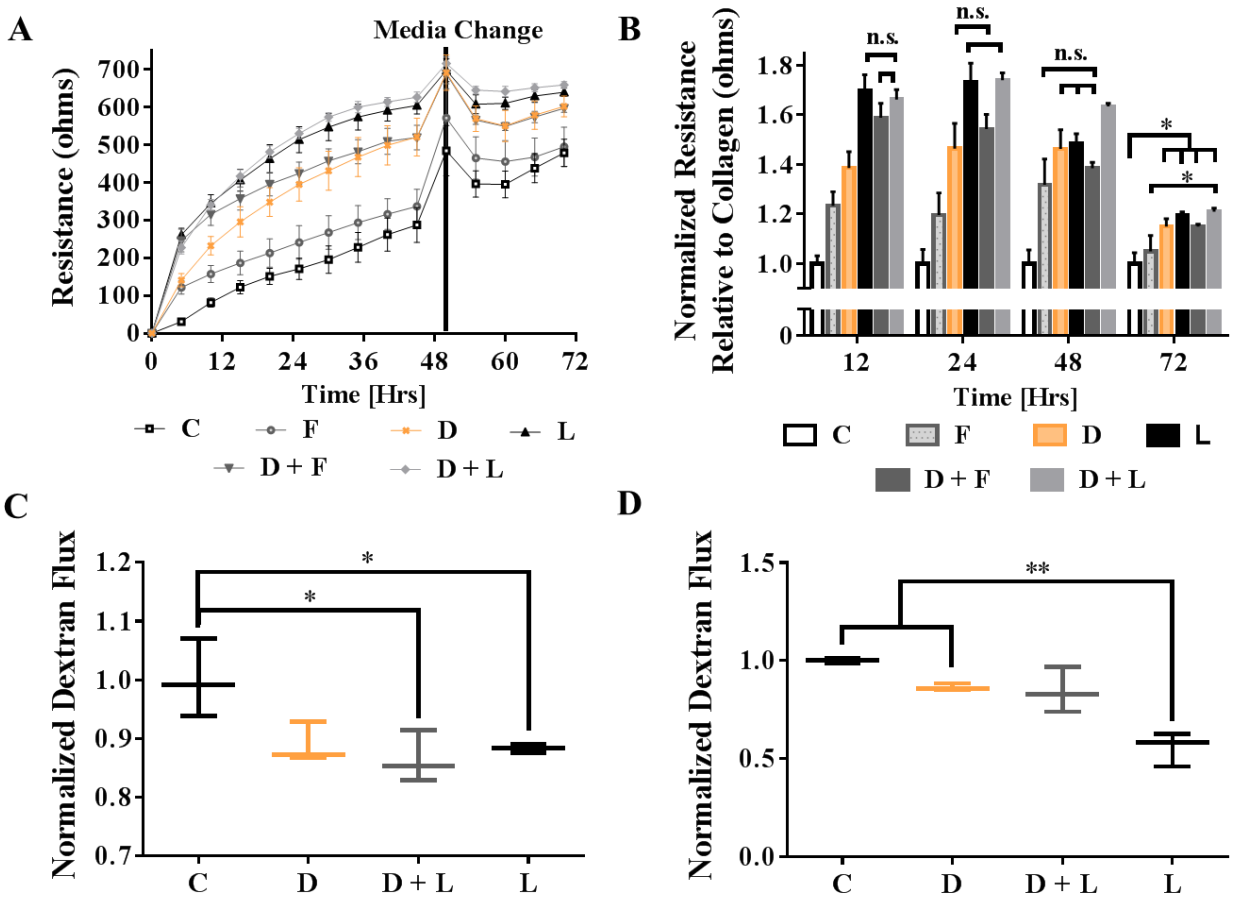

Figure 4.2. The effect of dECM composition on alveolar epithelial barrier formation. TEER of MLE12 cells cultured on collagen I (C), dECM (D), laminin (L), or fibronectin (F) ECM coating combinations over 72 hours is shown by (A) a representative real-time graph of one sample with 3 experimental replicates and (B) binned at 12, 24, 48 and 72 hours with 3 experimental replicates to show statistical differences. MLE12 monolayer permeability to small molecules with respect to ECM coating after (C) 2 and (D) 4 days of cultures was determined by a 4 kDa FITC-Dextran Transwell permeability assay. Normalized dextran flux is shown as absorbance values from the bottom chamber of the Transwell, correlating to dextran transported across the membrane. Data

are normalized to the collagen control and presented as mean +/- standard deviation. $N \geq 3$ for each coating condition. n.s, *, and ** indicates $p > 0.05$, $p < 0.05$, and $p < 0.001$, respectively.

MLE12 junction expression on ECM coatings

Increased barrier function with laminin led us to investigate the underlying mechanisms further by gene expression and immunofluorescent staining within both AJ and TJ complexes. Immunofluorescence staining of vinculin, E-cadherin, and F-Actin colocalization was done (Figure 4.3) to understand the maturity of tight junction structures on dECM and dECM with laminin coatings compared to collagen. This staining suggests that cells cultured on dECM, compared to collagen, had "healthier" barriers with vinculin localized to the junctions. dECM junctions had more abundant and linear staining of all three proteins at the junction, with less vinculin and E-cadherin within the cytoplasm. Since vinculin strengthens the links between E-cadherin and the cytoskeleton, this could give insight into changes of TEER between collagen and dECM. The disconnect seen between the mRNA and protein levels of E-cadherin (Figure 4.6), with E-cadherin expression only being upregulated in the presence of laminin, suggests that other components within dECM may be causing inhibition of E-cadherin endocytosis or translocation to the junction instead of upregulation. Addition of laminin to dECM shows dense staining of both vinculin and E-cadherin throughout each cell, with only a few cells with enhanced localization at the junction. With upregulation of E-cadherin with laminin, there may be increased transcription of E-cadherin that has not fully assembled at the junction.

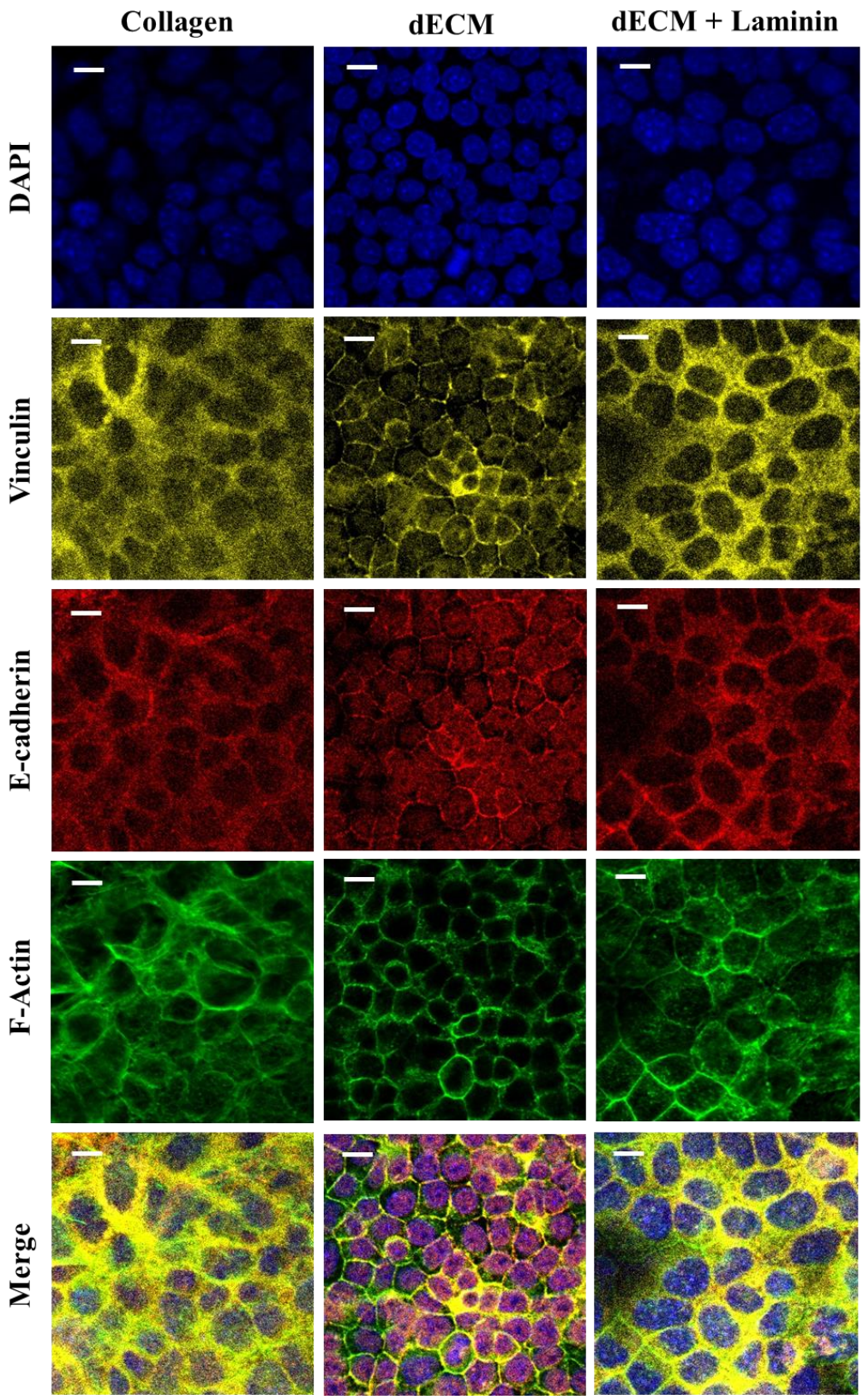

Figure 4.3. AJ protein localization with variations in ECM coatings. Representative immunofluorescent images of MLE12s cultured onto collagen, dECM or dECM with laminin with DAPI (blue), Vinculin (yellow), E-cadherin (red), and F-Actin (green) staining. Scale bar = 10 μm.

Subtle increases in JAM-A expression overall and at the junction between cells cultured on Collagen and dECM (Figure 4.4) match gene upregulation of JAM-A. All groups except collagen have distinct outlines of the cells with JAM-A, indicating that ECM proteins other than collagen and laminin are causing JAM-A localization at the cell interfaces.

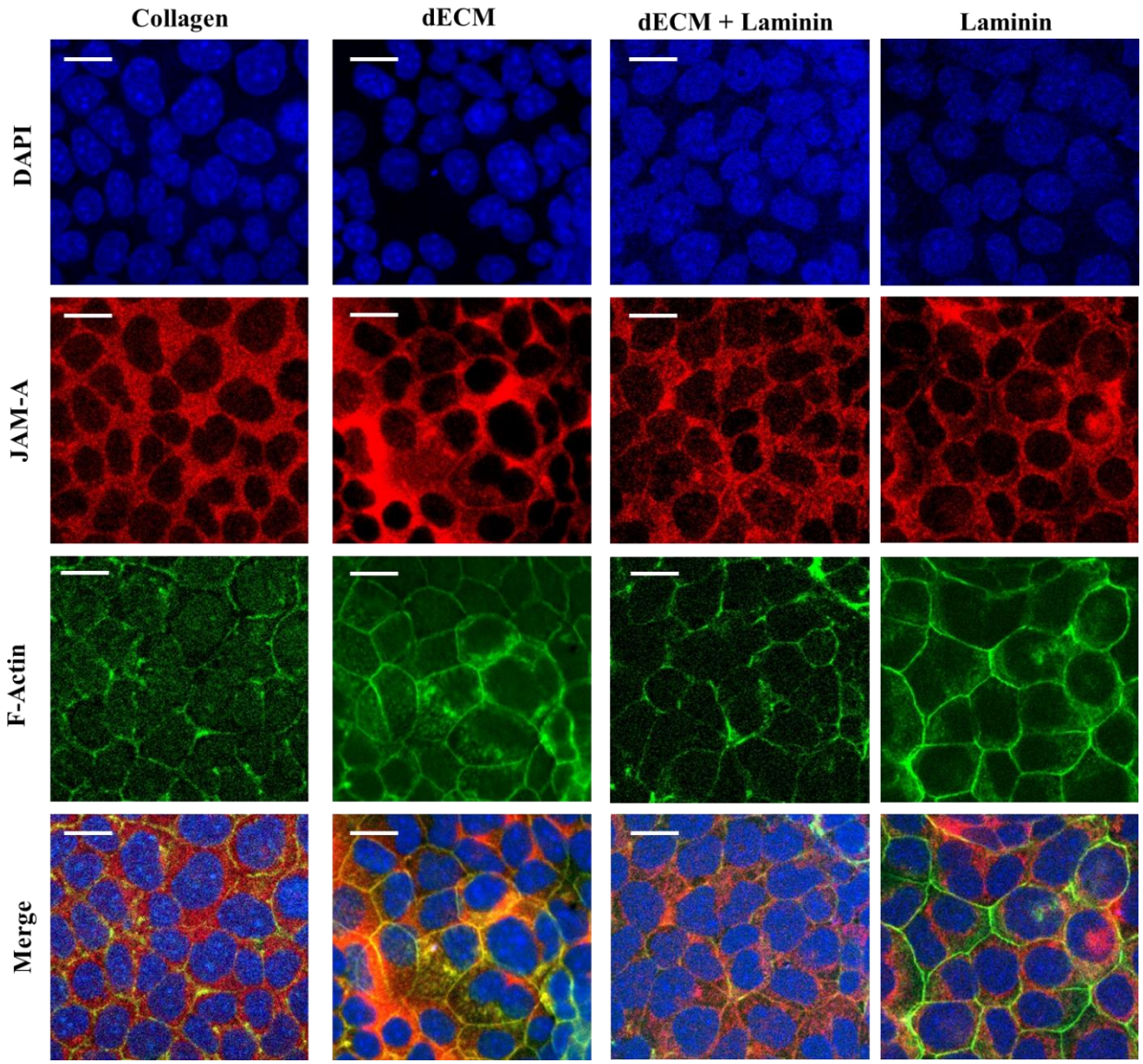

Figure 4.4. TJ protein localization with variations in ECM coatings. Representative immunofluorescent images of MLE12s cultured onto collagen, dECM, dECM with laminin, or laminin alone with DAPI (blue), JAM-A (red), and F-Actin (green) staining. Scale bar = 10 µm.

Immunostaining of AF-6 (Figure 4.5) shows distinct localization that the junction of all cells regardless of ECM. dECM has some variability in staining across the monolayer, possibly

due to processing, but localization is considered to be similar to the other groups based on overall sample appearance.

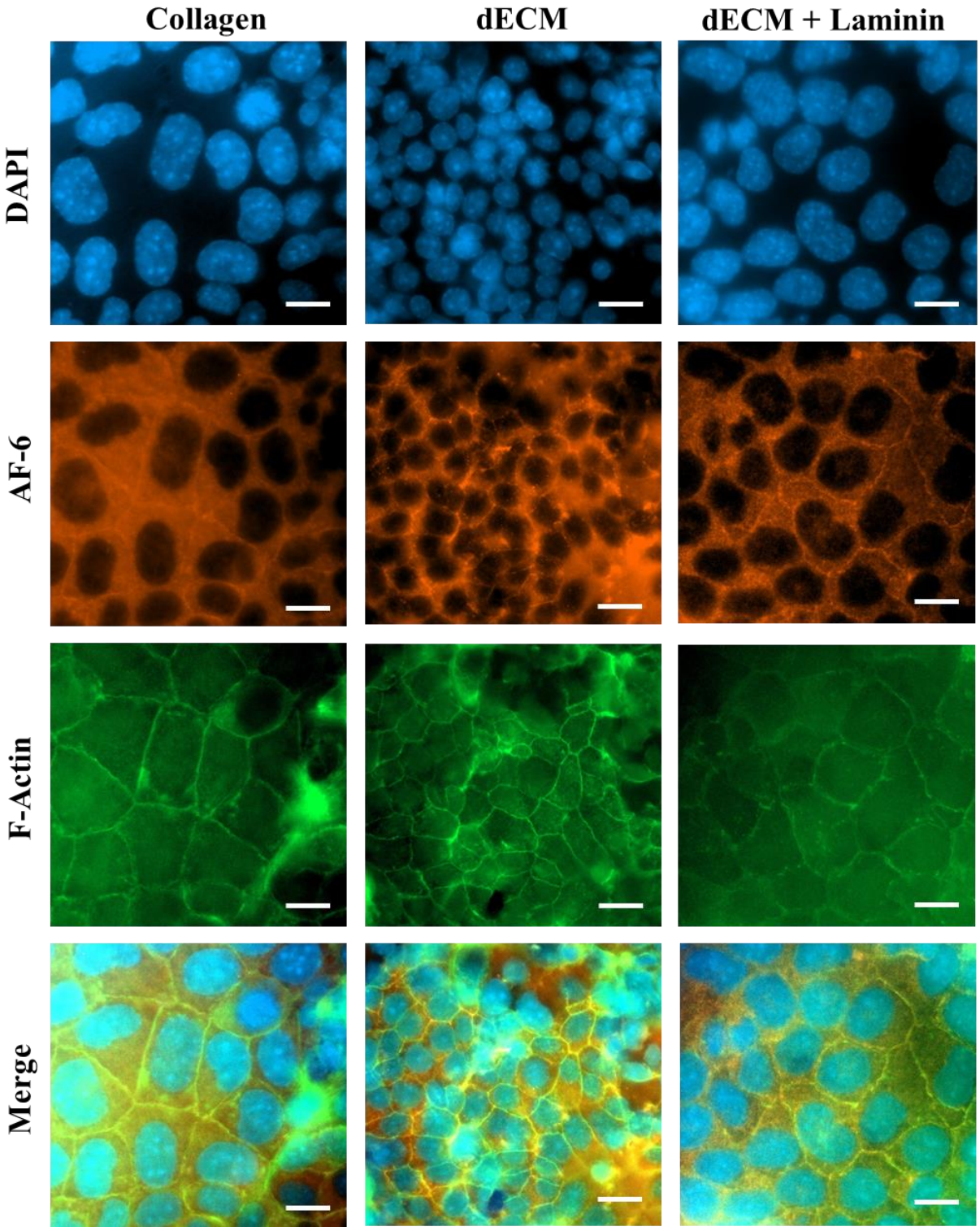

Figure 4.5. AF-6 localization with variations in ECM coatings. Representative immunofluorescent images of MLE12s cultured onto collagen, dECM, dECM with laminin, or laminin alone with DAPI (blue), AF-6 (red), and F-Actin (green) staining. Scale bar = 10 μm.

MLE12s were seeded on ECM coatings for 5 days to evaluate mRNA expression with qPCR (Figure 22A-F). The laminin concentration of 0.1 mg/mL was chosen based on decreased junction gene expression with higher coating concentrations (data not shown). We concluded that 0.1 mg/mL laminin is the most effective concentration for further experimentation. Gene expression of Claudin 18, Epac, and AF-6 all increased with cells cultured onto laminin-supplemented matrices. E-cadherin and JAM-A gene expression were highest with the combination of laminin and dECM. The Rap1 expression only had significant differences between cells cultured on dECM with laminin and dECM with fibronectin. More significant differences between other coating groups may be seen in Rap1 localization or activation. Expression of all genes was either decreased or not significantly different by cells cultured on coatings containing laminin compared to all other coating groups. Additionally, there is an increasing trend in expression of AF-6, JAM-A, and Rap1 with cells cultured on dECM compared to on collagen alone, suggesting that collagen alone is not enough to stimulate this pathway and the remnants of laminin or other proteins trigger Epac/Rap1 activation.

Throughout all immunofluorescent staining of the epithelial junctions, the most considerable differences by coating type were seen in ZO-1 staining. ZO-1 protein expression (Figure 4.6G) shows a qualitative increase in the amount of ZO-1 stabilizing the junctions of MLE12s cultured on dECM with laminin and laminin alone. Compared to cells cultured on collagen, there is also more uniformity in cell and junctional morphology of MLE12s on both

dECM and dECM with laminin. Junction formed on dECM or collagen coatings both exhibit gaps within the ZO-1 lining the junction (indicated by arrows, Figure 4.6G), and a zipper arrangement of the ZO-1 at the junction. Alternatively, laminin coatings induce a more continuous, linear ZO-1 formation at the junction. Overall, cell uniformity was quantified by lacunarity index (Figure 4.6H), and while junction morphology is different between groups leading to higher error, overall cell shape is consistent within each coating, causing no significant difference. There still may be a difference between cell shape and uniformity between coating types, but this may not be considered with this lacunarity index analysis. A decrease in the number of junctions per cell with laminin added to the coating before culture has been confirmed quantitatively by ImageJ analysis (Figure 4.6).

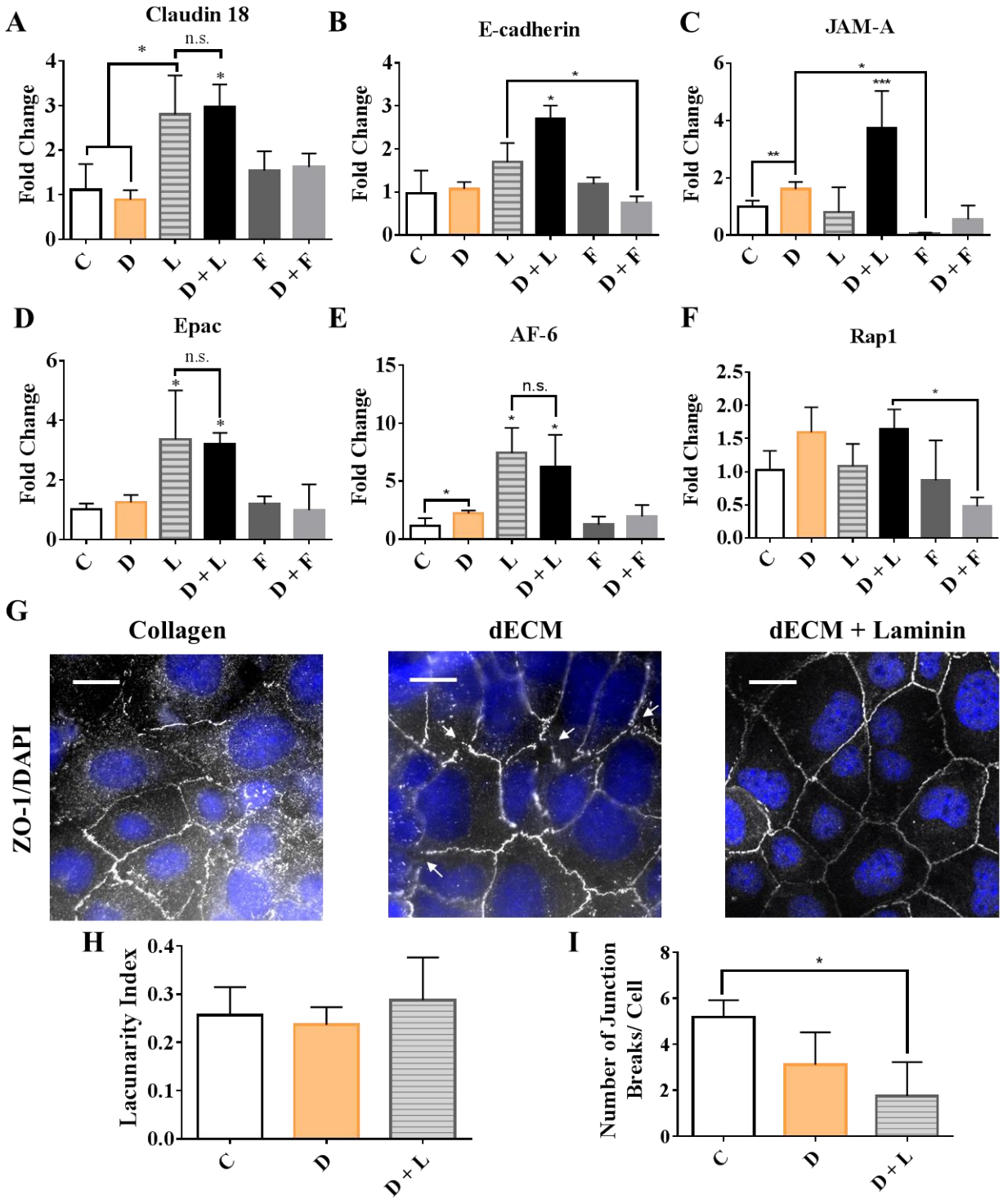

Figure 4.6. Changes in junctional gene expression and ZO-1 localization with dECM coatings dictates alveolar epithelial junction regulation. MLE12 alveolar epithelial cells were cultured on TCP coated with collagen (C), dECM (D), laminin (L), fibronectin (F) or a combination of two

for 5 days before collecting mRNA. Gene expression of the (A-C) junction proteins, claudin-18, E-cadherin, and JAM-A, and (D-F) junction regulators, Epac, AF-6, and Rap1, were quantified using qPCR and normalized to collagen coating controls. Upon barrier formation by alveolar epithelial cells, (G, scale bar = 20 μm) immunofluorescent staining of ZO-1 (white) and Dapi (blue) shows stabilization of the junctions depending on coating type by a representative confocal image. Arrows indicate breaks within the cell junctions. Quantification of confocal images from 3 experimental replicates using AngioTool determined the (H) lacunarity index and (I) the number of junction interruptions per cell. Data are presented as mean +/- standard deviation. $N \geq 3$ with 2-3 technical replicates for each coating condition. n.s, *, and ** indicate $p > 0.05$, $p < 0.05$, and $p < 0.01$, respectively.

Epithelial progenitor cell barrier formation

To determine if similar findings would translate to a progenitor cell population that is commonly used for lung tissue engineering, basal epithelial stem cell (BESC) junction formation through the Epac/Rap1/AF-6 pathway was probed. BESCs were cultured onto collagen, dECM, and dECM with laminin-coated TCP for a week prior to examination with TEER (Figure 4.7A-B). Initially, there were few differences in resistance means between BESCs cultured on dECM and dECM with laminin coatings. Changes were observed after 168 hours when the barrier function of cells cultured on dECM with laminin begins to reach higher resistances overall. Collagen shows meager resistance throughout the entire culture, caused by lack of BESC junction formation and persistence of a round morphology.

Similar to MLE12s cultured on laminin coatings, dECM causes significant upregulation of JAM-A and Claudin-18, but not in Epac. Contrasting MLE12 gene expression, BESCs do not show

significant increases in AF-6 expression when cells are cultured on dECM and dECM with laminin compared to collagen.

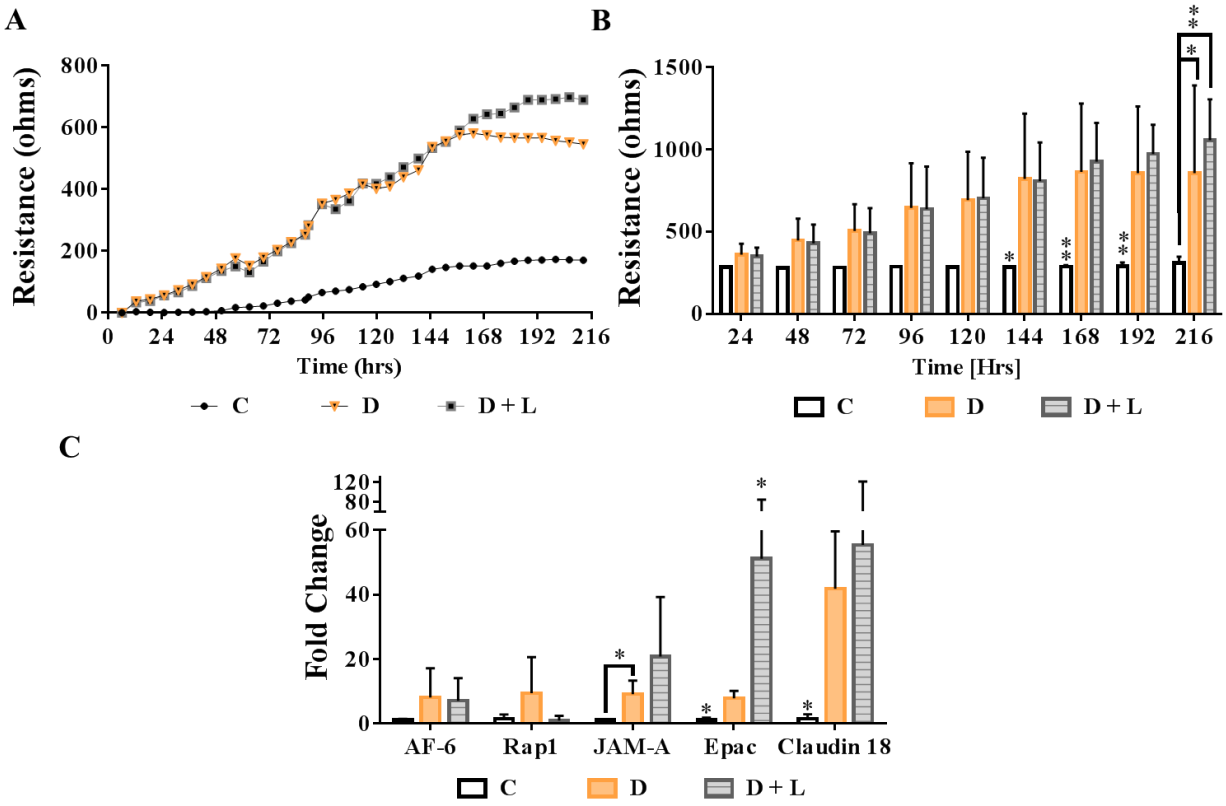

Figure 4.7. BESC barrier function and Epac/Rap1 pathway expression. TEER of BESCs was examined over 9 days after being cultured on collagen (C), dECM (D), or dECM + Laminin (D +L) coatings for 1 week. (A) A representative graph with adjusted means and (B) binned into 24-hour periods with raw resistances are shown. (C) Gene expression of AF-6, Rap1, JAM-A, Epac, and Claudin-18 after 5 days of culture on each respective coating quantified with qPCR. Unless otherwise stated, all data are presented as mean +/- standard deviation. $N \geq 3$ for each coating condition. * and ** indicates $p < 0.05$, and $p < 0.01$, respectively.

Role of Epac in laminin-mediated attachment and barrier formation

Epac has been implicated in both barrier regulation and cell attachment. Relative amounts of cell metabolites detected by a CCK8 assay show that Epac treatment does affect MLE12 attachment (Figure 4.8). MLE12 cells normally exhibit relatively low attachment on collagen alone compared to dECM and dECM with laminin; however, when 007-AM Epac activator is added into the media, there is a significant increase in cell attachment onto collagen coatings. No effect is seen with ESI-09 Epac inhibitor treatment. Unexpectedly, the opposite is seen with dECM compared to collagen, where 007-AM treatment causes decreases in cell attachment, but ESI-09 also causes no change. dECM and dECM with laminin have a similar attachment, as seen previously, but no change is seen when 007-AM is added while an increase is seen with ESI-09. Unanticipated changes in cell attachment to dECM and dECM with laminin coatings with Epac treatment could be caused by other ECM components within dECM could be causing feedback attachment responses that are not investigated within this research.

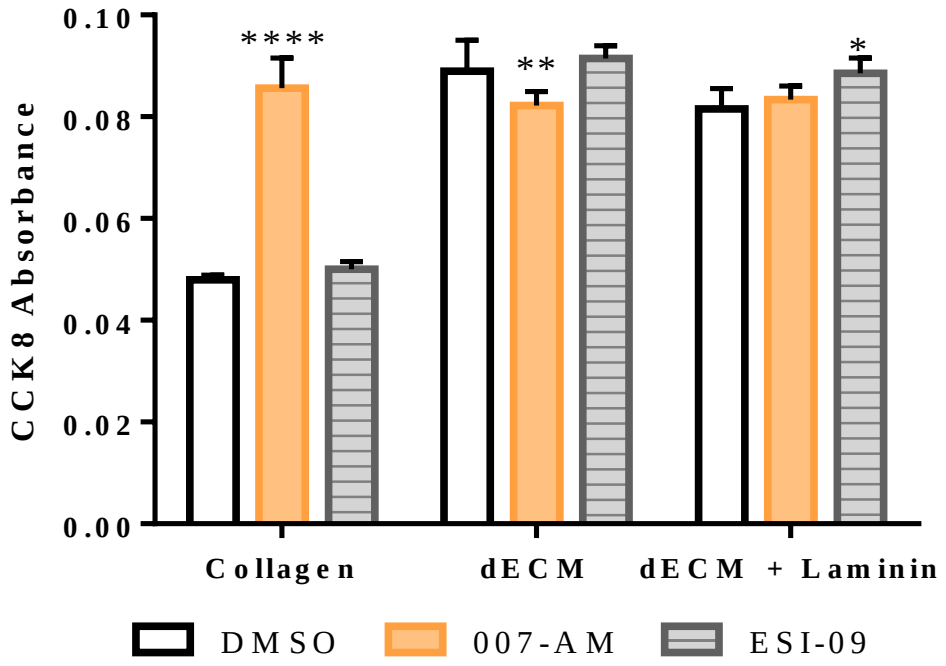

Figure 4.8. Epac inhibition and activation effects on MLE12 cell attachment. Relative cell viability determined by a cck8 assay at 4 hours. Data are presented as mean +/- standard deviation. $N \geq 3$ per group. *, **, and *** indicates $p < 0.05$, $p < 0.01$ and $p < 0.001$, respectively.

To more fully understand the effects of the Epac/Rap1 upregulation on laminin-rich matrices, inhibition or activation of Epac with ESI-09 or 007-AM, respectively, was used to evaluate if laminin-mediated barrier reinforcement could be abolished or induced. TEER analysis of MLE12 cells treated with EPAC inhibitor or agonist for 24 hours shows significantly decreased barrier resistance with ESI-09 Epac inhibition and barrier strengthening with 007-AM Epac activation over 24 hours (Figure 4.9A). Epac treatments were reversible upon media change, shown by the convergence of both groups with their DMSO counterpart.

While TEER of cells cultured on dECM with laminin can be reduced with ESI-09, 4 kDa dextran permeability does not change significantly from DMSO (Figure 4.9B). However, a barrier disruption is seen when ESI-09 is added to MLE12 culture on laminin alone after 4 days, shown by an increase in dextran flux (Figure 4.9B) compared to the DMSO vehicle control. An increase in barrier resistance was also seen when ESI-09 was added to cells cultured on collagen. The reason for this is unknown, but we speculate that it could be caused by a feedback loop when laminin is not present. To determine if laminin-mediated barrier function can be induced in cells cultured without laminin supplemented coatings with Epac activation, similar dextran permeability assays were also conducted on collagen and dECM with 007-AM (Figure 4.9C). Treatment of cells on collagen and laminin with 007-AM after 2 days of culture were the only groups to show significant decreases in junction permeability.

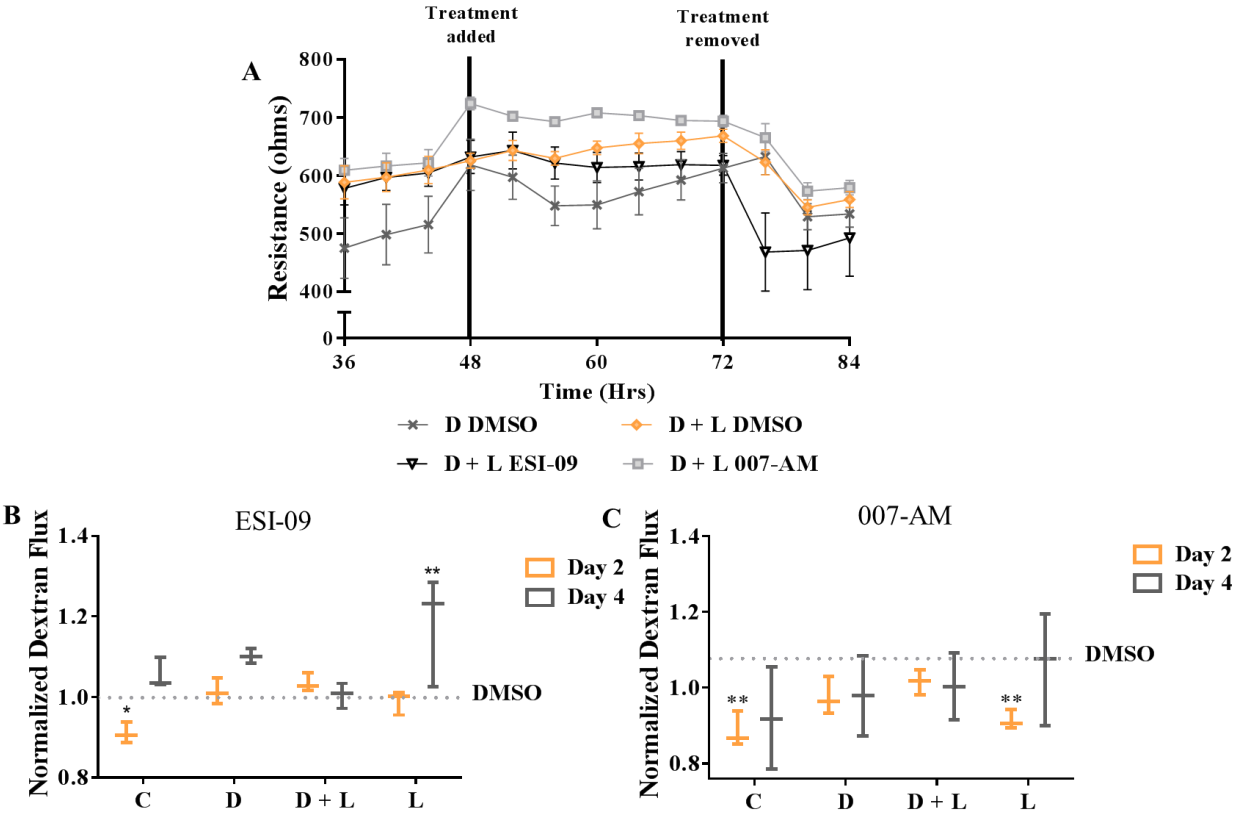

Figure 4.9. Both Epac activation and inhibition cause ECM-dependent barrier function changes. (A) MLE12 cells cultured on dECM (D) or dECM with laminin (D + L) were treated with either ESI-09 Epac inhibitor or 007-AM Epac agonist for 24 hours to examine TEER. (B) Cells cultured on collagen I (C), dECM (D), dECM with laminin (D+ L) and laminin only (L) coatings were treated with ESI-09 to determine if barrier permeability to 4 kDa molecules can be abolished. (C) 4 kDa FITC-dextran permeability of cells cultured on collagen I (C), dECM (D), dECM with laminin (D+ L) and laminin only (L) coatings with 007-AM treatment was evaluated to determine whether barrier permeability of 4 kDa molecules could be further reduced. Dextran flux is defined as the amount of dextran that has permeabilized through the transwell support into the bottom chamber. Samples treated with the Epac inhibitor (ESI-09) and Epac agonist (007-AM) are reported as normalized values to their DMSO vehicle control counterparts. All data are

presented as mean +/- standard deviation. $N \geq 3$ for each coating condition. * and ** indicates $p < 0.05$, and $p < 0.001$, respectively.

Delving further into the mechanisms of Epac, we also examined junctional gene and protein expression with Epac inhibition. All junctional gene expression was decreased significantly compared to the vehicle control except for Rap1, which showed a decreasing trend when treated with ESI-09 (Figure 4.10A). ZO-1 localization to the junction was also disrupted with the treatment of ESI-09 (Figure 4.10B). Additionally, F-actin arrangement and cell morphology were drastically altered with increased stress fiber formation and junctional degradation. This was confirmed quantitatively by image analysis (Figure 4.10C-D), showing decreased mean lacunarity with ESI-09; however, a non-significant decrease in the number of junction endpoints per cell potentially caused by lack of junctions.

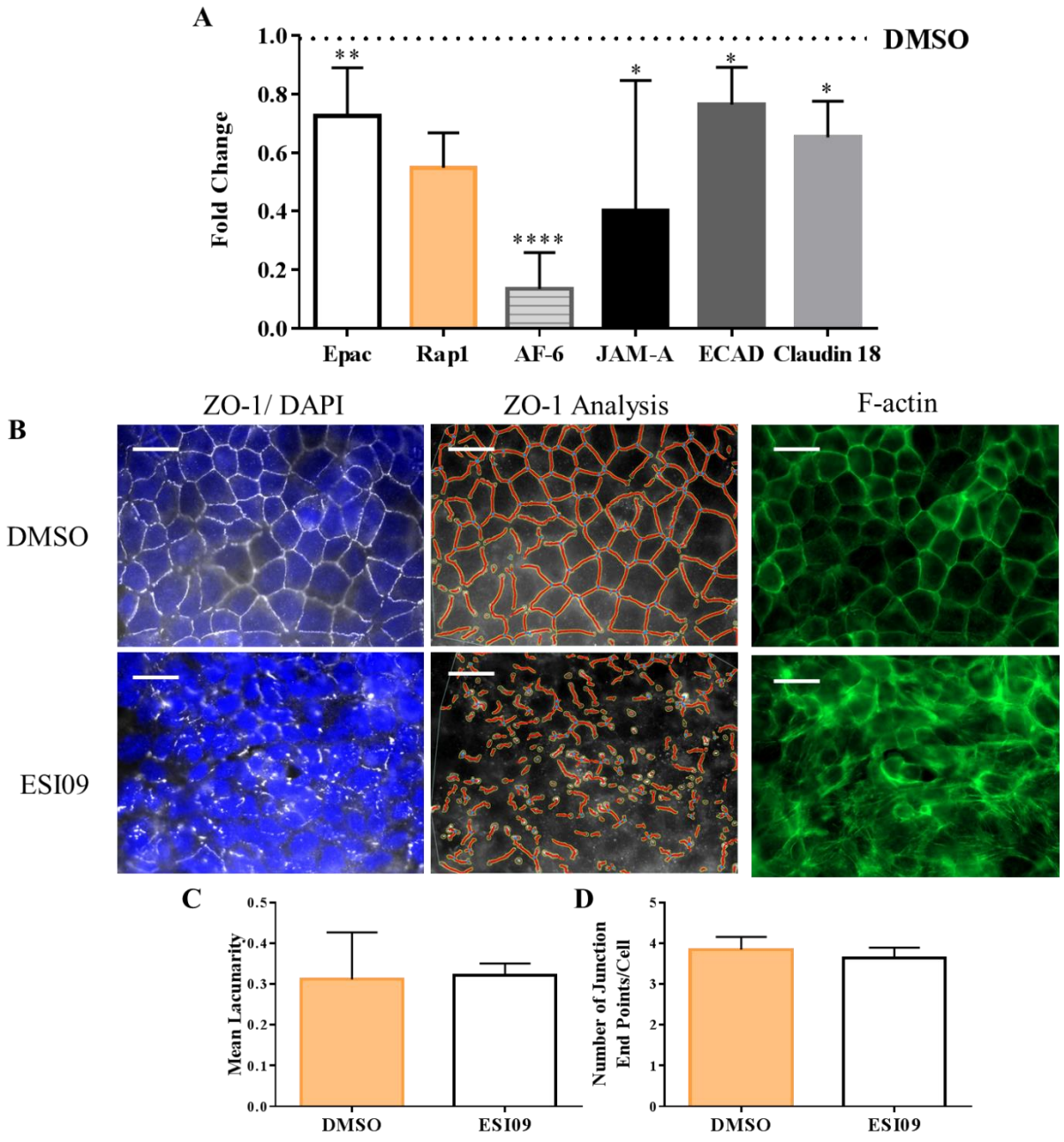

Figure 4.10. Effect of Epac inhibition on junction protein and gene expression. (A) Gene expression of claudin-18, E-cadherin, JAM-A, Epac, AF-6, and Rap1 by MLE12 alveolar epithelial cells cultured onto TCP coated with dECM with laminin for 5 days before treatment with ESI-09 was quantified and normalized to the vehicle control. (B, scale bar = 20 μm) Upon confluency, MLE12s were treated for 4 hours with ESI-09 and stained for ZO-1 (white) and F-

actin (green). Representative confocal images and AngioTool analysis junction outlines show disorganized junctions with Epac inhibition. Quantification of confocal images from 3 experimental replicates using AngioTool determined (C) the lacunarity index and (D) the number of junction interruptions per cell with ESI-09 treatment. Data is presented as mean +/- standard deviation from 3 experimental replicates with a minimum of 2 technical replicates each and *, **, **** indicates $p < 0.05$, $p< 0.01$, and $p < 0.0001$, respectively.

Conversely, Epac activation with 007-AM increases gene expression of both Rap1 and JAM-A (Figure 4.11A). Immunofluorescence staining cells cultured on collagen matrices with and without 007-AM staining shows ZO-1 localization to the junctions and f-actin cortical organization (Figure 4.11B), more resembling junctions formed on laminin-rich matrices. Image quantification characterizes these changes by finding an increase in cell shape uniformity (lacunarity, Figure 4.11C) and a decrease in the number of junction-breaks per cell (Figure 4.11D). These data show that 007-AM increases expression while other AJ and TJ maturation may be caused by stabilization of ZO-1 or translocation to the junction.

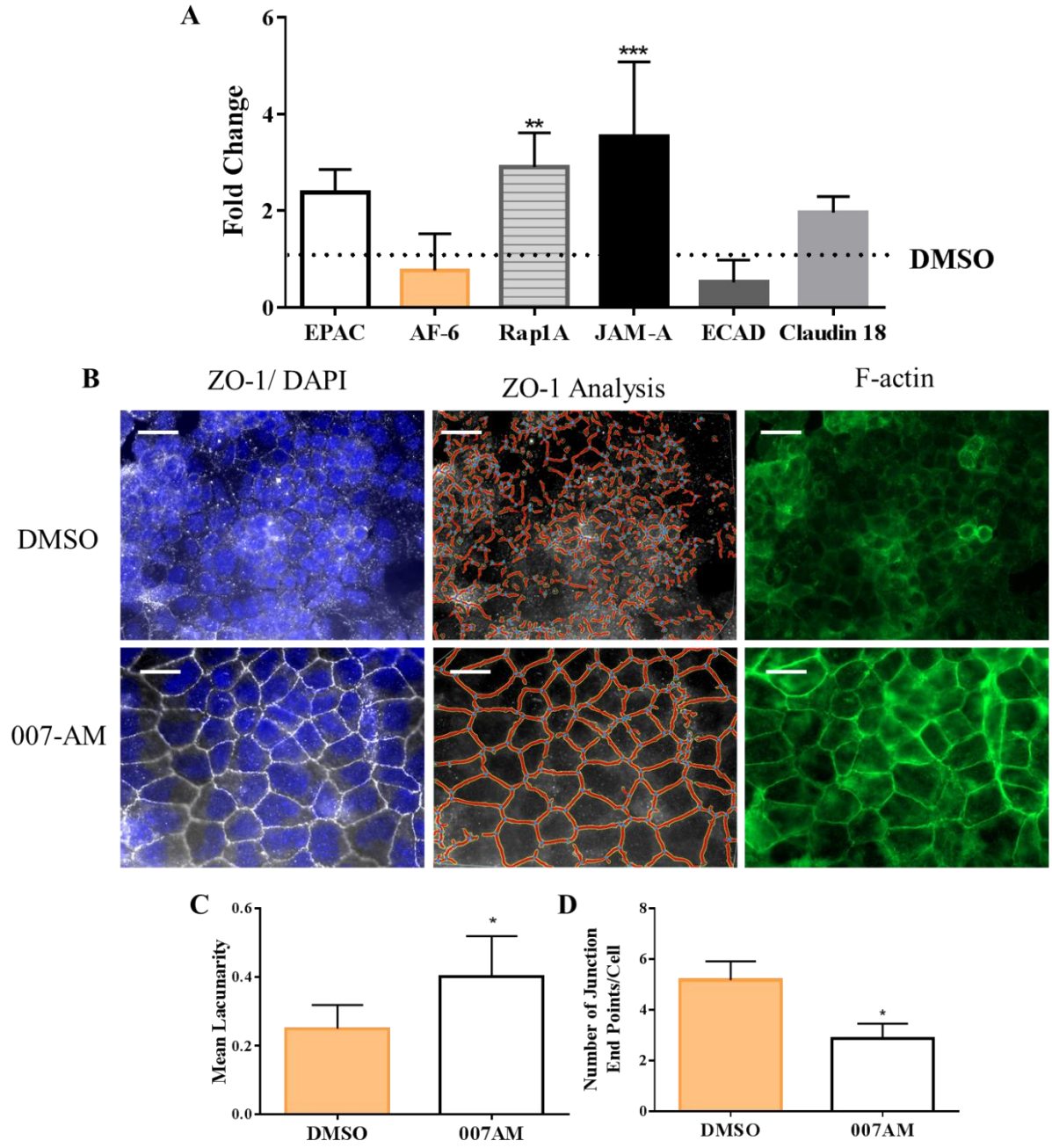

Figure 4.11. Junction reorganization with Epac agonist. (A) Gene expression of claudin-18, E-cadherin, JAM-A, Epac, AF-6, and Rap1 by MLE12 alveolar epithelial cells cultured onto TCP coated with collagen for 5 days before treatment with 007-AM was quantified and normalized to the vehicle control. (B, scale bar = 20 μm) Upon confluency, MLE12s were treated for 4 hours

with 007-AM and stained for ZO-1 (white) and F-actin (green). Representative confocal images show more organized junctions with 007-AM treatment. Quantification of confocal images from 3 experimental replicates using AngioTool determined (C) the lacunarity index or the uniformity of junction formation and (D) the number of junction interruptions per cell with 007-AM treatment. Data are presented as mean +/- standard deviation from 3 experimental replicates with a minimum of 2 technical replicates each and *, **, *** indicates $p < 0.05$, $p< 0.01$, and $p < 0.001$, respectively.

4.4 Discussion

This research aims to expand the basic knowledge of epithelial barrier physiology and to elucidate how decellularization can alter engineered alveolar barriers. To achieve this, we have investigated whether the epithelial barrier function can be improved by systematically replenishing laminin or fibronectin within dECM. Laminin and fibronectin were chosen for their abundance within epithelial basement membranes, and the drastic effects both can have on epithelial differentiation and propagation of disease pathologies if concentrations are dysregulated [17], [62], [174]–[177].

Through TEER and dextran permeability studies, we have identified laminin as a critical protein in alveolar junction formation over collagen I and fibronectin. Fibronectin causes a prolonged decrease in barrier function but an increase in initial attachment rate, seen both in TEER before 12 hours and CCK8 viability assays at 4 and 24 hours. These results are constant with previous studies showing increased cell attachment onto fibronectin and laminin-rich matrices, but only laminin enhances barrier maturation within decellularized lungs and *in vitro* [9], [89]. Analysis of epithelial barrier formation on dECM shows some similarities in the characteristics of barriers formed on both fibronectin and laminin, yet at a fraction of the resistance. At earlier time points, dECM had a similar attachment rate to fibronectin, but a long-term slope resembled cells on laminin coatings. This confirms that previously identified concentrations of both laminin and fibronectin within dECM [7] are promoting initial attachment and steady increases in barrier resistance by alveolar epithelial cells. Nevertheless, to achieve prolonged barrier maturation, laminin would need to be added.

Similarly, small molecule permeability with laminin coatings also decreased; however, dECM and dECM with laminin did not show significant changes from that of collagen, mainly

after 4 days of culture. Dextran permeability showed unexpected differences from the TEER results, but we postulate that after 4 days, collagen and dECM may have formed tight enough barriers concerning pore size and can also reflect transcellular transport, although the changes in TEER may give more insight into prolonged paracellular ion movement associated with edema [178].

To further understand how laminin is increasing the barrier function of the alveolar epithelium, we sought to identify which junction structures are being regulated. Both AJ and TJ proteins, E-cadherin and JAM-A, and the stabilizing scaffold protein, vinculin, show the most significant changes in colocalization with dECM compared to collagen and laminin enriched coatings. Localization of vinculin within epithelial monolayers can help to distinguish the strength of focal adhesions or adherens junctions[179]. Vinculin has a high turnover rate and therefore, can make it difficult to visualize its behavior [180]. We suspect that other matrix proteins within dECM aid in the initial formation of these structures, but other scaffolding proteins must help to maintain and strengthen these junction complexes. JAM-A and E-cadherin are also closely associated with AF-6, as AF-6 aids in its recruitment to early junctions [181], [182]. AF-6 is also found at nectin and claudin complexes with ZO-1 to stabilize and recruit more junction proteins. Without AF-6 present during junction formation, both cell junction formation and cell polarity are inhibited [183]. Even during very early stages of cell-cell contacts, AF-6 is at the junction to organize all of these structures and may be why there is AF-6 distinctly localized that the junction of all cells regardless of ECM, while collagen does not cause the same effect with other junction proteins. AF-6 is localizing to many structures at the junction even if the junctions are still immature and produce low resistance barriers. Upregulation of Claudin-18, JAM-A, Epac, AF-6 and E-cadherin gene expression with laminin or dECM with laminin matrices, but only very subtle changes in

protein localization suggest both TJ, AJ, and focal adhesion complexes are potentially altered by an alternative method to achieve the overall barrier strengthening with laminin-coated substrates. We believe this is due in part by the stabilization of multiple junction structures by the scaffolding protein ZO-1, seen by translocation of ZO-1 to the junction in a continuous band with laminin enriched coatings. Analysis of ZO-1 immunofluorescent staining at the cell junction showed that there was a significant decrease in the number of breaks in the ZO-1 junction staining per cell and a more linear junction morphology when cells were cultured on laminin. ZO-1 recruitment to the cell junction in an organized morphology is a strong correlation to alveolar permeability because it is required for assembly of AJs, TJs, and the actin cytoskeleton [63], [152], [184]–[186].

MLE12 cells offer fully differentiated alveolar epithelial cells and high expansion rates for investigating these fundamental questions concerning alveolar epithelial junctions; however, lung bioengineering requires stem populations that can repopulate with more than 21 types of cells within the lungs. Several groups have identified basal epithelial stem cells (BESCs) as a promising multipotent stem cell candidate for lung regeneration [13], [151] that would differentiate into ciliated, club and pneumocyte populations [187], [188]. To demonstrate the potential translation of laminin treatments into stem cell repopulation of bioengineered lungs, we conducted similar coating experiments with BESCs with TEER and qPCR analysis. Like the MLE12 cells, BESCs formed higher resistance barriers on dECM and dECM with laminin compared to a complete lack of barrier formation on collagen-coated plates. Gene expression of JAM-A, EPAC, and claudin-18 were increased with both dECM and laminin compared to collagen alone. These data suggest that laminin is a stimulator of Epac and junction formation within both stem cell and fully differentiated lung epithelial cell populations.

Epac is widely known as a driver of actin organization and barrier formation within the context of the endothelium, but less is known about Epac's role in alveolar epithelial barrier formation. Initial assessment of gene expression with laminin and fibronectin showed upregulation of Epac and AF-6 with laminin coatings. Rap1 and AF6 were only upregulated in the presence of additional laminin, but not fibronectin, suggesting that laminin mediates barrier function causing upregulation of JAM-A, E-cadherin, and Claudin-18, as expected from previous literature linking Epac activation to TJ and AJ expression and stabilization [189]–[193]. These data led us to investigate further Epac's role in laminin-mediated barrier function by inhibiting the interaction of Epac with downstream effectors. Epac inhibition can abolish laminin-mediated barrier resistance, as observed by TEER and ZO-1 localization.

Also of interest is how we can apply Epac activation to enhance barrier formation without the addition of laminin. An Epac agonist, 007-AM was applied to collagen coatings, significantly increasing JAM-A and Rap1 gene expression, rearranging ZO-1 and the actin cytoskeleton cortically, and decreasing barrier permeability. 007-AM has recently been established as a long-lasting treatment for endothelial barriers within bioengineered lungs [152] and treatment of vascular permeability within acute lung injury [155], [194]. These data now confirm that Epac activation and laminin-enriched ECM coatings can both benefit the epithelial barriers to produce functional lung biomaterials and potentially serve as therapies for edema-related diseases.

Future studies will be conducted to confirm that these findings can be translated to *ex vivo* lung tissue engineering and *in vivo* treatment of diseases. However, this high throughput and definitive *in vitro* approach has allowed us to answer basic questions about junction physiology that would not be possible within a whole lung model. Also, while these experiments have definitively established the role of both laminin and fibronectin in alveolar epithelial barrier formation, the role

of other critical epithelial differentiators such as collagen IV, nidogens, GAGs, other glycoproteins will need to be investigated.

CHAPTER 5: ROTATIONAL BIOREACTORS FOR LUNG RECELLULARIZATION

5.1 Rationale

Designing methods for the culture of 3D tissue engineering requires strategies that do not typically apply to 2D culture. The intricate architecture necessary to create the natural tissue microenvironment, such as within decellularized lungs, involves consideration of adequate cell seeding to all alveoli, airways, and capillaries, delivery of fresh media to all cells, and tissue orientation during culture to ensure proper cell dispersal to all dimensions. Currently, there are several challenges hindering lung bioengineering from creating viable transplant alternatives, including insufficient scaffold cell coverage, partial cell differentiation, and lack of uniform organ function. Perfecting bioreactor designs and seeding techniques with the addition of cell-specific dynamic seeding protocols to current methods may aid in overcoming some of these challenges.

The latest advances in both commercially available and custom lung bioreactor systems include artificial pleural membranes, gas exchange units, waste removal, real-time monitoring of oxygen and lung mechanics, and high-throughput automation [195]. These advancements have extended the length of culture and reproducibility; however, with insufficient cell attachment and differentiation, current efforts have not resulted in fully functional tissue even after one month of culture [196]. To accomplish bioengineered lung function, alternative seeding procedures need to be considered to combine with current bioreactor advancements [197].

Specifically for recellularization of acellular lung scaffolds, two main bioreactor designs have been developed to apply media flow and cell dispersal; a perfusion bioreactor system [2] and a rotating wall vessel (RWV, [11]). These systems have been designed and commercialized for both rodent lung culture and more complex porcine and human-sized organs [10], [91], [100]. Both

designs have their limitations caused by cell settling during prolonged static culture periods or constant cell movement inhibiting attachment.

The branching airway structures of the lungs are ideal for efficient delivery of fluids and cells, but challenges arise with keeping cells stationary for attachment throughout all dimensions of all alveolar structures. Alveoli are spherical structures lined with a very thin alveolar epithelium that is vital to the function of the lung. The 200 μm structure is spherical and would require attachment or migration of approximately ten, 20 μm type 1 epithelial cells around the entirety of the sphere [198]. Due to the complex 3D structure, distribution of the cells within the alveoli and throughout all alveoli may require dynamic seeding regimens [11]; however, during the first hours of culture, when cells are first attaching, periodically repositioning the lung may be needed for epithelial attachment.

In vivo, migratory cells such as immune or metastatic cells require flow to initiate cell adhesion. In the case of epithelial cells, laminar flow can decrease the rate of attachment [104] and even increase metastatic potential [199]. Alternatively, to ensure sufficient epithelial attachment, periods of static culture are required to allow for cell adhesion complexes to be formed. Cells first make attachments to their ECM substrates through integrin-based focal adhesions. Epithelial cells then spread, reorganize their cytoskeleton, and initiate more integrin interactions with the ECM to strengthen adhesion over time. Adhesion complexes begin cooperatively binding after just one minute, but it takes up to 10 to 20 minutes after seeding for the cell adhesion structures to withstand substantial shear forces [200]. Once epithelial attachments have matured, fluid flow and shear stresses become an essential driver of cell differentiation. After attachment, a long-term culture within a perfusion bioreactor system is used to distribute nutrients and apply biophysical stimuli.

Static seeding protocols used for RWV and some perfusion culture systems cause extended cell settling and therefore, non-uniform cell attachment. Alternatively, other perfusion culture system methods include seeding with a constant flow of media and cells through the tissue. Constant fluid shear stress could disrupt adhesion complexes immediately upon formation. These two systems do provide beneficial advanced media dispersal and mechanical cues that aid in tissue maturation but may need refining concerning seeding procedures. Given the importance of maximum attachment of delivered cells throughout recellularized lungs, the goal of this study is to increase cell dispersal using a rotational seeding method for *ex vivo* culture of decellularized lungs.

5.2 Materials and Methods

Bioreactor design

A rotational seeding system designed for improved attachment and dispersal of cells within decellularized lung scaffolds. The rotational system supports a 50 mL conical tube on two long cylinders (Figure 5.1). One cylinder was attached to a stepper motor programmed using an Arduino Mega (See Appendix A for code) controller system to rotate the tissue every 20 minutes for 3 hours. This rotation rate ensures uniform coverage of the airways over 4 hours using the cell coating routine illustrated in figure 5.1B. This rotation procedure allows attachment at every 45º angle of the lung throughout the entire culture. The degree of rotation between resting positions is large to allow for optimal cell movement throughout the tissue. After seeding completion, the lung was transferred into a perfusion bioreactor system (Figure 5.2) for static overnight culture without vascular or airway flow to ensure optimal cell adhesion. 24 hours after initial seeding, vascular perfusion through the pulmonary artery was initiated at 2 mL/minute by a pulsatile pump (CellMax). Media ventilation was also applied into the trachea at 1 breath/minute, driven by negative pressure within the main chamber, created by a syringe pump. One-way valves were placed into the breathing loop to allow new media exchange during ventilation. Pressure and pH were monitored by sensors also controlled by the Arduino system to ensure pressure did not vary more than 15 mmHg [106] from atmospheric pressure and oxygenation of the media was maintained.

Cell Culture

Mouse alveolar type II cells (MLE12, ATCC) were cultured with HITES medium containing 2% fetal bovine serum at 37 °C with 5% CO_2, according to the manufacturer's protocols. Male and female Sprague Dawley rat lungs were decellularized without processing by lyophilization and milling, as previously mentioned in the decellularization section of Chapter 3. The trachea and pulmonary artery were cannulated for the addition of the cells and bioreactor attachment. Before recellularization, the lung was rinsed 3 times with PBS with 5% Antibiotic/Antimycotic. All bioreactor components were autoclaved, rinsed with PBS with 5% Antibiotic/Antimycotic for 1 day, and handled within a sterile hood before use. 50 x 10^6 MLE12s in 12 mL of media were perfused intratracheally. Inoculated lungs were either rotationally cultured for 4 hours in a 50 ml tube or placed directly into the perfusion bioreactor chamber for static culture overnight. After initial seeding on rotation bioreactor, as described in the bioreactor design, pulsatile vascular flow and media ventilation was administered for 24 hours.

MLE12 cell attachment rate assay

250,000 cells/cm^2 were seeded onto 0.1 mg/mL dECM or collagen I coatings as previously described in Chapter 4. Every 20 minutes for 3 hours, unadhered cells and media were aspirated from the well and rinsed gently before fixation with 4 % PFA. Cell nuclei were stained using DAPI Prolong Gold Antifade Mounting agent, and the number of nuclei was counted within 3 pre-determined regions of each well using a Zeiss AxioObserver Z1 fluorescence microscope. Percent of cell attachment was calculated by dividing the number of cells attached by the number of cells seeded.

Resazurin Reduction Assay

After 48 hours of perfusion culture, media was removed from the main chamber and replaced with 50 μM resazurin media solution. This solution remained within the lung for 4 hours until absorbance (544 nm (ex)/590 nm (em)) levels of the resazurin solution and qualitative images were taken to evaluate metabolic activity of the cells. Absorbance values were subtracted from the non-metabolized stock concentration of the 50 μM resazurin solution.

Histology

Each lung (right or left) was divided into dorsal or ventral portions, that were further divided into upper and lower regions. Dissected tissue for histology and other assays were chosen based on resazurin cell viability throughout the lung, to attempt to isolate regions with similar cell viability for histology and Picogreen. An entire ventral or dorsal portion of each lung was fixed with 4% paraformaldehyde, embedded, and sectioned through the frontal plane to see the distribution of cells throughout the entirety of the lung. Two histological sections, several millimeters apart were taken from each tissue region for staining with hematoxylin and eosin (H & E) and imaged using a Vectra Polaris Automated Quantitative Pathology Imaging System.

dsDNA quantification

A Picogreen dsDNA quantification assay (ThermoFisher) was performed on the remaining portions of the lungs not used for histological sectioning. Each sample was normalized to its wet weight and graphed as total dsDNA throughout the tissue or as maximum fold change between regions. Fold change of total dsDNA was determined by adding the dsDNA values within all regions of one sample and dividing by the average total dsDNA for all of the control group. To

calculate the maximum dsDNA concentration difference, the highest and lowest dsDNA values from one lung were subtracted from each other and then divided by the average maximum difference for all control lungs.

Statistical Analysis

All data are presented as mean +/- standard deviation with an $N \geq 3$ unless otherwise stated. Statistical significance was determined by a Two or One-way ANOVA and a Tukey's multiple comparisons tests using GraphPad Prism.

5.3 Results

Bioreactor design

To enhance cell dispersal and mimic the mechanics, temperature, and pH within the lungs, we have designed a novel bioreactor system. The first portion of the bioreactor system is a rotational seeding unit (Figure 5.1) that will turn the lung every 20 minutes in a pattern illustrated in figure 5.1B for 4 hours during the initial cell attachment period. Large degrees of rotation were used between resting periods to tumble the cells through multiple regions of the lungs before settling at the desired location. The duration of the resting periods was determined by the rate of MLE12 attachment (Figure 5.1A) to allow 10 percent of cells to attach at each position. This aided in the attachment of cells more evenly throughout the lung. Seeding efficiency was characterized by H & E staining and Picogreen dsDNA quantification. After 4 hours of cell attachment, the lung was moved to the perfusion bioreactor (Figure 5.2) for mechanical conditioning and media perfusion. The perfusion bioreactor design was adapted from a previously published design [10], [106] without the endothelial seeding chamber.

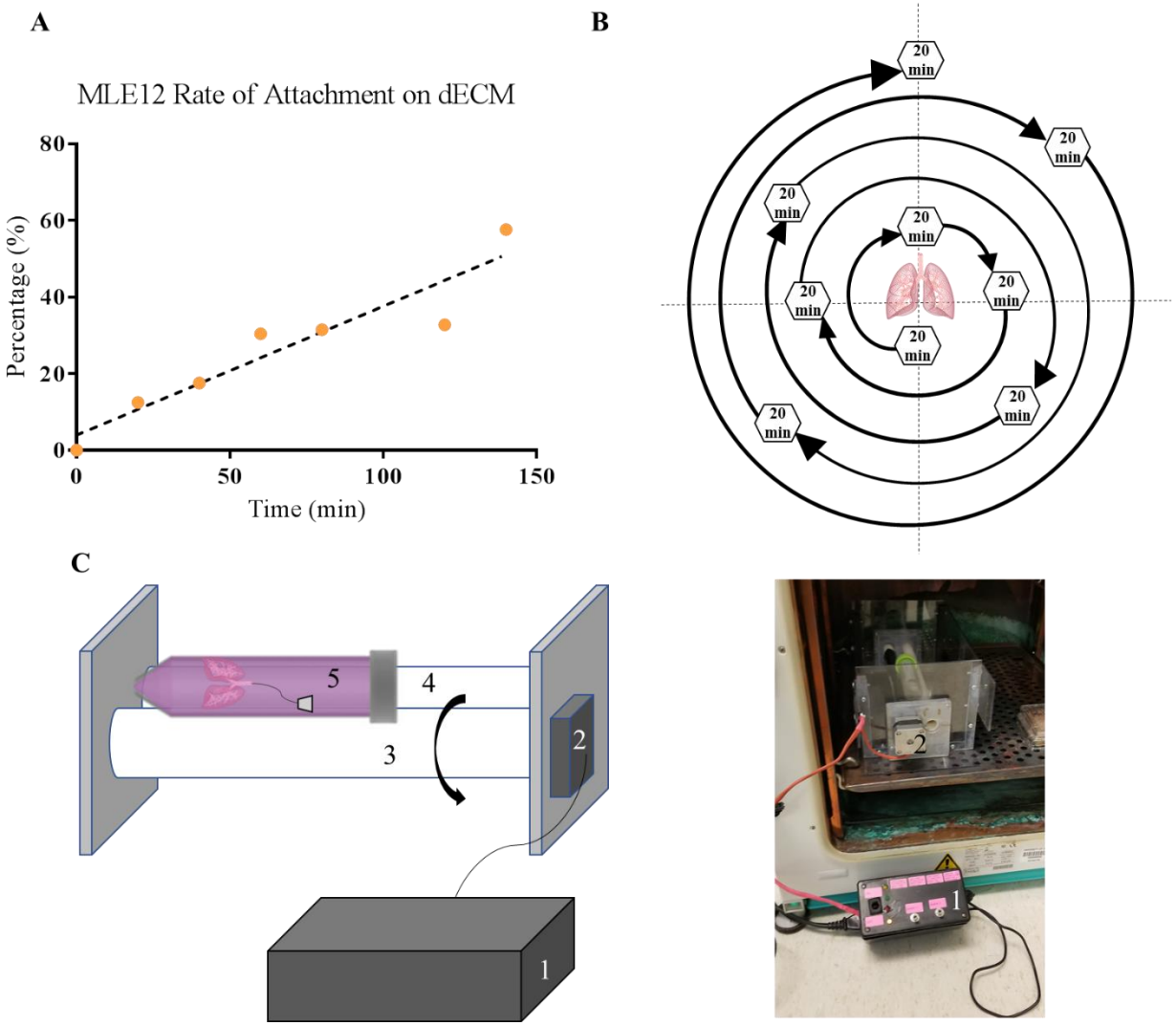

Figure 5.1. Rotational seeding unit design. (A) MLE12 rate of attachment was determined by counting the percentage of cells that had attached with respect to number seeded every 20 minutes for 4 hours. Attachment rate was used to inform our (B) programmed rotation schedule that will rest at every 45° angle of the lung for 20-minute intervals before turning to a new location. Large angles of rotation between each resting position allow for coating of the cells. (C) A schematic and (B) a picture of the actual system that was housed within a cell culture incubator is shown. An Arduino Mega within a protective box (1) powered and controlled the stepper motor (2). The

stepper motor actively turns one pipe (3) and through friction with the (5) 50 mL conical tube containing the seeded lung, the other pipe (4) will also turn.

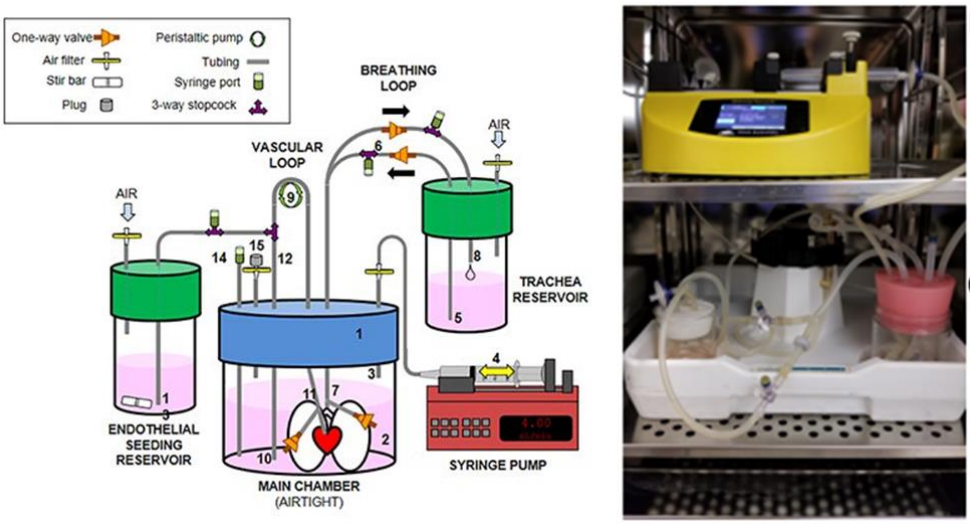

Figure 5.2. Perfusion bioreactor design for long-term culture. A previously designed perfusion bioreactor system (left, reprinted from [10]) was modified for our culture procedures. An image of the modified perfusion bioreactor system (right) includes a breathing loop that is controlled by a syringe pump and a vascular circuit driven by a pulsatile pump, but no endothelial seeding reservoir.

Resazurin and Picogreen assessment of cell distribution within cultured lungs

50 million MLE12 cells were cultured into decellularized rat lungs with rotational or static seeding to assess if periods of dynamic culture can increase cell dispersal throughout the lung. Resazurin was perfused through the airways and cultured for 4 hours to allow for metabolites to gradually change the color of the resazurin solution from a dark blue to pink for whole-lung cell viability assessments. After 48 hours of culture, rotationally seeded lungs exhibited a more uniform pink or light purple color distribution, correlating to viable cells throughout, while static seeding

causes several distinct regions with either viable cells (pink) or dark purple to blue (less cellular metabolism, Figure 5.3A). Resazurin absorbance of the lung perfusate (Figure 5.3B) was collected from the tracheal cannula and showed increased cell viability with rotational seeding. There was no significant increase between rotationally and statically seeded lungs because the collection of the perfusate from the trachea had mixed with the resazurin from all regions of the lung upon removal. To better understand where cells attached with both seeding methods, after 48 hours of culture, the lung was dissected into several regions for assessment. Summing the dsDNA within all areas of each lung showed total dsDNA concentrations (Figure 5.3C) that resembled the results seen by resazurin absorbance, as expected. To assess regional differences, the maximum difference between dissected tissue regions was calculated (Figure 5.3D). There were no significant differences found because of a large degree of viability caused by an outlier within the static group that had little cell viability throughout.

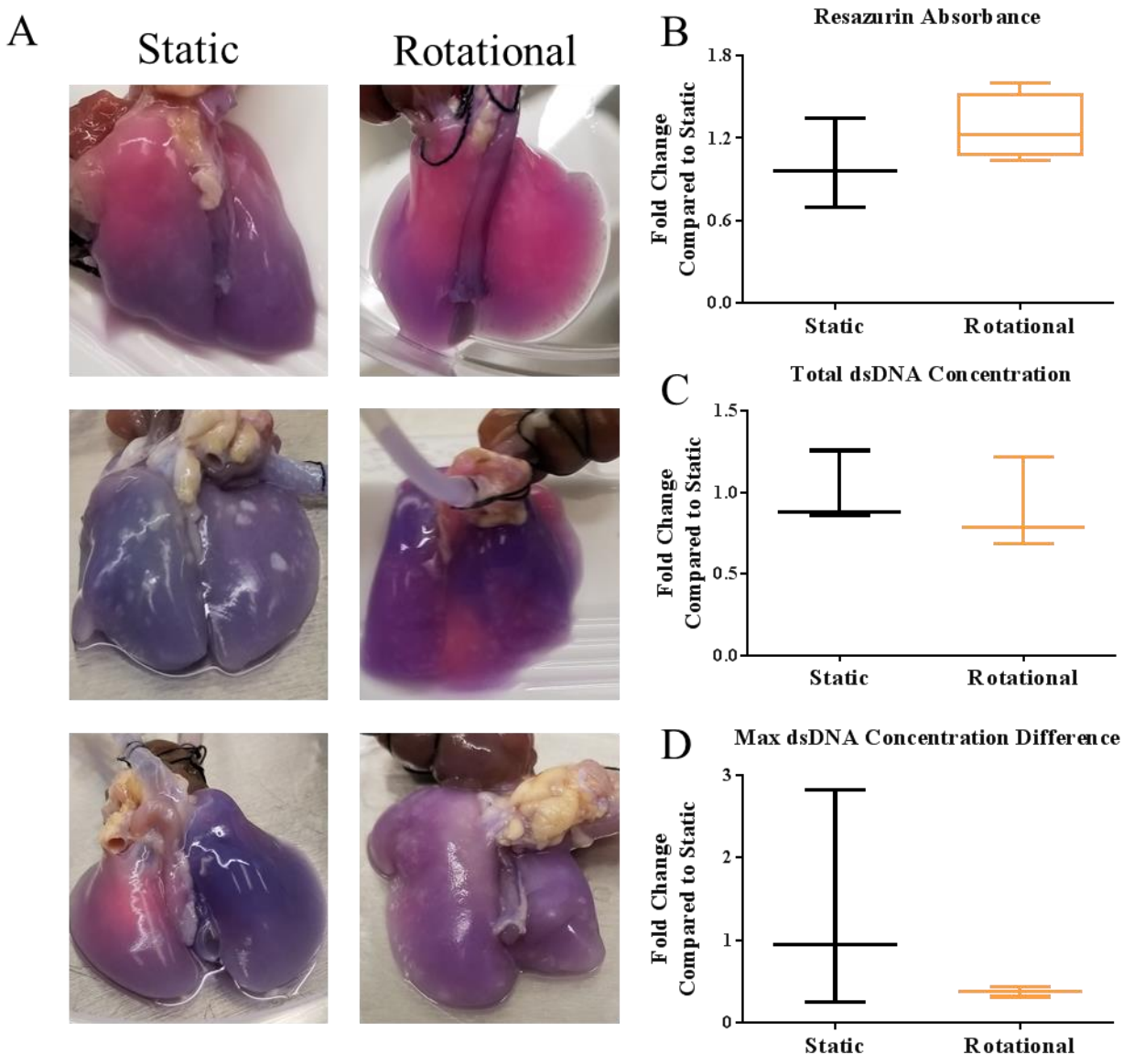

Figure 5.3. Cell distribution and viability within statically or dynamically seeded lung scaffolds. (A) Images of regenerated lungs after resazurin perfusion (pink indicates viable regions). (B) Resazurin perfusate absorbance quantification after collection from the tracheal cannula and (C) overall Picogreen dsDNA concentration indicates whole lung viability. (D) dsDNA concentration differences between the dorsal and ventral regions of the right and left lung give insight into the regional distribution of cells with a static and dynamic culture. Data are

represented as mean +/- the minimum and maximum. N ≥ 3 for each condition with no significant changes seen between either group.

Cell dispersal within dynamically culture lungs

Histology was also done to verify the findings from resazurin and Picogreen cell distribution studies. After 48 hours of culture (Figure 5.4), there were increases in cell attachment and distribution. Cell morphology within both conditions does not show cell spreading with some clumping of cells within the airways, that may be attenuated with longer culture times.

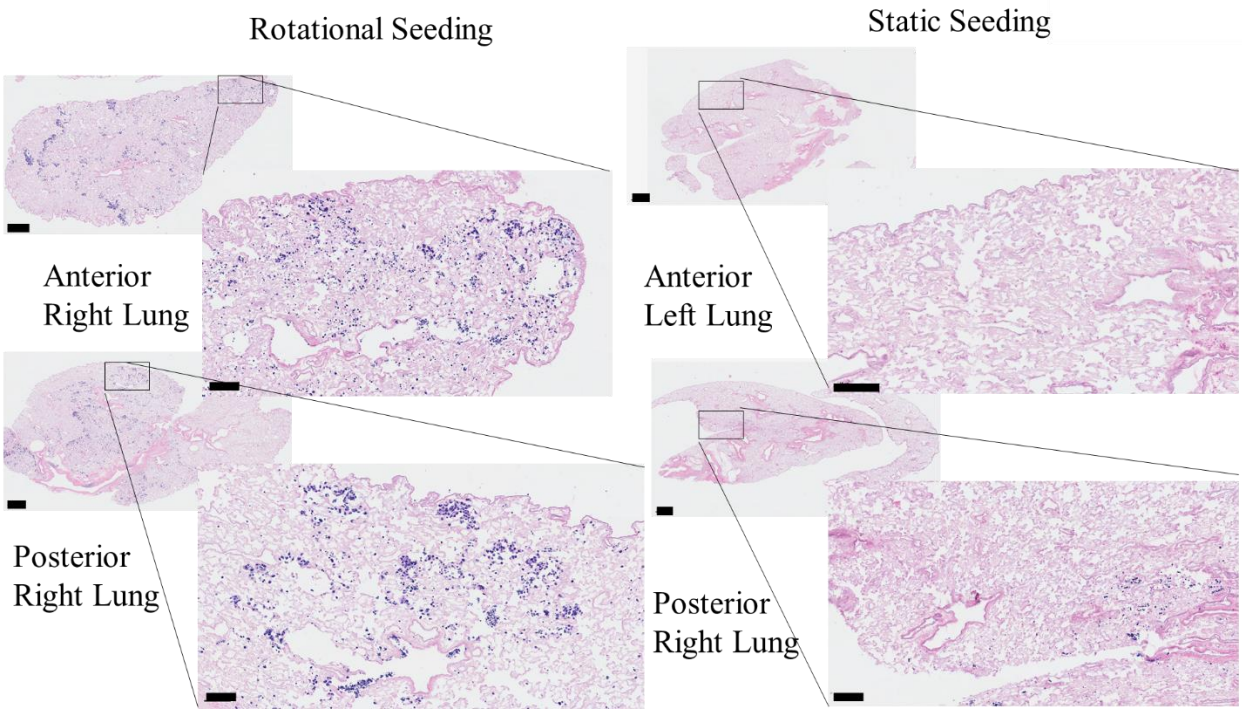

Figure 5.4. Histological analysis of cell attachment after static or dynamic seeding. Representative images from the histological sections from either the anterior or posterior regions of the left or right lungs are shown. Scale bars on larger images indicate 100 μm and scale bars on smaller, magnified images indicate 600 μm.

5.4 Discussion

Several other groups have concluded that dynamic seeding of cells onto biomaterials is necessary to enhance cellular differentiation or cell dispersal throughout the entirety of a scaffold [13], [201]–[205]. Within whole lung bioengineering, implementation of these methods has faced challenges caused by cellular settling or premature detachment of cells by fluid flow. In this study, we have developed a seeding protocol that enhances cell dispersal to use in tandem with other long-term culture methods. This two-phase culture system includes a rotational cell attachment step, followed by traditional *ex vivo* lung perfusion culture. Alterations to rotation durations and speeds can create custom seeding routines based on cell attachment characteristics.

Resazurin metabolic assays have been previously used as an efficient, non-invasive way to assess tissue viability during *ex vivo* culture [13], [206], [207]. With perfusion into the seeded scaffold, cells will encounter resazurin and undergo reduction into a pink colored resorufin. Pink and purple regions with high cellular viability will easily be distinguished from dark blue regions with little cell content. Rotationally seeded lungs exhibited pink and light purple regions throughout the lung scaffold while statically seeded scaffolds had some bright pink areas that rapidly transition to a dark purple or blue color. The average resazurin absorbance showed similar cell viability results between the two groups, but a closer examination of cell attachment by regional Picogreen measurements shows that dispersal was limited to small regions with static seeding. While Picogreen dsDNA concentration differences between static and rotationally seeded lungs are not significantly different, the fold change is decreased by an outlier within the static culture group. The outlier has little difference in dsDNA concentrations between each area because overall, there are very few cells throughout the lung.

To confirm our previous findings, histology through the frontal plane of the cultured lung shows a broader distribution of cells throughout dynamically seeded lungs. Cells within statically seeded lungs exhibit sedimentation in a small portion of the lung, that would limit overall function after long-term culture. Cell clumping within alveolar and airway spaces and rounded cell morphologies may indicate that longer culture times are needed. Various epithelial cell lineages or stem cell populations may also be used in the future to induce phenotypic morphologies and increase airway and alveoli coverage.

Careful consideration of epithelial attachment *in vitro* was used to determine the ideal attachment rate within a whole lung scaffold and improved cell coverage. These studies help to inform all types of 3D culture methods and emphasize the importance of intermittent motion in cellular seeding. The development of a portable, rotation system that is not in direct contact with the lung or media allows for reduced contamination and adaptation of these methods to biomaterial applications. Overall, these are promising results highlighting the importance of dynamic culture in *ex vivo* cell culture to increase recellularization efficiency.

CHAPTER 6: REPLENISHING MATRIX COMPONENTS IN dECM: PILOT STUDIES

6.1 Rationale

Findings from this research and other groups [89], [208], [209] have demonstrated the importance of dECM structure and composition on the differentiation and homeostasis of lung tissues. Current decellularization protocols cause overall reductions in elastin, collagen, and BM ECM components, causing drastic changes in lung mechanics [150], [210]. While the lung is equipped with an efficient route for administering decellularization chemicals intratracheally and vascularly, ventilation decellularization preferentially strips the BM proteins from the airway and alveolar surfaces [211]. Depletion of some ECM proteins more than others can be detrimental if the resulting matrix profile recapitulates diseased or aged ratios [17]. Due to "dynamic reciprocity" between cells sensing and regulating the surrounding microenvironment, ECM alterations must be restored to ensure "healthy" regeneration [212], [213]. We hypothesize that removal of these vital components, specifically at the airway and alveolar walls of decellularized lungs, may cause detrimental effects on the formation of the gas exchange barrier upon re-epithelialization and tissue maturation.

Two approaches are being considered to promote a tissue-specific ECM environment within decellularization, either cell removal techniques can be further optimized, or the matrix can be artificially replenished. Several groups have attempted to add ECM components such as Fibrillin-2, Tenascin-C, collagen, [12], [88] or pretreatment with matrix-producing cells [92], [93], [214] and have improved recellularization efficiency. However, selectively reintroducing only a few ECM components may not address all ECM deficiencies and pre-treatment of cells may propagate negatively influenced dynamic reciprocity. We hypothesize that all ECM proteins must

be concentrated and deposited at the airway and alveolar surfaces to restore the BM profile and structure before a few selected differentiating proteins can further be supplemented. These proof of concept studies aims to translate the benefits of concentrated dECM coatings on the epithelial barrier that we have shown previously to whole lung epithelial regeneration.

6.2 Materials and Methods

Decellularized rat lung dECM coating

Mouse or rat lungs were decellularized without lyophilization and milling, as previously mentioned in Chapters 3 and 5. The trachea and pulmonary artery were cannulated for dECM coating pretreatment, the addition of the cells, and bioreactor attachment. The decellularized lungs were perfused intratracheally with 5 ml of 8 mg/mL dECM pregel solution [72], [130] and stored at 4° C overnight. The coated lung was rinsed 3 times with PBS containing 5% Antibiotic/Antimycotic and stored at 4° C until inoculated.

Histology

dECM coated or non-coated lungs, with and without recellularization were fixed with 4% PFA, embedded, and sectioned for H & E staining. As an attempt to represent the regional cell viability between end-point assessments, an entire ventral or dorsal portion of each lung was used for histology, and the remaining half of the lung was distributed between the remaining assays. The tissue was sectioned through the frontal plane to see the distribution of cells throughout the entirety of the lung. Two histological sections, several millimeters apart, were stained H & E and imaged using a Vectra Polaris Automated Quantitative Pathology Imaging System.

Recellularization

Preliminary static recellularization studies were performed with decellularized mouse lungs. Each dECM-coated and non-coated lung was seeded with 1 x 10^6 human alveolar basal adenocarcinoma cells (A549s) intratracheally. Seeded lungs were then placed into 15 mL conical

tubes and placed on a shaker in an incubator for 4 or 7 days. The A549 populated lungs were cultured in RPMI media containing 1% Antimycotic/Antibiotic and 10% FBS.

For all other recellularization with perfusion bioreactor culture, decellularized rat lungs were cultured with mouse alveolar type II cell (MLE12, ATCC) in HITES medium containing 2% fetal bovine serum. Further experimentation was performed with rat lungs because of size limitations with smaller mice lungs. Also, MLE12s were chosen for further experimentation because they form more optimal barriers compared to A549s. dECM-coated and non-coated lungs were perfused with 12 ml of 50 x 10^6 MLE12 cells in media intratracheally. A 4 hour initial seeding period was completed on the rotation bioreactor as described in the bioreactor design of Chapter 5. The recellularized lungs were then transferred to the perfusion bioreactor system, also described in Chapter 5, for 12 hours of static culture and 4 days of mechanical conditioning. Air was exchanged daily, media pH was monitored, and the media was exchanged a maximum of every 3 days.

Resazurin Reduction Assay

After 3 and 5 days of perfusion culture, the media was removed from the main chamber, and a 50 μM resazurin solution in media was infused into the airways of the lungs and main chamber. This solution remained within the lungs for 4 hours before photos of the entire lung appearance were taken, and absorbance (590 nm) of the resazurin solution was measured using a microplate reader. Absorbance values were subtracted from the stock resazurin solution. After the resazurin assessment on the 3rd day, the residual resazurin solution was removed from the chamber, resazurin was rinsed from the lungs with media, and the bioreactor was refilled with new medium before resuming normal perfusion and ventilation.

dsDNA quantification

DNA content of a portion of the lung section not utilized for histology was quantified using a Picogreen dsDNA quantification assay (ThermoFisher). The dsDNA concentration for each tissue was determined using the tissue's initial wet weight. The summed dsDNA of all lung sections from each set of coated lungs was normalized to the non-coated lungs.

qPCR

mRNA was extracted using Trizol (ThermoFisher) from the remaining regenerated tissue not utilized for Picogreen or histology according to the manufacturer's protocols. The mRNA was purified with an RNeasy Mini Kit (Qiagen) and quantified using a Pierce BCA protein assay kit (Thermo Fisher). After each sample was balanced to the lowest concentration, the mRNA was converted to cDNA with an iScript cDNA synthesis kit (Biorad). The cDNA was then used for qPCR analysis with the alveolar epithelium-specific junction primers found in table 1 of Chapter 4.

Ex vivo recellularized lung barrier permeability

Previously mentioned 4 kDa FITC-labeled dextran (Chapter 4) was administered to the trachea of intact and recellularized lungs with or without coatings to assess leakage into the vasculature system. This method was adapted from previously tested protocols [94], [215]. Multiple fractions of PBS were run through the vasculature to collect any FITC-labeled dextran that has crossed the barrier. The immunofluorescence intensity of the PBS perfusate was assessed

using a fluorescent microplate reader with an excitation wavelength of 485 nm and an emission wavelength of 528mm.

Statistical Analysis

All data are presented as mean +/- standard deviation with an $N \geq 3$ unless otherwise stated. Statistical significance was determined by a Two or One-way ANOVA and a Tukey's multiple comparisons tests using GraphPad Prism.

6.3 Results

dECM coating deposition

To evaluate coating efficiency of the dECM, histology was performed on decellularized rat lungs with and without dECM coatings. H & E staining of dECM-coated and non-coated lungs (Figure 6.1) shows a denser matrix structure within the airways and alveoli throughout the histological section. This confirmed our method of coating provided efficient delivery throughout the tissue to proceed.

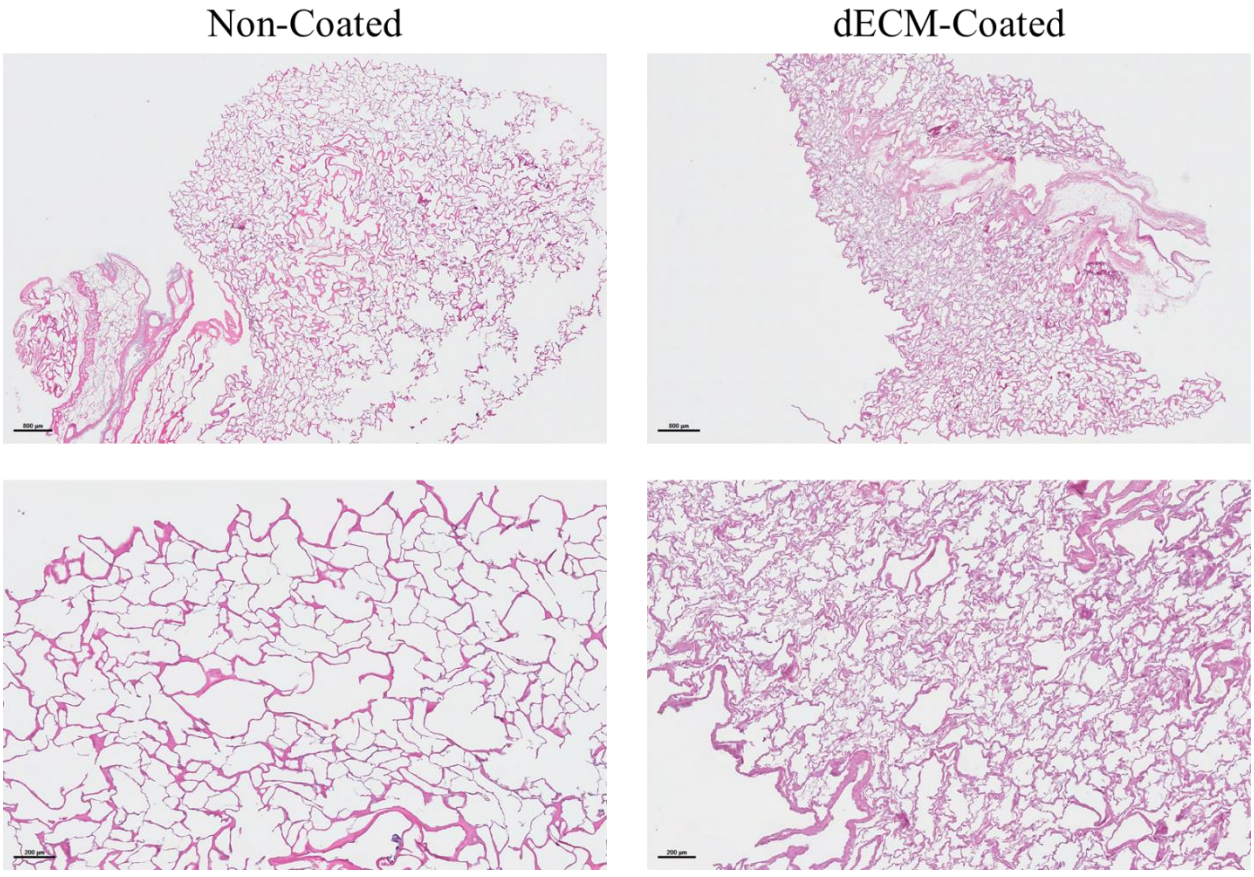

Figure 6.1. dECM coating deposition in decellularized rat lungs. H & E staining of non-coated and dECM-coated rat lungs showing ECM distribution within the alveoli and airway structures.

Scale bar represents 800 μm in the low magnification images (top) and 200 μm in the higher magnification images (bottom).

Non-bioreactor culture of dECM coated decellularized mouse lungs

A preliminary recellularization study was done using decellularized mouse lungs with human alveolar basal adenocarcinoma cells (A549s) to assess attachment and proliferation. Picogreen DNA quantification was performed after 4 and 7 days of culture with ECM coated and non-coated mice lungs (Figure 6.2). The increase between dECM coated lungs and the control lungs was not significant after just 4 days, but after 7 days there was a significant increase in proliferation. This preliminary data supports our hypothesis that dECM may increase epithelial attachment and proliferation.

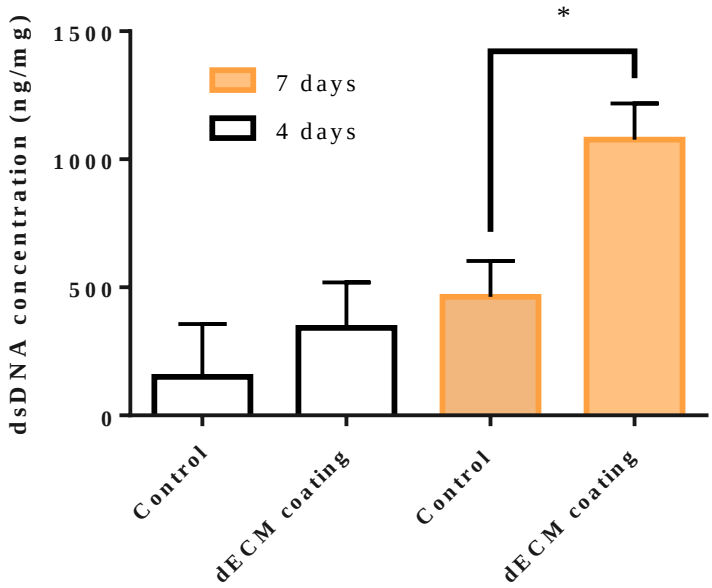

Figure 6.2. Picogreen dsDNA quantification of A549's cultured in decellularized lungs. dECM-coated or non-coated mouse lungs were cultured for 4 and 7 days on a rocker. Each group

has a minimum sample size of 2-3 (4-day control has a sample size of 2) and is represented as mean +/- standard deviation.

MLE12 recellularization with dECM coatings

After 5 days of culture in the dynamic bioreactor system, the recellularized rat lungs that were coated with a dECM coating before MLE12 seeding showed higher cell viability throughout the lung, demonstrated by pink resazurin dye throughout the lung at day 3 and 5. Recellularization without the dECM coating has regions will severely reduce tissue viability at day 3 and decreases further by day 5 (Figure 6.3A). Resazurin absorbance of the tracheal perfusate by microplate reader confirmed increased absorbance of resazurin caused by increased cellular metabolic activity (Figure 6.3B). Picogreen dsDNA quantification (Figure 6.4) further confirms these findings with more cells engrafted within the lung at the conclusion of the 5-day culture.

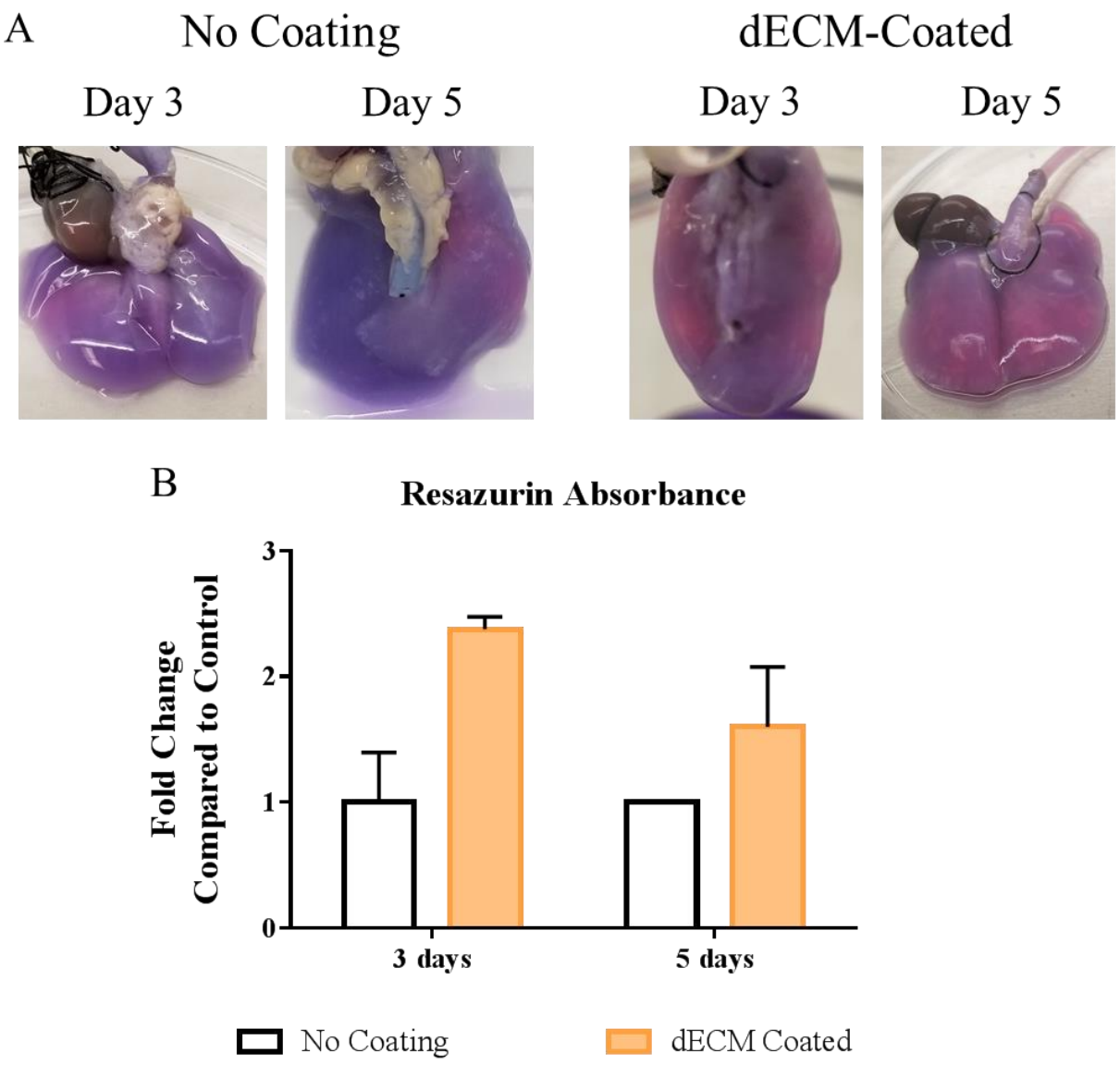

Figure 6.3. **MLE12 resazurin viability with dECM coatings.** (A) Representative images of regenerated lungs with and without dECM coatings after resazurin perfusion (pink indicates viable regions). (B) Resazurin perfusate absorbance quantification after collection from the tracheal cannula. $N \geq 2$.

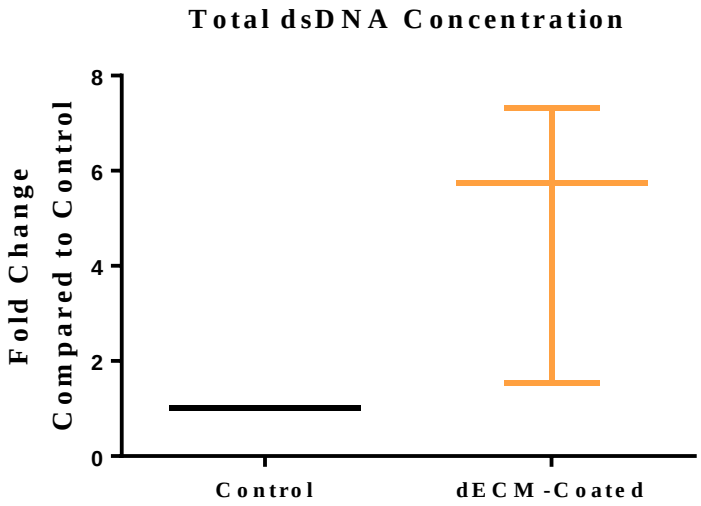

Figure 6.4. Picogreen dsDNA concentration within dECM-coated and non-coated lungs. MLE12s were recellularized and cultured for 5 days. N=1 for non-coated controls and N=3 for dECM-Coated lungs. Data is represented as mean +/- the minimum and maximum.

To then investigate the morphology of the cultured cells and the overall distribution within the lung, histological sections were stained with H&E (Figure 6.5). The culture within dECM-coated lungs exhibited increases in cells attached throughout the lung, with denser regions of cells seen in the superior regions. Even in areas with lower cell density, cells were found anchored to the walls of many alveoli, with some instances of cell clumping in the alveolar and airway lumens.

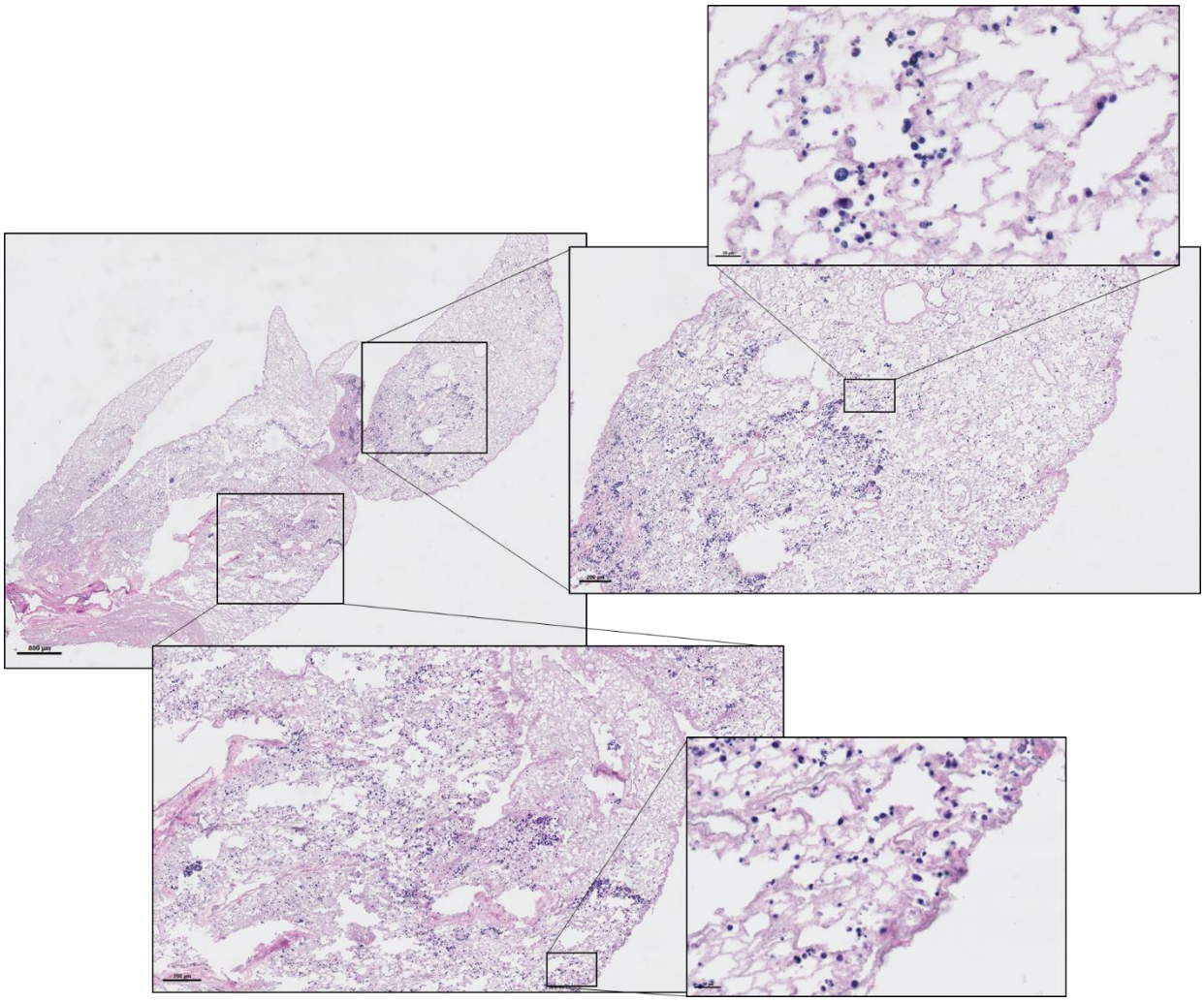

Figure 6.5. Histological analysis of dECM coated recellularized lung after 5 days of perfusion/ventilation culture. Representative bright-field images from dECM-coated lungs cultured with MLE12 cells are shown with the magnification of several regions. Scale bars are 800 μm, 200 μm, and 20 μm with increasing magnification, respectively.

Lastly, to delve further into the function of the cells within the recellularized lungs, we evaluated cell junction gene expression and dextran permeability. MLE12 cells cultured in dECM-coated lungs had increased gene expression of AF-6, Claudin 18, and E-cadherin compared to non-coated lungs (Figure 6.6A), though more experiments are needed to reach a definitive conclusion.

We then performed a dextran *ex vivo* permeability assay by administering a dextran and PBS solution to the lung and collecting the perfusate from the pulmonary artery. PBS was rinsed through the trachea 5 to 6 more times to retrieve any dextran that had permeabilized to the vasculature. dECM-coated lungs had less dextran pass into the vasculature immediately after dextran perfusion compared to non-coated lungs. With additional PBS rinsing fractions, they both had similar levels of dextran permeability.

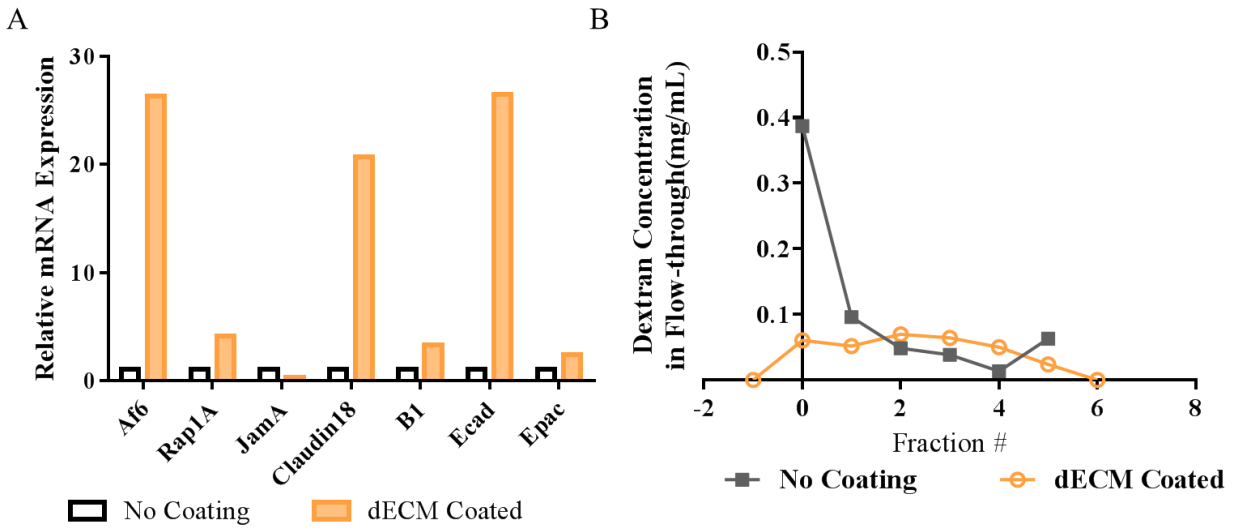

Figure 6.6. Cell-junction gene expression and dextran permeability of dECM coated recellularized lungs. (A) qPCR analysis after 5 days of perfusion/ventilation culture. (B) Dextran permeability after perfusion of dextran into the trachea and collection of flow throughout of the PA. Fraction number indicates the number of PBS washes before and after initial dextran perfusion. Data are represented as the mean with a sample size of 1.

6.4 Discussion

Alterations to dECM composition by decellularization detergents can disrupt the tissue-specific ECM profile that cells are accustom to *in vivo*. Adverse cellular responses to abnormal ECM environments can lead to the failure of regenerative materials [216]–[218]. Minor variations in ECM composition are expected between all non-homologous tissues throughout the body and are sensed by cells to properly redirect cell fate [53], [219], [220]. Even with tissue matching, decellularization can disrupt the matrix component ratio [211] in regions of the tissue that are repetitively and directly exposed to decellularization chemicals. Within decellularized lungs, the most damaged ECM region would be the BM because of its proximity to harsh chemicals. Since the structure and composition of the BM ECM is radically different the connective tissue within the submucosal layer [221], [222], seeding epithelium into decellularized lungs that have BM ECM partially removed could interrupt epithelial barrier formation. For these reasons, in this chapter, we have attempted to concentrate the tissue-specific matrix and apply it to decellularized lungs in a dense matrix coating before epithelial culture.

Preliminary studies utilizing the dECM coating with the non-bioreactor culture of decellularized lungs with A549 cells validated the hypothesis that even with basic culture methods, dECM can increase cell viability within recellularized lungs. Overall assessments of recellularization efficiency with dECM coatings by resazurin staining and Picogreen dsDNA quantification also showed that dECM coatings foster epithelial attachment and proliferation within a 3D whole organ system. A more detailed investigation into the reasons for increased recellularization by histological staining shows deposition of the dECM coating throughout the lung and increase cell attachment. The enhanced attachment could be attributed to overall increases in scaffolding for cells to attach to or the diversification of biochemical cues promoting attachment.

Some airway structures and alveoli show more dECM within the lumen of the airway and alveoli, indicating that the concentration of dECM may need to be reduced or rinsing procedures should be modified to decrease deposition. Similar studies applying collagen and Matrigel coatings to decellularized lungs show comparable matrix deposition and increased alveolar cell differentiation with ECM coatings [88], indicating that, even with alveolar and airway filling, additional tissue-specific ECM can be beneficial for cell attachment or stabilizing cells within the airways and alveoli during culture.

Also of interest was determining whether the dECM coatings could aid in barrier formation as seen *in vitro*. Preliminary gene expression studies show that cells are exhibiting characteristic epithelial gene expression and may be preparing junction complexes for barrier formation. Decreases in dextran permeability with dECM coatings are also promising evidence to support this hypothesis but are more likely caused by increased matrix or cellular coverage at this early stage in culture. Further implementation of strategies developed in Chapter 4 on barrier formation with dECM tissues may also improve functional outcomes of lung recellularization by supplementing laminin or other basement membrane proteins into the dECM pre-treatment coating.

In conclusion, dECM coatings increased attachment, epithelial junction gene expression, and overall function of the lung that will aid in faster maturation and remodeling of the tissue. More importantly, the added insights uncovered from this work about epithelial attachment and junction expression within decellularized tissues will help to inform future research with decellularized ECM.

CHAPTER 7: CONCLUSIONS AND FUTURE DIRECTIONS

Successful recellularization and culture of whole-organ grafts would expand the possibilities of regenerative medicine treatments exponentially. Increasing the number of available tissues for transplantation would also offer cures for hundreds of thousands of patients waiting for organ donations [223]. There is a critical need for innovation with this technology to overcome challenges that prevent final regeneration. Several main findings would help to complete this goal, including obtaining a more detailed understanding of cell-dECM interactions, development of long-term fully biomimetic culture systems, and enhanced cellular attachment of progenitor populations that can repopulate many cell phenotypes. The research within this dissertation aims to get a step further by answering some of these questions.

During this investigation, we have thoroughly characterized hydrogels and coatings derived from lung extracellular matrix to understand the self-assembly and processing of dECM. Understanding how protease digestion can alter hydrogel and coating mechanical and biochemical characteristics is a valuable tool within biomaterials research that has yet to be examined. These findings informed our application of a minimally digested dECM coating for investigations into alveolar epithelial-matrix interactions. Barrier function assays and junction characterization uncovered that dECM aids in the formation of the epithelial gas exchange barrier; however, dECM has been depleted of vital basement membrane proteins, mainly laminin, that need to be replenished for natural regulation of ZO-1 scaffolding proteins.

Each ECM protein plays a different but crucial role in the differentiation of every tissue, and that is why ECM is considered the “blueprint” of the lung. To exemplify that, a preliminary TEER study showing MLE12 barrier function on alveolar and airway enriched dECM shows that region-specific dECM can elicit increased barrier resistance from native cell types to that region

(Figure 7.1). Alveolar and airway enriched dECM was developed through careful dissection of each region after decellularization. Data finding increased barrier resistance on alveolar ECM sparks a need for future investigations into the composition of the dECM from the different tissues to inform dECM coating development. A logical next step within this research is to also apply similar systematic micro-level investigations to examine the effects of matrix proteins, such as GAGs and Collagen IV, in barrier formation, but also cellular differentiation and attachment.

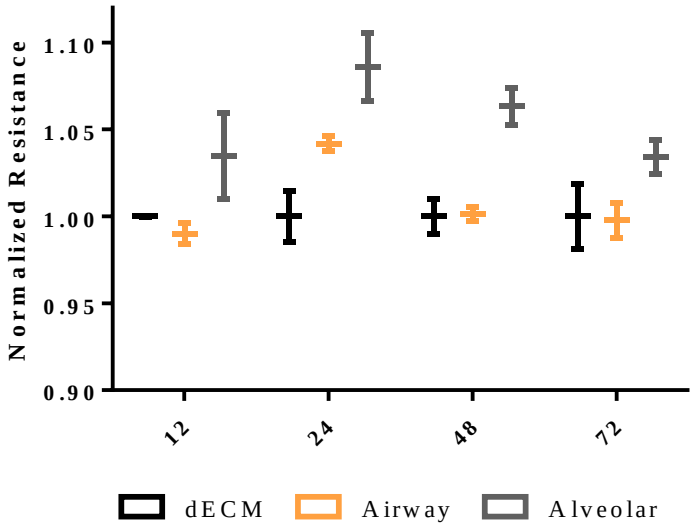

Figure 7.1. Alveolar-specific ECM increases barrier function. TEER of MLE12 cells culture on region-specific dECM coatings for 5 days. N=1 with the mean +/- standard deviation of 3 replicates shown.

Finally, this research applied our initial *in vitro* findings to our ultimate goal of improving a whole-organ regeneration model. We aimed to progress lung recellularization in two ways: 1) by developing cell seeding techniques for *ex vivo* lung culture and 2) revitalize the ECM composition at the surface of the airways and alveoli that have been depleted by harsh

decellularization chemicals. dECM coatings offer concentrated ECM from throughout the lung that can be used to replenish the basement membrane of decellularized lungs for re-epithelialization. Through this research, we developed a rotational seeding bioreactor and protocol for increased dispersal of cells throughout the lung. Secondly, we verified that dECM coatings are a promising technique to increase epithelial viability within *ex vivo* culture of decellularized lungs as a proof of concept study. The next stages of this research would be to apply the tailored dECM coatings to *ex vivo* culture with other identified recellularization investigations, such as stem cell differentiation. Bright-field images (Figure 7.2), TEER, and gene expression (Figure 4.8) of basal epithelial cells cultured for 10 days displays drastic differences in morphology and barrier formation on different dECM coatings. The limited investigation that this research has done into BESC barrier formation shows that the composition of dECM can elicit different behaviors from epithelial populations. Future experimentation is needed to fully understand the extent of BESC differentiation with these recellularization techniques *ex vivo*.

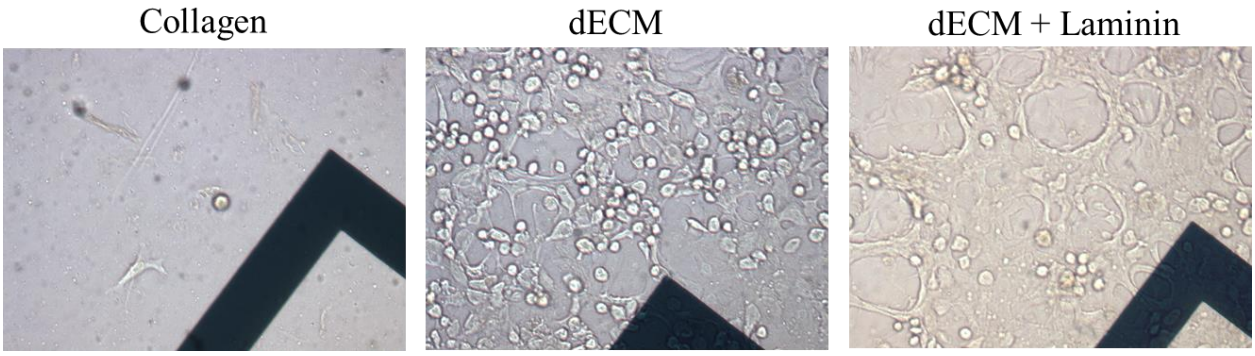

Figure 7.2. Basal epithelial stem cell (BESC) morphology varies with ECM composition. Bright-field images from 3 different coated ECIS (electrodes seen in images) wells cultured with BESCs for 10 days is shown.

Understanding this mechanism of alveolar junction reinforcement not only improves the recellularization of ECM lung scaffolds but will also lead to a broader understanding of ECM protein interaction with epithelial cells *in vitro* and potential mediators for therapeutic targets. Increased function of recellularized lungs would be a significant step towards a lung replacement strategy for the thousands of patients with end-stage lung pathologies. To bring this research even closer to producing a viable lung replacement, these techniques can be scaled-up to a human lung with the help of established systems in other laboratories.

APPENDIX A

A1. Rotation Bioreactor Arduino Code

```
//**********************MAIN POWER SWITCH MUST BE IN ON POSITION TO
UPLOAD*****************************
// Used to check if switches have changed
int PREVIOUS_STATE=0;
int PRESENT_STATE=0;
// Inputs
int SwSA=7; // inputs for the left pin - this pin is backwards- HIGH is down
int SwSB=4; // inputs for the right pin - this pin is correct- HIGH is up
//leds
int Speed0_LED=8;
int Speed1_LED=9;
int Speed2_LED=10;
int Speed3_LED=11;
int main_power=0;
const int stepPin=13; //dictates the step size
const int dirPin=12;  //dictates the direction
const int onoff=2;
int move_count=0;
```

```
unsigned long main_time=millis();
unsigned long break_time= millis();
unsigned long HOLD_TIME=0;

void setup()
{Serial.begin(9600);
pinMode(main_power, OUTPUT);
pinMode(Speed0_LED, OUTPUT);
pinMode(Speed1_LED, OUTPUT);
pinMode(Speed2_LED, OUTPUT);
pinMode(Speed3_LED, OUTPUT);
pinMode(SwSA, INPUT);
pinMode(SwSB, INPUT);
pinMode(dirPin, OUTPUT);
pinMode(stepPin, OUTPUT);
pinMode(onoff, OUTPUT);
}

/// ***********************************************
///  Overall main power and code
/// ***********************************************
void loop()
{
```

```
if (digitalRead(main_power) == true)
      {
      reactor_state();
      digitalWrite(onoff, HIGH);
      }
      else
      {
      digitalWrite(onoff, HIGH);
      Serial.print(" system off \n");
      main_time=millis();
      move_count=0;
      case_leds(LOW, LOW, LOW, LOW);
      }
      delay(100);
}

/// ********************************************
///  Switch matching
/// ********************************************

void reactor_state()
{
```

```
      PRESENT_STATE= switch_inputs(digitalRead(SwSA), digitalRead(SwSB));    // converts
switches to cases for state machine
      if (PREVIOUS_STATE != PRESENT_STATE)
      {
       main_time=millis();
       move_count=0;
       HOLD_TIME=0;
       PREVIOUS_STATE=PRESENT_STATE;              // Switch to the new State to monitor
the switches
       Serial.print(" reset state");
      }
      else
      {
        case_outputs(PRESENT_STATE);              // state machine to run the system
       ///Serial.print("same state");
      }
return;
}

/// ***********************************************
// defines rotation speeds and directions
/// ***********************************************
```

```
void reactor_rotation(int deg, int stepP, int dirP, bool dir)
{
  delay(1000);                          //this gives a function to make the motor move that will have a
set rate
  digitalWrite(dirP, dir);
  delay(1000);
  for(int x=0; x < deg; x++)
    {
      digitalWrite(stepP, HIGH);
      delay(10);              //THis is where you set the rate of the turn. You can increase the time
between on and off
      digitalWrite(stepP, LOW);
      delay(10);  //delay(100);
    }
}

/// ***********************************************
// asigns led to switches
/// ***********************************************
void case_leds(bool speed0_led,  bool speed1_led, bool speed2_led, bool speed3_led) //this gives
a function for the lights
{     digitalWrite(Speed0_LED, speed0_led);
      digitalWrite(Speed1_LED, speed1_led);
```

```
    digitalWrite(Speed2_LED, speed2_led);
    digitalWrite(Speed3_LED, speed3_led);
}

/// ***************************************
///  Switch cases (roatation schemes)
/// ***************************************
void case_outputs(int PRESENT_STATE)
 {
  ///Serial.print("  00  \n");
  switch(PRESENT_STATE)
//int would return a value
  {
    case 0:  // pin9 orange both down - This will rotate every 20 min
     {
        digitalWrite(onoff, HIGH);
        case_leds(LOW, HIGH, LOW, LOW);
        ///Serial.print("  0  \n");

        unsigned long time_since_break= millis()-break_time;
        if (time_since_break >= HOLD_TIME)
        {
            if (move_count == 0 || move_count ==8)
```

```
  {       delay(1200000); //20 min
          digitalWrite(onoff, LOW);
          Serial.print(" move_count0 \n");
          reactor_rotation(100, stepPin, dirPin, false);  //100= 180 degrees
          digitalWrite(onoff, HIGH);
          move_count+=1;
          break_time=millis();
          HOLD_TIME=1200000; //HOLD_TIME -change this for different wait times
          break;
  }
if (move_count == 1 || move_count ==9)
  {       digitalWrite(onoff, LOW);
          reactor_rotation(50, stepPin, dirPin, false);
          Serial.print(" move_count1 \n");
          digitalWrite(onoff, HIGH);
          move_count+=1;
          break_time=millis();
          HOLD_TIME=1200000;
          break;
  }
if (move_count == 2 || move_count ==10)
  {       digitalWrite(onoff, LOW);
          reactor_rotation(100, stepPin, dirPin, true);
```

```
        digitalWrite(onoff, HIGH);
        Serial.print(" move_count2 \n");
        move_count+=1;
        break_time=millis();
        HOLD_TIME=1200000;
        break;
    }
  if (move_count == 3 || move_count ==11)
    {     digitalWrite(onoff, LOW);
        reactor_rotation(125, stepPin, dirPin, true);
        digitalWrite(onoff, HIGH);
        Serial.print(" move_count3 \n");
        move_count+=1;
        break_time=millis();
        HOLD_TIME=1200000;
        break;
    }
  if (move_count == 4 || move_count ==12)
    {     digitalWrite(onoff, LOW);
        reactor_rotation(100, stepPin, dirPin, true);
        digitalWrite(onoff, HIGH);
        move_count+=1;
        Serial.print(" move_count4 \n");
```

```
        break_time=millis();
        HOLD_TIME=1200000;
        break;
    }
  if (move_count == 5 || move_count ==13)
    {     digitalWrite(onoff, LOW);
        reactor_rotation(150, stepPin, dirPin, true);
        digitalWrite(onoff, HIGH);
        Serial.print(" move_count5 \n");
        move_count+=1;
        break_time=millis();
        HOLD_TIME=1200000;
        break;
    }
  if (move_count == 6 || move_count ==14)
    {     digitalWrite(onoff, LOW);
        reactor_rotation(100, stepPin, dirPin, true);
        digitalWrite(onoff, HIGH);
        Serial.print(" move_count6 \n");
        move_count+=1;
        break_time=millis();
        HOLD_TIME=1200000;
        break;
```

```
            }
          if (move_count == 7 || move_count ==15)
            {       digitalWrite(onoff, LOW);
                    reactor_rotation(175, stepPin, dirPin, true);
                    digitalWrite(onoff, HIGH);
                    Serial.print(" move_count6 \n");
                    move_count+=1;
                    break_time=millis();
                    HOLD_TIME=0;
                    break;
            }
        }

        break;
    }

    case 1:  // pin9 yellowtop both down -- green light -This will rotate 40 degrees every 20
minutes
    {
        digitalWrite(onoff, HIGH);
        case_leds(LOW, LOW, LOW, HIGH);
        //int CASE1_HOLDTIME= 12000000; //20 min
        Serial.print("  1  \n");
```

```
    unsigned long time_since_break= millis()-break_time;
    if (time_since_break >= HOLD_TIME)
    {
          digitalWrite(onoff, LOW);
          reactor_rotation(22, stepPin, dirPin, false);
          digitalWrite(onoff, HIGH);
          move_count+=1;
          break_time=millis();
          HOLD_TIME=1200000;
          break;
     }
     break;
}

case 2:     //blue light - constant roation 1 turn per 30 min (12 degrees every minute)
{
    digitalWrite(onoff, HIGH);
    case_leds(LOW, LOW, HIGH, LOW);
    Serial.print("  2  \n");
    //int CASE2_HOLDTIME= 60000; // 1 minute
    unsigned long time_since_break= millis()-break_time;
    if (time_since_break >= HOLD_TIME)
    {
```

```
            digitalWrite(onoff, LOW);
            reactor_rotation(7, stepPin, dirPin, false);
            digitalWrite(onoff, HIGH);
            move_count+=1;
            break_time=millis();
            HOLD_TIME=60000;
            break;
    }
    break;
  }

case 3:  // rotate 360 wait 30 min rotate back 360 and repeat 3x
{
    digitalWrite(onoff, HIGH);
    case_leds(HIGH, LOW, LOW, LOW);
    Serial.print("  3  \n");
    //int CASE3_HOLDTIME= 1800000; // 30 minute
    unsigned long time_since_break= millis()-break_time;
    if (time_since_break >= HOLD_TIME)
    {
       if (move_count == 0 || move_count ==2 || move_count == 4)
           {digitalWrite(onoff, LOW);
            Serial.print(" move_count0 \n");
```

```
            reactor_rotation(200, stepPin, dirPin, false);
            digitalWrite(onoff, HIGH);
            move_count+=1;
            break_time=millis();
            HOLD_TIME=1800000;
            break;
           }
        if (move_count == 1 || move_count ==3 || move_count == 5)
           {digitalWrite(onoff, LOW);
            reactor_rotation(200, stepPin, dirPin, true);
            Serial.print(" move_count1 \n");
            digitalWrite(onoff, HIGH);
            move_count+=1;
            break_time=millis();
            HOLD_TIME=1800000;
            break;
           }
     }
    break;
 }

default:
{
```

```
      case_leds(LOW, LOW, LOW, LOW);
      break;
    }
  }
}



/// ***********************************************
// Tests the case that the switches are in
/// ***********************************************
int switch_inputs(bool swsa, bool swsb)   //this will read what position the switches are in and
give it a case number
{
  int S_C;
  if ((swsa) == HIGH && (swsb) == LOW)
  {
    S_C = 0;
  }
    if ((swsa) == HIGH && (swsb) == HIGH)
  {
    S_C = 1;
  }
```

```
  if ((swsa) == LOW && (swsb) == LOW)
  {
    S_C = 2;
  }

  if ((swsa) == LOW && (swsb) == HIGH)
  {
    S_C = 3;
  }

  return(S_C);
}
```

REFERENCES

[1] D. E. Wagner *et al.*, "Can Stem Cells be Used to Generate New Lungs? Ex Vivo Lung Bioengineering with Decellularized Whole Lung Scaffolds," *Respirol. Carlton Vic*, vol. 18, no. 6, Aug. 2013.

[2] T. H. Petersen *et al.*, "Tissue-Engineered Lungs for in Vivo Implantation," *Science*, vol. 329, no. 5991, pp. 538–541, Jul. 2010.

[3] H. Zhou *et al.*, "Bioengineering Human Lung Grafts on Porcine Matrix," *Ann. Surg.*, vol. Publish Ahead of Print, Jan. 2017.

[4] S. E. Gilpin *et al.*, "Perfusion decellularization of human and porcine lungs: Bringing the matrix to clinical scale," *J. Heart Lung Transplant.*, vol. 33, no. 3, pp. 298–308, Mar. 2014.

[5] Angela Panoskaltsis-Mortari, Ph.D., Andrew P. Price, B.S, and Kristen A. England, Ph.D., "Development of a Decellularized Lung Bioreactor System for Bioengineering the Lung: The Matrix Reloaded."

[6] JennaL. Balestrini and LauraE. Niklason, "Extracellular Matrix as a Driver for Lung Regeneration," *Ann. Biomed. Eng.*, vol. 43, no. 3, pp. 568–576, Mar. 2015.

[7] F. E. Uhl, D. E. Wagner, and D. J. Weiss, "Preparation of Decellularized Lung Matrices for Cell Culture and Protein Analysis," in *Fibrosis*, Humana Press, New York, NY, 2017, pp. 253–283.

[8] A. Sorkio, H. Hongisto, K. Kaarniranta, H. Uusitalo, K. Juuti-Uusitalo, and H. Skottman, "Structure and Barrier Properties of Human Embryonic Stem Cell–Derived Retinal Pigment Epithelial Cells Are Affected by Extracellular Matrix Protein Coating," *Tissue Eng. Part A*, vol. 20, no. 3–4, pp. 622–634, Sep. 2013.

[9] M. Koval, C. Ward, M. K. Findley, S. Roser-Page, M. N. Helms, and J. Roman, "Extracellular Matrix Influences Alveolar Epithelial Claudin Expression and Barrier Function," *Am. J. Respir. Cell Mol. Biol.*, vol. 42, no. 2, pp. 172–180, Feb. 2010.

[10] R. W. Bonvillain *et al.*, "Nonhuman Primate Lung Decellularization and Recellularization Using a Specialized Large-organ Bioreactor," *JoVE J. Vis. Exp.*, no. 82, pp. e50825–e50825, Dec. 2013.

[11] A. Crabbé *et al.*, "Recellularization of Decellularized Lung Scaffolds Is Enhanced by Dynamic Suspension Culture," *PLOS ONE*, vol. 10, no. 5, p. e0126846, May 2015.

[12] S. E. Gilpin *et al.*, "Fibrillin-2 and Tenascin-C bridge the age gap in lung epithelial regeneration," *Biomaterials*, vol. 140, pp. 212–219, Sep. 2017.

[13] S. E. Gilpin *et al.*, "Regenerative potential of human airway stem cells in lung epithelial engineering," *Biomaterials*, vol. 108, pp. 111–119, Nov. 2016.

[14] R. D. Kamm, "Airway Wall Mechanics," *Annu. Rev. Biomed. Eng.*, vol. 1, no. 1, pp. 47–72, Aug. 1999.

[15] A. Pozzi, P. D. Yurchenco, and R. V. Iozzo, "The nature and biology of basement membranes," *Matrix Biol.*, vol. 57–58, pp. 1–11, Jan. 2017.

[16] G. Burgstaller, B. Oehrle, M. Gerckens, E. S. White, H. B. Schiller, and O. Eickelberg, "The instructive extracellular matrix of the lung: basic composition and alterations in chronic lung disease," *Eur. Respir. J.*, vol. 50, no. 1, p. 1601805, Jul. 2017.

[17] C. Bonnans, J. Chou, and Z. Werb, "Remodelling the extracellular matrix in development and disease," *Nat. Rev. Mol. Cell Biol.*, vol. 15, no. 12, pp. 786–801, Dec. 2014.

[18] M. D. Shoulders and R. T. Raines, "COLLAGEN STRUCTURE AND STABILITY," *Annu. Rev. Biochem.*, vol. 78, pp. 929–958, 2009.

[19] J. Bella, “Collagen structure: new tricks from a very old dog,” *Biochem. J.*, vol. 473, no. 8, pp. 1001–1025, Apr. 2016.
[20] J. Bella and D. J. S. Hulmes, “Fibrillar Collagens,” in *Fibrous Proteins: Structures and Mechanisms*, D. A. D. Parry and J. M. Squire, Eds. Cham: Springer International Publishing, 2017, pp. 457–490.
[21] B. Bätge, C. Winter, H. Notbobm, Y. Acil, J. Brinckmann, and P. K. Müller, “Glycosylation of Human Bone Collagen I in Relation to Lysylhydroxylation and Fibril Diameter,” *J. Biochem. (Tokyo)*, vol. 122, no. 1, pp. 109–115, 1997.
[22] K. E. Kadler, A. Hill, and E. G. Canty-Laird, “Collagen fibrillogenesis: fibronectin, integrins, and minor collagens as organizers and nucleators,” *Curr. Opin. Cell Biol.*, vol. 20, no. 5, pp. 495–501, Oct. 2008.
[23] T. Lisman *et al.*, “A single high-affinity binding site for von Willebrand factor in collagen III, identified using synthetic triple-helical peptides,” *Blood*, vol. 108, no. 12, pp. 3753–3756, Dec. 2006.
[24] A. D. Konitsiotis, N. Raynal, D. Bihan, E. Hohenester, R. W. Farndale, and B. Leitinger, “Characterization of High Affinity Binding Motifs for the Discoidin Domain Receptor DDR2 in Collagen,” *J. Biol. Chem.*, vol. 283, no. 11, pp. 6861–6868, Mar. 2008.
[25] S. W. Manka *et al.*, “Structural insights into triple-helical collagen cleavage by matrix metalloproteinase 1,” *Proc. Natl. Acad. Sci.*, vol. 109, no. 31, pp. 12461–12466, Jul. 2012.
[26] E. G. Canty and K. E. Kadler, “Procollagen trafficking, processing and fibrillogenesis,” *J. Cell Sci.*, vol. 118, no. 7, pp. 1341–1353, Apr. 2005.
[27] Y. Zhou *et al.*, “Extracellular matrix in lung development, homeostasis and disease,” *Matrix Biol.*, Mar. 2018.
[28] Y.-M. Lin, A. Zhang, H. J. Rippon, A. Bismarck, and A. E. Bishop, “Tissue Engineering of Lung: The Effect of Extracellular Matrix on the Differentiation of Embryonic Stem Cells to Pneumocytes,” *Tissue Eng. Part A*, vol. 16, no. 5, pp. 1515–1526, Dec. 2009.
[29] B. Alberts, A. Johnson, J. Lewis, M. Raff, K. Roberts, and P. Walter, “The Extracellular Matrix of Animals,” 2002.
[30] G.-M. B, P. Cs, S. Pb, G. Mg, M.-F. M, and R. Mjg, “The Role of the Basal Lamina in Nerve Regeneration,” *J. Cytol. Histol.*, vol. 7, no. 4, Nov. 2016.
[31] D. Sheppard, “Functions of Pulmonary Epithelial Integrins: From Development to Disease,” *Physiol. Rev.*, vol. 83, no. 3, pp. 673–686, Jul. 2003.
[32] D. Sheppard, “Airway Epithelial Integrins: Why So Many?,” *Am. J. Respir. Cell Mol. Biol.*, vol. 19, no. 3, pp. 349–351, Sep. 1998.
[33] H. J. Kim, D. H. Ingbar, and C. A. Henke, “Integrin mediation of type II cell adherence to provisional matrix proteins,” *Am. J. Physiol.-Lung Cell. Mol. Physiol.*, vol. 271, no. 2, pp. L277–L286, Aug. 1996.
[34] J.-P. Xiong *et al.*, “Crystal Structure of the Extracellular Segment of Integrin αVβ3 in Complex with an Arg-Gly-Asp Ligand,” *Science*, vol. 296, no. 5565, pp. 151–155, Apr. 2002.
[35] N. M. Nguyen and R. M. Senior, “Laminin isoforms and lung development: All isoforms are not equal,” *Dev. Biol.*, vol. 294, no. 2, pp. 271–279, Jun. 2006.
[36] J. H. Miner *et al.*, “The Laminin α Chains: Expression, Developmental Transitions, and Chromosomal Locations of α1-5, Identification of Heterotrimeric Laminins 8–11, and Cloning of a Novel α3 Isoform,” *J. Cell Biol.*, vol. 137, no. 3, pp. 685–701, May 1997.
[37] R. A. Pierce *et al.*, “Expression of Laminin α3, α4, and α5 Chains by Alveolar Epithelial Cells and Fibroblasts,” *Am. J. Respir. Cell Mol. Biol.*, vol. 19, no. 2, pp. 237–244, Aug. 1998.
[38] D. Vllasaliu, F. H. Falcone, S. Stolnik, and M. Garnett, “Basement membrane influences intestinal epithelial cell growth and presents a barrier to the movement of macromolecules,” *Exp. Cell Res.*, vol. 323, no. 1, pp. 218–231, Apr. 2014.

[39] J. M. Enserink *et al.*, "The cAMP-Epac-Rap1 Pathway Regulates Cell Spreading and Cell Adhesion to Laminin-5 through the α3β1 Integrin but Not the α6β4 Integrin," *J. Biol. Chem.*, vol. 279, no. 43, pp. 44889–44896, Oct. 2004.
[40] C.-M. Horejs *et al.*, "Biologically-active laminin-111 fragment that modulates the epithelial-to-mesenchymal transition in embryonic stem cells," *Proc. Natl. Acad. Sci.*, vol. 111, no. 16, pp. 5908–5913, Apr. 2014.
[41] A. I. Alford and D. E. Rannels, "Extracellular matrix fibronectin alters connexin43 expression by alveolar epithelial cells," *Am. J. Physiol.-Lung Cell. Mol. Physiol.*, vol. 280, no. 4, pp. L680–L688, Apr. 2001.
[42] W. P. Daley, S. B. Peters, and M. Larsen, "Extracellular matrix dynamics in development and regenerative medicine," *J. Cell Sci.*, vol. 121, no. 3, pp. 255–264, Feb. 2008.
[43] L. A. Griggs *et al.*, "Fibronectin fibrils regulate TGF-β1-induced Epithelial-Mesenchymal Transition," *Matrix Biol.*, vol. 60–61, pp. 157–175, Jul. 2017.
[44] D. K. Olivero and L. T. Furcht, "Type IV collagen, laminin, and fibronectin promote the adhesion and migration of rabbit lens epithelial cells in vitro," *Invest. Ophthalmol. Vis. Sci.*, vol. 34, no. 10, pp. 2825–2834, Sep. 1993.
[45] J. T. Hjelle, E. C. Carlson, K. Brendel, and E. Meezan, "Biosynthesis of basement membrane matrix by isolated rat renal glomeruli," *Kidney Int.*, vol. 15, no. 1, pp. 20–32, Jan. 1979.
[46] A. P. Price, K. A. England, A. M. Matson, B. R. Blazar, and A. Panoskaltsis-Mortari, "Development of a Decellularized Lung Bioreactor System for Bioengineering the Lung: The Matrix Reloaded," *Tissue Eng. Part A*, vol. 16, no. 8, pp. 2581–2591, Aug. 2010.
[47] H. C. Ott *et al.*, "Perfusion-decellularized matrix: using nature's platform to engineer a bioartificial heart," *Nat. Med.*, vol. 14, no. 2, p. 213, Feb. 2008.
[48] P. M. Crapo *et al.*, "Biologic scaffolds composed of central nervous system extracellular matrix," *Biomaterials*, vol. 33, no. 13, pp. 3539–3547, May 2012.
[49] P. M. Crapo, T. W. Gilbert, and S. F. Badylak, "An overview of tissue and whole organ decellularization processes," *Biomaterials*, vol. 32, no. 12, pp. 3233–3243, Apr. 2011.
[50] B. Schlingmann, S. A. Molina, and M. Koval, "Claudins: Gatekeepers of lung epithelial function," *Semin. Cell Dev. Biol.*, vol. 42, no. Supplement C, pp. 47–57, Jun. 2015.
[51] G. Li *et al.*, "Knockout Mice Reveal Key Roles for Claudin 18 in Alveolar Barrier Properties and Fluid Homeostasis," *Am. J. Respir. Cell Mol. Biol.*, vol. 51, no. 2, pp. 210–222, Mar. 2014.
[52] M. J. LaFemina *et al.*, "Claudin-18 Deficiency Results in Alveolar Barrier Dysfunction and Impaired Alveologenesis in Mice," *Am. J. Respir. Cell Mol. Biol.*, vol. 51, no. 4, pp. 550–558, May 2014.
[53] J. Cortiella *et al.*, "Influence of Acellular Natural Lung Matrix on Murine Embryonic Stem Cell Differentiation and Tissue Formation," *Tissue Eng. Part A*, vol. 16, no. 8, pp. 2565–2580, Apr. 2010.
[54] "The effect of matrix composition of 3D constructs on embryonic stem cell differentiation - ScienceDirect." [Online]. Available: https://www.sciencedirect.com/science/article/pii/S0142961205002899?via%3Dihub. [Accessed: 14-Apr-2019].
[55] O. Rosmark *et al.*, "Quantifying extracellular matrix turnover in human lung scaffold cultures," *Sci. Rep.*, vol. 8, no. 1, p. 5409, Apr. 2018.
[56] N. Higuita-Castro *et al.*, "Using a Novel Microfabricated Model of the Alveolar-Capillary Barrier to Investigate the Effect of Matrix Structure on Atelectrauma," *Sci. Rep.*, vol. 7, no. 1, p. 11623, Sep. 2017.
[57] L. M. Godin *et al.*, "Decreased Laminin Expression by Human Lung Epithelial Cells and Fibroblasts Cultured in Acellular Lung Scaffolds from Aged Mice," *PLOS ONE*, vol. 11, no. 3, p. e0150966, Mar. 2016.

[58] D. Sokocevic *et al.*, "The effect of age and emphysematous and fibrotic injury on the re-cellularization of de-cellularized lungs," *Biomaterials*, vol. 34, no. 13, pp. 3256–3269, Apr. 2013.
[59] L. Cao *et al.*, "Detection of an Integrin-Binding Mechanoswitch within Fibronectin during Tissue Formation and Fibrosis," *ACS Nano*, vol. 11, no. 7, pp. 7110–7117, Jul. 2017.
[60] K. A. Rickard, S. Shoji, J. R. Spurzem, and S. I. Rennard, "Attachment Characteristics of Bovine Bronchial Epithelial Cells to Extracellular Matrix Components," *Am. J. Respir. Cell Mol. Biol.*, vol. 4, no. 5, pp. 440–448, May 1991.
[61] C. T. Lefort, K. Wojciechowski, and D. C. Hocking, "N-cadherin Cell-Cell Adhesion Complexes Are Regulated by Fibronectin Matrix Assembly," *J. Biol. Chem.*, vol. 286, no. 4, pp. 3149–3160, Jan. 2011.
[62] C.-M. Horejs *et al.*, "Preventing tissue fibrosis by local biomaterials interfacing of specific cryptic extracellular matrix information," *Nat. Commun.*, vol. 8, p. 15509, Jun. 2017.
[63] F. Wang *et al.*, "Heterogeneity of claudin expression by alveolar epithelial cells," *Am. J. Respir. Cell Mol. Biol.*, vol. 29, no. 1, pp. 62–70, Jul. 2003.
[64] B. M. Young *et al.*, "An Electrospun Decellularized Lung Matrix Scaffold for Airway Smooth Muscle Culture," *ACS Biomater. Sci. Eng.*, Nov. 2017.
[65] B. Schoen *et al.*, "Electrospun Extracellular Matrix: Paving the Way to Tailor-Made Natural Scaffolds for Cardiac Tissue Regeneration," *Adv. Funct. Mater.*, vol. 27, no. 34, p. n/a-n/a, Sep. 2017.
[66] D. J. Rosario, G. C. Reilly, E. Ali Salah, M. Glover, A. J. Bullock, and S. Macneil, "Decellularization and sterilization of porcine urinary bladder matrix for tissue engineering in the lower urinary tract," *Regen. Med.*, vol. 3, no. 2, pp. 145–156, Mar. 2008.
[67] Z. Mosala Nezhad, A. Poncelet, L. de Kerchove, P. Gianello, C. Fervaille, and G. El Khoury, "Small intestinal submucosa extracellular matrix (CorMatrix®) in cardiovascular surgery: a systematic review," *Interact. Cardiovasc. Thorac. Surg.*, vol. 22, no. 6, pp. 839–850, Jun. 2016.
[68] T. W. Gilbert, D. B. Stolz, F. Biancaniello, A. Simmons-Byrd, and S. F. Badylak, "Production and characterization of ECM powder: implications for tissue engineering applications," *Biomaterials*, vol. 26, no. 12, pp. 1431–1435, Apr. 2005.
[69] M. Ali, A. K. Pr, J. J. Yoo, F. Zahran, A. Atala, and S. J. Lee, "A Photo-Crosslinkable Kidney ECM-Derived Bioink Accelerates Renal Tissue Formation," *Adv. Healthc. Mater.*, vol. 8, no. 7, p. e1800992, Apr. 2019.
[70] M. D. Santis *et al.*, "Development of a hybrid alginate-ECM hydrogel as a potential bioink for 3D bioprinting," *Eur. Respir. J.*, vol. 52, no. suppl 62, p. LSC-1090, Sep. 2018.
[71] L. T. Saldin, M. C. Cramer, S. S. Velankar, L. J. White, and S. F. Badylak, "Extracellular matrix hydrogels from decellularized tissues: Structure and function," *Acta Biomater.*, vol. 49, pp. 1–15, Feb. 2017.
[72] R. A. Pouliot *et al.*, "Development and characterization of a naturally derived lung extracellular matrix hydrogel," *J. Biomed. Mater. Res. A*, p. n/a-n/a, Apr. 2016.
[73] S. D. Sackett *et al.*, "Extracellular matrix scaffold and hydrogel derived from decellularized and delipidized human pancreas," *Sci. Rep.*, vol. 8, no. 1, p. 10452, Jul. 2018.
[74] S. B. Seif-Naraghi *et al.*, "Safety and Efficacy of an Injectable Extracellular Matrix Hydrogel for Treating Myocardial Infarction," *Sci. Transl. Med.*, vol. 5, no. 173, pp. 173ra25-173ra25, Feb. 2013.
[75] T. D. Johnson *et al.*, "Human versus porcine tissue sourcing for an injectable myocardial matrix hydrogel," *Biomater. Sci.*, vol. 2, no. 5, pp. 735–744, Apr. 2014.
[76] L. Zhang *et al.*, "Effect of an Inductive Hydrogel Composed of Urinary Bladder Matrix Upon Functional Recovery Following Traumatic Brain Injury," *Tissue Eng. Part A*, vol. 19, no. 17–18, pp. 1909–1918, Apr. 2013.

[77] J. A. Claudio-Rizo, J. Delgado, I. A. Quintero-Ortega, J. L. Mata-Mata, and B. Mendoza-Novelo, "Decellularized ECM-Derived Hydrogels: Modification and Properties," *Hydrogels*, Aug. 2018.
[78] J. B. Orens and E. R. Garrity, "General Overview of Lung Transplantation and Review of Organ Allocation," *Proc. Am. Thorac. Soc.*, vol. 6, no. 1, pp. 13–19, Jan. 2009.
[79] National Center for Health Statistics, "Health, United States, 2016: With Chartbook on Long-term Trends in Health.," *CDC*, Hyattsville, MD, May-2017.
[80] "Data resources | UNOS." [Online]. Available: https://unos.org/data/data-resources/. [Accessed: 28-Nov-2017].
[81] M. Shafa *et al.*, "Human induced pluripotent stem cell–derived lung progenitor and alveolar epithelial cells attenuate hyperoxia-induced lung injury," *Cytotherapy*, vol. 20, no. 1, pp. 108–125, Jan. 2018.
[82] K. A. A. Schilders *et al.*, "Regeneration of the lung: Lung stem cells and the development of lung mimicking devices," *Respir. Res.*, vol. 17, p. 44, Apr. 2016.
[83] A. V. Le *et al.*, "Efficient and Functional Endothelial Repopulation of Whole Lung Organ Scaffolds," *ACS Biomater. Sci. Eng.*, vol. 3, no. 9, pp. 2000–2010, Sep. 2017.
[84] H. C. Ott *et al.*, "Regeneration and orthotopic transplantation of a bioartificial lung," *Nat. Med.*, vol. 16, no. 8, p. 927, Aug. 2010.
[85] E. Chavakis, C. Urbich, and S. Dimmeler, "Homing and engraftment of progenitor cells: A prerequisite for cell therapy," *J. Mol. Cell. Cardiol.*, vol. 45, no. 4, pp. 514–522, Oct. 2008.
[86] R. L. Heise, P. A. Link, and L. Farkas, "From Here to There, Progenitor Cells and Stem Cells Are Everywhere in Lung Vascular Remodeling," *Front. Pediatr.*, vol. 4, Aug. 2016.
[87] G. Hatachi *et al.*, "Transplantation of bioengineered rat lungs recellularized with endothelial and adipose-derived stromal cells," *Sci. Rep.*, vol. 7, no. 1, p. 8447, Dec. 2017.
[88] T. Jensen *et al.*, "A rapid lung de-cellularization protocol supports embryonic stem cell differentiation in vitro and following implantation," *Tissue Eng. Part C Methods*, vol. 18, no. 8, pp. 632–646, Aug. 2012.
[89] A. B. Daly *et al.*, "Initial Binding and Recellularization of Decellularized Mouse Lung Scaffolds with Bone Marrow-Derived Mesenchymal Stromal Cells," *Tissue Eng. Part A*, vol. 18, no. 1–2, pp. 1–16, Jan. 2012.
[90] M. Ghaedi *et al.*, "Bioengineered lungs generated from human iPSCs-derived epithelial cells on native extracellular matrix," *J. Tissue Eng. Regen. Med.*, vol. 12, no. 3, pp. e1623–e1635, 2018.
[91] J. E. Nichols *et al.*, "Giving new life to old lungs: methods to produce and assess whole human paediatric bioengineered lungs," *J. Tissue Eng. Regen. Med.*, vol. 11, no. 7, pp. 2136–2152, Jul. 2017.
[92] S. Lecht *et al.*, "Enhanced reseeding of decellularized rodent lungs with mouse embryonic stem cells," *Biomaterials*, vol. 35, no. 10, pp. 3252–3262, Mar. 2014.
[93] J. E. Nichols *et al.*, "Production and transplantation of bioengineered lung into a large-animal model," *Sci. Transl. Med.*, vol. 10, no. 452, p. eaao3926, Aug. 2018.
[94] C. T. Stabler *et al.*, "Enhanced Re-Endothelialization of Decellularized Rat Lungs," *Tissue Eng. Part C Methods*, vol. 22, no. 5, pp. 439–450, May 2016.
[95] X. Ren *et al.*, "Engineering pulmonary vasculature in decellularized rat and human lungs," *Nat. Biotechnol.*, vol. 33, no. 10, pp. 1097–1102, Oct. 2015.
[96] N. V. Dorrello *et al.*, "Functional vascularized lung grafts for lung bioengineering," *Sci. Adv.*, vol. 3, no. 8, p. e1700521, Aug. 2017.
[97] M. Zamir, J. E. Moore, H. Fujioka, and D. P. Gaver, "BIOFLUID MECHANICS OF SPECIAL ORGANS AND THE ISSUE OF SYSTEM CONTROL," *Ann. Biomed. Eng.*, vol. 38, no. 3, pp. 1204–1215, Mar. 2010.

[98] F. Peták *et al.*, "Lung mechanical and vascular changes during positive- and negative-pressure lung inflations: importance of reference pressures in the pulmonary vasculature," *J. Appl. Physiol. Bethesda Md 1985*, vol. 106, no. 3, pp. 935–942, Mar. 2009.
[99] S. E. Gilpin, J. M. Charest, X. Ren, and H. C. Ott, "Bioengineering Lungs for Transplantation," *Thorac. Surg. Clin.*, vol. 26, no. 2, pp. 163–171, May 2016.
[100] M. S. B. Raredon *et al.*, "Biomimetic Culture Reactor for Whole-Lung Engineering," *BioResearch Open Access*, vol. 5, no. 1, pp. 72–83, Apr. 2016.
[101] T. H. Petersen, E. A. Calle, M. B. Colehour, and L. E. Niklason, "Bioreactor for the Long-Term Culture of Lung Tissue," *Cell Transplant.*, vol. 20, no. 7, pp. 1117–1126, Aug. 2011.
[102] A. Guyot and J. W. Hanrahan, "ATP release from human airway epithelial cells studied using a capillary cell culture system," *J. Physiol.*, vol. 545, no. Pt 1, pp. 199–206, Nov. 2002.
[103] "Biomimetic Culture Reactor for Whole-Lung Engineering." [Online]. Available: https://www.ncbi.nlm.nih.gov/pmc/articles/PMC4827315/. [Accessed: 14-Apr-2019].
[104] N. W. Karuri *et al.*, "Biological length scale topography enhances cell-substratum adhesion of human corneal epithelial cells," *J. Cell Sci.*, vol. 117, no. 15, pp. 3153–3164, Jul. 2004.
[105] "Culturing and Applications of Rotating Wall Vessel Bioreactor Derived 3D Epithelial Cell Models." [Online]. Available: https://www.ncbi.nlm.nih.gov/pmc/articles/PMC3567125/. [Accessed: 14-Apr-2019].
[106] E. A. Calle, T. H. Petersen, and L. E. Niklason, "Procedure for Lung Engineering," *J. Vis. Exp. JoVE*, no. 49, Mar. 2011.
[107] C. Zihni, C. Mills, K. Matter, and M. S. Balda, "Tight junctions: from simple barriers to multifunctional molecular gates," *Nat. Rev. Mol. Cell Biol.*, vol. 17, no. 9, p. nrm.2016.80, Jun. 2016.
[108] J. Cai, M. K. Culley, Y. Zhao, and J. Zhao, "The role of ubiquitination and deubiquitination in the regulation of cell junctions," *Protein Cell*, Oct. 2017.
[109] T. Sato *et al.*, "Regulation of the Assembly and Adhesion Activity of E-cadherin by Nectin and Afadin for the Formation of Adherens Junctions in Madin-Darby Canine Kidney Cells," *J. Biol. Chem.*, vol. 281, no. 8, pp. 5288–5299, Feb. 2006.
[110] C. E. Overgaard, L. A. Mitchell, and M. Koval, "Roles for claudins in alveolar epithelial barrier function," *Ann. N. Y. Acad. Sci.*, vol. 1257, no. 1, pp. 167–174, Jun. 2012.
[111] L. A. Mitchell *et al.*, "Junctional Adhesion Molecule A Promotes Epithelial Tight Junction Assembly to Augment Lung Barrier Function," *Am. J. Pathol.*, vol. 185, no. 2, pp. 372–386, Feb. 2015.
[112] L. Gonzalez-Mariscal, M. Quiros, M. Diaz-Coranguez, and P. Bautista, "Tight Junctions," 2012.
[113] K. Ebnet, "Organization of multiprotein complexes at cell–cell junctions," *Histochem. Cell Biol.*, vol. 130, no. 1, pp. 1–20, Jul. 2008.
[114] A. García-Ponce, S. Chánez Paredes, K. F. Castro Ochoa, and M. Schnoor, "Regulation of endothelial and epithelial barrier functions by peptide hormones of the adrenomedullin family," *Tissue Barriers*, vol. 4, no. 4, Aug. 2016.
[115] A. A. Birukova, P. Fu, J. Xing, and K. G. Birukov, "Rap1 mediates protective effects of iloprost against ventilator-induced lung injury," *J. Appl. Physiol.*, vol. 107, no. 6, pp. 1900–1910, Dec. 2009.
[116] J. M. Enserink *et al.*, "The cAMP-Epac-Rap1 Pathway Regulates Cell Spreading and Cell Adhesion to Laminin-5 through the α3β1 Integrin but Not the α6β4 Integrin," *J. Biol. Chem.*, vol. 279, no. 43, pp. 44889–44896, Oct. 2004.
[117] X. Cheng, Z. Ji, T. Tsalkova, and F. Mei, "Epac and PKA: a tale of two intracellular cAMP receptors," *Acta Biochim. Biophys. Sin.*, vol. 40, no. 7, pp. 651–662, Jul. 2008.
[118] F. Balzac *et al.*, "E-cadherin endocytosis regulates the activity of Rap1: a traffic light GTPase at the crossroads between cadherin and integrin function," *J. Cell Sci.*, vol. 118, no. 20, pp. 4765–4783, Oct. 2005.

[119] Monteiro Ana C. and Parkos Charles A., "Intracellular mediators of JAM-A–dependent epithelial barrier function," *Ann. N. Y. Acad. Sci.*, vol. 1257, no. 1, pp. 115–124, Jun. 2012.
[120] M. R. H. Kooistra, N. Dubé, and J. L. Bos, "Rap1: a key regulator in cell-cell junction formation," *J. Cell Sci.*, vol. 120, no. 1, pp. 17–22, Jan. 2007.
[121] E. Severson, A. Ivanov, L. Jiang, K. Mandell, A. Nusrat, and C. Parkos, "Junctional Adhesion Molecule A (JAM-A) signals through Afadin and Rap1," *FASEB J.*, vol. 20, no. 4, pp. A201–A201, Mar. 2006.
[122] T. Ooshio *et al.*, "Involvement of the Interaction of Afadin with ZO-1 in the Formation of Tight Junctions in Madin-Darby Canine Kidney Cells," *J. Biol. Chem.*, vol. 285, no. 7, pp. 5003–5012, Feb. 2010.
[123] K. Pajęcka, M. N. Nielsen, T. K. Hansen, and J. M. Williams, "The formation of quiescent glomerular endothelial cell monolayer in vitro is strongly dependent on the choice of extracellular matrix coating," *Exp. Cell Res.*, vol. 353, no. 1, pp. 16–25, 01 2017.
[124] A. Arai, Y. Nosaka, E. Kanda, K. Yamamoto, N. Miyasaka, and O. Miura, "Rap1 Is Activated by Erythropoietin or Interleukin-3 and Is Involved in Regulation of β1 Integrin-mediated Hematopoietic Cell Adhesion," *J. Biol. Chem.*, vol. 276, no. 13, pp. 10453–10462, Mar. 2001.
[125] A. Oldenburger, H. Maarsingh, and M. Schmidt, "Multiple Facets of cAMP Signalling and Physiological Impact: cAMP Compartmentalization in the Lung," *Pharmaceuticals*, vol. 5, no. 12, pp. 1291–1331, Dec. 2012.
[126] T. D. Johnson, S. Y. Lin, and K. L. Christman, "Tailoring material properties of a nanofibrous extracellular matrix derived hydrogel," *Nanotechnology*, vol. 22, no. 49, p. 494015, Nov. 2011.
[127] C. L. Hoop, J. Zhu, A. M. Nunes, D. A. Case, and J. Baum, "Revealing Accessibility of Cryptic Protein Binding Sites within the Functional Collagen Fibril," *Biomolecules*, vol. 7, no. 4, p. 76, Dec. 2017.
[128] G. A. D. Lullo, S. M. Sweeney, J. Körkkö, L. Ala-Kokko, and J. D. S. Antonio, "Mapping the Ligand-binding Sites and Disease-associated Mutations on the Most Abundant Protein in the Human, Type I Collagen," *J. Biol. Chem.*, vol. 277, no. 6, pp. 4223–4231, Feb. 2002.
[129] J. Heino, "Cellular Signaling by Collagen-Binding Integrins," in *I Domain Integrins*, D. Gullberg, Ed. Dordrecht: Springer Netherlands, 2014, pp. 143–155.
[130] P. A. Link, R. A. Pouliot, N. S. Mikhaiel, B. M. Young, and R. L. Heise, "Tunable Hydrogels from Pulmonary Extracellular Matrix for 3D Cell Culture," *JoVE J. Vis. Exp.*, no. 119, pp. e55094–e55094, Jan. 2017.
[131] R. Pouliot, "DEVELOPMENT AND CHARACTERIZATION OF LUNG DERIVED EXTRACELLULAR MATRIX HYDROGELS," *Theses Diss.*, Jan. 2016.
[132] Y. Hamuro, S. J. Coales, K. S. Molnar, S. J. Tuske, and J. A. Morrow, "Specificity of immobilized porcine pepsin in H/D exchange compatible conditions," *Rapid Commun. Mass Spectrom. RCM*, vol. 22, no. 7, pp. 1041–1046, Apr. 2008.
[133] J. Ahn, M.-J. Cao, Y. Q. Yu, and J. R. Engen, "Accessing the Reproducibility and Specificity of Pepsin and other Aspartic Proteases," *Biochim. Biophys. Acta*, vol. 1834, no. 6, pp. 1222–1229, Jun. 2013.
[134] S. Özbek, P. G. Balasubramanian, R. Chiquet-Ehrismann, R. P. Tucker, and J. C. Adams, "The Evolution of Extracellular Matrix," *Mol. Biol. Cell*, vol. 21, no. 24, pp. 4300–4305, Dec. 2010.
[135] J. A. McDonald, D. G. Kelley, and T. J. Broekelmann, "Role of fibronectin in collagen deposition: Fab' to the gelatin-binding domain of fibronectin inhibits both fibronectin and collagen organization in fibroblast extracellular matrix.," *J. Cell Biol.*, vol. 92, no. 2, pp. 485–492, Feb. 1982.
[136] K. E. Kubow *et al.*, "Mechanical forces regulate the interactions of fibronectin and collagen I in extracellular matrix," *Nat. Commun.*, vol. 6, p. 8026, Aug. 2015.
[137] M. C. Erat *et al.*, "Identification and structural analysis of type I collagen sites in complex with fibronectin fragments," *Proc. Natl. Acad. Sci.*, vol. 106, no. 11, pp. 4195–4200, Mar. 2009.

[138] K. Sekiguchi, S. Hakomori, M. Funahashi, I. Matsumoto, and N. Seno, “Binding of fibronectin and its proteolytic fragments to glycosaminoglycans. Exposure of cryptic glycosaminoglycan-binding domains upon limited proteolysis,” *J. Biol. Chem.*, vol. 258, no. 23, pp. 14359–14365, Dec. 1983.
[139] M. Pagano and M. Reboud-Ravaux, “Cryptic activities of fibronectin fragments, particularly cryptic proteases,” *Front. Biosci. Landmark Ed.*, vol. 16, pp. 698–706, Jan. 2011.
[140] A. Uemura *et al.*, “Effect of Plasmin on Laminin and Fibronectin During Plasmin-Assisted Vitrectomy,” *Arch. Ophthalmol.*, vol. 123, no. 2, pp. 209–213, Feb. 2005.
[141] A. M. Milan, R. V. Sugars, G. Embery, and R. J. Waddington, “Modulation of Collagen Fibrillogenesis by Dentinal Proteoglycans,” *Calcif. Tissue Int.*, vol. 76, no. 2, pp. 127–135, Feb. 2005.
[142] M. Németh-Csóka and A. Kovácsay, “The effect of glycosaminoglycans on the in vitro fibril formation of collagen type I and type III,” *Exp. Pathol. (Jena)*, vol. 17, no. 2, pp. 82–87, Jan. 1979.
[143] Y. Izu *et al.*, “Dysfunctional tendon collagen fibrillogenesis in collagen VI null mice,” *Matrix Biol.*, vol. 30, no. 1, pp. 53–61, Jan. 2011.
[144] D. R. Stamov, T. A. Khoa Nguyen, H. M. Evans, T. Pfohl, C. Werner, and T. Pompe, “The impact of heparin intercalation at specific binding sites in telopeptide-free collagen type I fibrils,” *Biomaterials*, vol. 32, no. 30, pp. 7444–7453, Oct. 2011.
[145] Y. Bi, P. Patra, and M. Faezipour, “Structure of collagen-glycosaminoglycan matrix and the influence to its integrity and stability,” in *2014 36th Annual International Conference of the IEEE Engineering in Medicine and Biology Society*, 2014, pp. 3949–3952.
[146] J. M. Mattson, R. Turcotte, and Y. Zhang, “Glycosaminoglycans contribute to extracellular matrix fiber recruitment and arterial wall mechanics,” *Biomech. Model. Mechanobiol.*, vol. 16, no. 1, pp. 213–225, Feb. 2017.
[147] A. J. Engler, S. Sen, H. L. Sweeney, and D. E. Discher, “Matrix Elasticity Directs Stem Cell Lineage Specification,” *Cell*, vol. 126, no. 4, pp. 677–689, 2006.
[148] Y. S. Pek, A. C. A. Wan, and J. Y. Ying, “The effect of matrix stiffness on mesenchymal stem cell differentiation in a 3D thixotropic gel,” *Biomaterials*, vol. 31, no. 3, pp. 385–391, Jan. 2010.
[149] H. Yuan, E. P. Ingenito, and B. Suki, “Dynamic properties of lung parenchyma: mechanical contributions of fiber network and interstitial cells,” *J. Appl. Physiol. Bethesda Md 1985*, vol. 83, no. 5, pp. 1420–1431; discussion 1418-1419, Nov. 1997.
[150] T. Jensen *et al.*, “A Rapid Lung De-cellularization Protocol Supports Embryonic Stem Cell Differentiation In Vitro and Following Implantation,” *https://home.liebertpub.com/tec*, 12-Apr-2012. [Online]. Available: https://www.liebertpub.com/doi/abs/10.1089/ten.TEC.2011.0584. [Accessed: 18-Dec-2018].
[151] S. Shojaie *et al.*, “Acellular Lung Scaffolds Direct Differentiation of Endoderm to Functional Airway Epithelial Cells: Requirement of Matrix-Bound HS Proteoglycans,” *Stem Cell Rep.*, vol. 4, no. 3, pp. 419–430, Feb. 2015.
[152] Y. Yuan *et al.*, “Epac agonist improves barrier function in iPSC-derived endothelial colony forming cells for whole organ tissue engineering,” *Biomaterials*, vol. 200, pp. 25–34, Apr. 2019.
[153] D. Tschumperlin, “Matrix, mesenchyme, and mechanotransduction,” *Ann Amer Thorac Soc*, vol. 12, Mar. 2015.
[154] A. A. Birukova, N. Zebda, P. Fu, V. Poroyko, I. Cokic, and K. G. Birukov, “Association between adherens junctions and tight junctions via Rap1 promotes barrier protective effects of oxidized phospholipids.,” *J. Cell. Physiol.*, vol. 226, no. 8, pp. 2052–2062, Aug. 2011.
[155] X. Wang *et al.*, “Activation of Epac alleviates inflammation and vascular leakage in LPS-induced acute murine lung injury,” *Biomed. Pharmacother.*, vol. 96, pp. 1127–1136, Dec. 2017.
[156] H. Lum, H. A. Jaffe, I. T. Schulz, A. Masood, A. RayChaudhury, and R. D. Green, “Expression of PKA inhibitor (PKI) gene abolishes cAMP-mediated protection to endothelial barrier dysfunction,” *Am. J. Physiol.*, vol. 277, no. 3, pp. C580-588, 1999.

[157] A. A. Birukova *et al.*, "Prostaglandins PGE2 and PGI2 promote endothelial barrier enhancement via PKA- and Epac1/Rap1-dependent Rac activation," *Exp. Cell Res.*, vol. 313, no. 11, pp. 2504–2520, Jul. 2007.
[158] A. A. Birukova, T. Zagranichnaya, E. Alekseeva, G. M. Bokoch, and K. G. Birukov, "Epac/Rap and PKA are novel mechanisms of ANP-induced Rac-mediated pulmonary endothelial barrier protection," *J. Cell. Physiol.*, vol. 215, no. 3, pp. 715–724, 2008.
[159] M. Laudette, H. Zuo, F. Lezoualc'h, and M. Schmidt, "Epac Function and cAMP Scaffolds in the Heart and Lung," *J. Cardiovasc. Dev. Dis.*, vol. 5, no. 1, Feb. 2018.
[160] S. Fukuhara *et al.*, "Cyclic AMP Potentiates Vascular Endothelial Cadherin-Mediated Cell-Cell Contact To Enhance Endothelial Barrier Function through an Epac-Rap1 Signaling Pathway," *Mol. Cell. Biol.*, vol. 25, no. 1, pp. 136–146, Jan. 2005.
[161] X. Cullere, S. K. Shaw, L. Andersson, J. Hirahashi, F. W. Luscinskas, and T. N. Mayadas, "Regulation of vascular endothelial barrier function by Epac, a cAMP-activated exchange factor for Rap GTPase," *Blood*, vol. 105, no. 5, pp. 1950–1955, Mar. 2005.
[162] A. A. Birukova, P. Fu, J. Xing, I. Cokic, and K. G. Birukov, "Lung endothelial barrier protection by iloprost in the 2-hit models of ventilator-induced lung injury (VILI) involves inhibition of Rho signaling," *Transl. Res. J. Lab. Clin. Med.*, vol. 155, no. 1, pp. 44–54, Jan. 2010.
[163] T. Sato *et al.*, "Regulation of the Assembly and Adhesion Activity of E-cadherin by Nectin and Afadin for the Formation of Adherens Junctions in Madin-Darby Canine Kidney Cells," *J. Biol. Chem.*, vol. 281, no. 8, pp. 5288–5299, Feb. 2006.
[164] A. C. Monteiro *et al.*, "JAM-A associates with ZO-2, afadin, and PDZ-GEF1 to activate Rap2c and regulate epithelial barrier function," *Mol. Biol. Cell*, vol. 24, no. 18, pp. 2849–2860, Jul. 2013.
[165] F. Rezaee *et al.*, "cAMP-dependent activation of protein kinase A attenuates respiratory syncytial virus-induced human airway epithelial barrier disruption," *PLoS ONE*, vol. 12, no. 7, Jul. 2017.
[166] B. Ponsioen *et al.*, "Detecting cAMP-induced Epac activation by fluorescence resonance energy transfer: Epac as a novel cAMP indicator," *EMBO Rep.*, vol. 5, no. 12, pp. 1176–1180, Dec. 2004.
[167] P. Conrotto, I. Yakymovych, M. Yakymovych, and S. Souchelnytskyi, "Interactome of Transforming Growth Factor-β Type I Receptor (TβRI): Inhibition of TGFβ Signaling by Epac1," *J. Proteome Res.*, vol. 6, no. 1, pp. 287–297, Jan. 2007.
[168] M. M. Murphy *et al.*, "Role of Rap1 in promoting sickle red blood cell adhesion to laminin via BCAM/LU," *Blood*, vol. 105, no. 8, pp. 3322–3329, Apr. 2005.
[169] M. J. Lorenowicz, J. van Gils, M. de Boer, P. L. Hordijk, and M. Fernandez-Borja, "Epac1-Rap1 signaling regulates monocyte adhesion and chemotaxis," *J. Leukoc. Biol.*, vol. 80, no. 6, pp. 1542–1552, 2006.
[170] "Our Science &Technology | Propagenix." [Online]. Available: http://www.propagenix.com/science-and-technology. [Accessed: 30-Nov-2017].
[171] "A Novel EPAC-Specific Inhibitor Suppresses Pancreatic Cancer Cell Migration and Invasion | Molecular Pharmacology." [Online]. Available: http://molpharm.aspetjournals.org/content/83/1/122.long. [Accessed: 21-May-2018].
[172] D. Guidolin, B. Nico, G. Mazzocchi, A. Vacca, G. G. Nussdorfer, and D. Ribatti, "Order and disorder in the vascular network," *Leukemia*, vol. 18, no. 11, pp. 1745–1750, Nov. 2004.
[173] E. Zudaire, L. Gambardella, C. Kurcz, and S. Vermeren, "A Computational Tool for Quantitative Analysis of Vascular Networks," *PLoS ONE*, vol. 6, no. 11, Nov. 2011.
[174] S. Li, Y. Qi, K. McKee, J. Liu, J. Hsu, and P. D. Yurchenco, "Integrin and dystroglycan compensate each other to mediate laminin-dependent basement membrane assembly and epiblast polarization," *Matrix Biol.*, vol. 57–58, pp. 272–284, Jan. 2017.

[175] K. M. Hodivala-Dilke, C. M. DiPersio, J. A. Kreidberg, and R. O. Hynes, "Novel Roles for α3β1 Integrin as a Regulator of Cytoskeletal Assembly and as a Trans-dominant Inhibitor of Integrin Receptor Function in Mouse Keratinocytes," *J. Cell Biol.*, vol. 142, no. 5, pp. 1357–1369, Sep. 1998.
[176] C. Margadant, K. Raymond, M. Kreft, N. Sachs, H. Janssen, and A. Sonnenberg, "Integrin α3β1 inhibits directional migration and wound re-epithelialization in the skin," *J. Cell Sci.*, vol. 122, no. 2, pp. 278–288, Jan. 2009.
[177] Y. Li *et al.*, "α1-antitrypsin promotes lung adenocarcinoma metastasis through upregulating fibronectin expression," *Int. J. Oncol.*, vol. 50, no. 6, pp. 1955–1964, Jun. 2017.
[178] B. Srinivasan, A. R. Kolli, M. B. Esch, H. E. Abaci, M. L. Shuler, and J. J. Hickman, "TEER measurement techniques for in vitro barrier model systems," *J. Lab. Autom.*, vol. 20, no. 2, pp. 107–126, Apr. 2015.
[179] N. D. Gallant, K. E. Michael, and A. J. García, "Cell adhesion strengthening: contributions of adhesive area, integrin binding, and focal adhesion assembly," *Mol. Biol. Cell*, vol. 16, no. 9, pp. 4329–4340, Sep. 2005.
[180] W. H. Ziegler, R. C. Liddington, and D. R. Critchley, "The structure and regulation of vinculin," *Trends Cell Biol.*, vol. 16, no. 9, pp. 453–460, Sep. 2006.
[181] K. Ebnet, C. U. Schulz, M.-K. M. zu Brickwedde, G. G. Pendl, and D. Vestweber, "Junctional Adhesion Molecule (JAM) interacts with the PDZ domain containing proteins AF-6 and ZO-1," *J. Biol. Chem.*, Jun. 2000.
[182] S. Garrido-Urbani, P. F. Bradfield, and B. A. Imhof, "Tight junction dynamics: the role of junctional adhesion molecules (JAMs)," *Cell Tissue Res.*, vol. 355, no. 3, pp. 701–715, Mar. 2014.
[183] A. B. Zhadanov *et al.*, "Absence of the tight junctional protein AF-6 disrupts epithelial cell–cell junctions and cell polarity during mouse development," *Curr. Biol.*, vol. 9, pp. 880-NaN, 1999.
[184] A. S. Fanning, C. M. Van Itallie, and J. M. Anderson, "Zonula occludens-1 and -2 regulate apical cell structure and the zonula adherens cytoskeleton in polarized epithelia," *Mol. Biol. Cell*, vol. 23, no. 4, pp. 577–590, Dec. 2011.
[185] J. Ikenouchi, K. Umeda, S. Tsukita, M. Furuse, and S. Tsukita, "Requirement of ZO-1 for the formation of belt-like adherens junctions during epithelial cell polarization," *J. Cell Biol.*, vol. 176, no. 6, pp. 779–786, Mar. 2007.
[186] B. Schlingmann *et al.*, "Regulation of claudin/zonula occludens-1 complexes by hetero-claudin interactions," *Nat. Commun.*, vol. 7, p. 12276, Jul. 2016.
[187] W. Zuo *et al.*, "$p63^{+}Krt5^{+}$ distal airway stem cells are essential for lung regeneration," *Nature*, vol. 517, no. 7536, pp. 616–620, Jan. 2015.
[188] K. U. Hong, S. D. Reynolds, S. Watkins, E. Fuchs, and B. R. Stripp, "Basal cells are a multipotent progenitor capable of renewing the bronchial epithelium," *Am. J. Pathol.*, vol. 164, no. 2, pp. 577–588, Feb. 2004.
[189] C. Hogan *et al.*, "Rap1 Regulates the Formation of E-Cadherin-Based Cell-Cell Contacts," *Mol. Cell. Biol.*, vol. 24, no. 15, pp. 6690–6700, Aug. 2004.
[190] L. S. Price, A. Hajdo-Milasinovic, J. Zhao, F. J. T. Zwartkruis, J. G. Collard, and J. L. Bos, "Rap1 Regulates E-cadherin-mediated Cell-Cell Adhesion," *J. Biol. Chem.*, vol. 279, no. 34, pp. 35127–35132, Aug. 2004.
[191] E. A. Severson, W. Y. Lee, C. T. Capaldo, A. Nusrat, and C. A. Parkos, "Junctional Adhesion Molecule A Interacts with Afadin and PDZ-GEF2 to Activate Rap1A, Regulate β1 Integrin Levels, and Enhance Cell Migration," *Mol. Biol. Cell*, vol. 20, no. 7, pp. 1916–1925, Apr. 2009.
[192] S. Asuri, J. Yan, N. C. Paranavitana, and L. A. Quilliam, "E-cadherin dis-engagement activates the Rap1 GTPase," *J. Cell. Biochem.*, vol. 105, no. 4, pp. 1027–1037, 2008.

[193] W.-J. Pannekoek, M. R. H. Kooistra, F. J. T. Zwartkruis, and J. L. Bos, "Cell–cell junction formation: The role of Rap1 and Rap1 guanine nucleotide exchange factors," *Biochim. Biophys. Acta BBA - Biomembr.*, vol. 1788, no. 4, pp. 790–796, Apr. 2009.
[194] X. Wang *et al.*, "Protective Effect of Quercetin in LPS-Induced Murine Acute Lung Injury Mediated by cAMP-Epac Pathway," *Inflammation*, vol. 41, no. 3, pp. 1093–1103, Jun. 2018.
[195] J. M. Charest *et al.*, "Design and validation of a clinical-scale bioreactor for long-term isolated lung culture," *Biomaterials*, vol. 52, pp. 79–87, Jun. 2015.
[196] "Production and transplantation of bioengineered lung into a large-animal model | Science Translational Medicine." [Online]. Available: https://stm-sciencemag-org.proxy.library.vcu.edu/content/10/452/eaao3926. [Accessed: 19-Apr-2019].
[197] Joan E Nichols, Stephanie P Vega, Lissenya B Argueta, and Jean A Niles, "Modeling the lung: Design and development of tissue engineered macro- and micro-physiologic lung models for research use."
[198] J. P. Wikswo *et al.*, "Scaling and systems biology for integrating multiple organs-on-a-chip," *Lab. Chip*, vol. 13, no. 18, pp. 3496–3511, Sep. 2013.
[199] I. Rizvi *et al.*, "Flow induces epithelial-mesenchymal transition, cellular heterogeneity and biomarker modulation in 3D ovarian cancer nodules," *Proc. Natl. Acad. Sci.*, vol. 110, no. 22, pp. E1974–E1983, May 2013.
[200] A. Taubenberger, D. A. Cisneros, J. Friedrichs, P.-H. Puech, D. J. Muller, and C. M. Franz, "Revealing Early Steps of α2β1 Integrin-mediated Adhesion to Collagen Type I by Using Single-Cell Force Spectroscopy," *Mol. Biol. Cell*, vol. 18, no. 5, pp. 1634–1644, Feb. 2007.
[201] L. Samuelson and D. A. Gerber, "Improved function and growth of pancreatic cells in a three-dimensional bioreactor environment," *Tissue Eng. Part C Methods*, vol. 19, no. 1, pp. 39–47, Jan. 2013.
[202] L. Adamo and G. García-Cardeña, "Directed Stem Cell Differentiation by Fluid Mechanical Forces," *Antioxid. Redox Signal.*, vol. 15, no. 5, pp. 1463–1473, Sep. 2011.
[203] G. A. Villalona *et al.*, "Cell-Seeding Techniques in Vascular Tissue Engineering," *Tissue Eng. Part B Rev.*, vol. 16, no. 3, pp. 341–350, Jun. 2010.
[204] M. S. B. Raredon, M. Ghaedi, E. A. Calle, and L. E. Niklason, "A Rotating Bioreactor for Scalable Culture and Differentiation of Respiratory Epithelium," *Cell Med.*, vol. 7, no. 3, pp. 109–121, Apr. 2015.
[205] C. Tresoldi *et al.*, "Alternating Air-Medium Exposure in Rotating Bioreactors Optimizes Cell Metabolism in 3D Novel Tubular Scaffold Polyurethane Foams," *J. Appl. Biomater. Funct. Mater.*, vol. 15, no. 2, pp. 122–132, Apr. 2017.
[206] X. Ren, L. F. Tapias, B. J. Jank, D. J. Mathisen, M. Lanuti, and H. C. Ott, "Ex vivo Non-invasive Assessment of Cell Viability and Proliferation in Bio-engineered Whole Organ Constructs," *Biomaterials*, vol. 52, pp. 103–112, Jun. 2015.
[207] J. S. Uzarski, M. D. DiVito, J. A. Wertheim, and W. M. Miller, "Essential Design Considerations for the Resazurin Reduction Assay to Noninvasively Quantify Cell Expansion within Perfused Extracellular Matrix Scaffolds," *Biomaterials*, vol. 129, pp. 163–175, Jun. 2017.
[208] L. Kass, J. T. Erler, M. Dembo, and V. M. Weaver, "Mammary epithelial cell: Influence of extracellular matrix composition and organization during development and tumorigenesis," *Int. J. Biochem. Cell Biol.*, vol. 39, no. 11, pp. 1987–1994, 2007.
[209] M. J. Mondrinos, Y.-S. Yi, N.-K. Wu, X. Ding, and D. Huh, "Native extracellular matrix-derived semipermeable, optically transparent, and inexpensive membrane inserts for microfluidic cell culture," *Lab. Chip*, vol. 17, no. 18, pp. 3146–3158, 12 2017.
[210] T. H. Petersen, E. A. Calle, M. B. Colehour, and L. E. Niklason, "Matrix composition and mechanics of decellularized lung scaffolds," *Cells Tissues Organs*, vol. 195, no. 3, pp. 222–231, 2012.

[211] T. Tsuchiya *et al.*, "Ventilation-Based Decellularization System of the Lung," *BioResearch Open Access*, vol. 5, no. 1, pp. 118–126, May 2016.
[212] M. J. Bissell and J. Aggeler, "Dynamic reciprocity: how do extracellular matrix and hormones direct gene expression?," *Prog. Clin. Biol. Res.*, vol. 249, pp. 251–262, 1987.
[213] J. T. Thorne, T. R. Segal, S. Chang, S. Jorge, J. H. Segars, and P. C. Leppert, "Dynamic Reciprocity Between Cells and Their Microenvironment in Reproduction," *Biol. Reprod.*, vol. 92, no. 1, Jan. 2015.
[214] N. J. Kristofik *et al.*, "Improving in vivo outcomes of decellularized vascular grafts via incorporation of a novel extracellular matrix," *Biomaterials*, vol. 141, pp. 63–73, Oct. 2017.
[215] H. Chen, S. Wu, R. Lu, Y. Zhang, Y. Zheng, and J. Sun, "Pulmonary Permeability Assessed by Fluorescent-Labeled Dextran Instilled Intranasally into Mice with LPS-Induced Acute Lung Injury," *PLOS ONE*, vol. 9, no. 7, p. e101925, Jul. 2014.
[216] A. Rastegarpour, M. Cheung, M. Vardhan, M. M. Ibrahim, C. E. Butler, and H. Levinson, "Surgical mesh for ventral incisional hernia repairs: Understanding mesh design," *Plast. Surg.*, vol. 24, no. 1, pp. 41–50, Mar. 2016.
[217] N. F. Davis, E. M. Cunnane, F. J. O'Brien, J. J. Mulvihill, and M. T. Walsh, "Tissue engineered extracellular matrices (ECMs) in urology: Evolution and future directions," *Surg. J. R. Coll. Surg. Edinb. Irel.*, vol. 16, no. 1, pp. 55–65, Feb. 2018.
[218] A. J. Booth *et al.*, "Acellular Normal and Fibrotic Human Lung Matrices as a Culture System for In Vitro Investigation," *Am. J. Respir. Crit. Care Med.*, vol. 186, no. 9, pp. 866–876, Nov. 2012.
[219] M. Gibson, V. Beachley, J. Coburn, P. A. Bandinelli, H.-Q. Mao, and J. Elisseeff, "Tissue Extracellular Matrix Nanoparticle Presentation in Electrospun Nanofibers," *BioMed Res. Int.*, vol. 2014, p. 469120, 2014.
[220] J. M. Aamodt and D. W. Grainger, "Extracellular Matrix-based Biomaterial Scaffolds and the Host Response," *Biomaterials*, vol. 86, pp. 68–82, Apr. 2016.
[221] W. Wu, B. Li, Y. Liu, X. Wang, and L. Tang, "Effect of Multilaminate Small Intestinal Submucosa as a Barrier Membrane on Bone Formation in a Rabbit Mandible Defect Model," *BioMed Research International*, 2018. [Online]. Available: https://www.hindawi.com/journals/bmri/2018/3270293/. [Accessed: 24-Apr-2019].
[222] G. E. Morris *et al.*, "A novel electrospun biphasic scaffold provides optimal three-dimensional topography for in vitro co-culture of airway epithelial and fibroblast cells," *Biofabrication*, vol. 6, no. 3, p. 035014, Sep. 2014.
[223] S. F. Badylak, D. Taylor, and K. Uygun, "Whole-Organ Tissue Engineering: Decellularization and Recellularization of Three-Dimensional Matrix Scaffolds," *Annu. Rev. Biomed. Eng.*, vol. 13, no. 1, pp. 27–53, 2011.

CURRICULUM VITA

Bethany M. Young

6919 Miami Ave. Richmond, VA 23226 • 804-357-0251 • youngbm2@vcu.edu

EDUCATION

***Doctor of Philosophy* in Biomedical Engineering** 2019
Virginia Commonwealth University (VCU), Richmond, VA
Advisor: Dr. Rebecca Heise
Doctoral Committee: Dr. Jennifer Peutzer, Dr. Daniel Weiss, Dr. Daniel Conway, Dr. Mary Peace McRae
Proposed Dissertation Title: "Engineering the Alveolar Gas Exchange Barrier by Tailoring the Extracellular Matrix Environment"

***Master of Science* in Biomedical Engineering** 2016
Virginia Commonwealth University (VCU), Richmond, VA
Advisor: Dr. Rebecca Heise
Thesis Title: "Novel Small Airway Model Using Electrospun Decellularized Lung Extracellular Matrix"

***Bachelor of Science* in Biology** 2014
The University of Richmond, Richmond, VA

RESEARCH AND RELATED EXPERIENCE

Graduate Research Assistant, *VCU*, Richmond, VA 2014- 2019
- Developed *ex vivo* lung recellularization strategies with extracellular matrix (ECM) coatings to improve cell attachment and barrier function
- Designed and programmed a rotational bioreactor system to increase cell dispersal prior to long-term *ex vivo* ventilation and vascular circulation within a high-throughput perfusion bioreactor
- Collaborated with industry through research with Propagenix© on a novel lung basal epithelial medium that maintained stem cell plasticity for tissue engineering applications
- Engineered electrospun scaffolds and other 3D matrix culture systems for monolayer and organoid culture

Engineering Technician; **Intern**, *Henrico County Public Works*, Richmond, VA 2012- 2016
- Managed field inspections and asset inventory of the county-wide stormwater system
- Digitized county stormwater structures using ESRI ArcGIS sourced from field review and civil plans

- Responsible for interpretation of EPA regulations to develop implementation strategies
- Trained all incoming Engineering Technicians

TEACHING AND MENTORING EXPERIENCE

Chesterfield Environmental and Biotechnology Intern Program, Chesterfield, VA 2019
- Initiated and organized a mentorship program with a local high school technical center to provide hands-on experience to four students

Mechanobiology Research Experience for Undergraduates, *VCU*, Richmond, VA 2018
- NSF- REU structured program mentoring an undergraduate in pulmonary mechanics research

Laboratory Student Mentor, *VCU*, Richmond, VA 2015-2019
- Mentored several undergraduate researchers including Brittany Allen (2015-2016), Gabrielle Cotman (2017-2018), Keerthana Shankar (2016-Present), and Cindy Tho (2018-Present)

Adjunct Biology Instructor, *John Tyler Community College*, Chesterfield, VA 2016- 2018
- Developed lesson plans, labs, and lectures on evolutionary biology and physiology

Graduate Teaching Assistant, *VCU*, Richmond, VA 2016- 2018
- Introduction to Biomechanics (1 semester), Advanced Biomechanics (2 semesters), and Computational Methods in Biomedical Engineering (1 semester)

Dean's Early/Undergraduate Research Initiative, *VCU*, Richmond, VA 2015-2017
- Mentored high school seniors and undergraduate students in tissue engineering research
- Received the 2016 DERI travel grant

LEADERSHIP

Biomedical Engineering Graduate Student Council, *VCU*, Richmond, VA 2017-Present
- Assisted in establishing the VCU charter while serving as Vice President and Recruitment Chair

Virginia Bio, *VCU*, Richmond, VA 2014- Present
- An active member of the organization, attending many networking events and industry seminars

Arts and Sciences NEXT, Biotechnology and Innovation Facilitator, *Uof R, VA* 2018
- Served as panelist and mentor during a weekend workshop for undergraduate students to aid in making professional connections and career planning

Virginia Academy of Science (VAS), *VCU*, Richmond, VA 2016-2018
- Biomedical and General Engineering Section Secretary
- Served as Discussion Panel Member for the 2018 Undergraduate Research Meeting

Beta Beta Beta, Biological Honor Society, *U of R*, Richmond, VA 2010- 2014

- Vice President, 2012-2014 - planned speakers and events for the members and held weekly meetings

HONORS

NIH travel scholarship to Jackson Laboratory Whole Scientist Workshop 2019

2018 BMES Career Development Award, Atlanta, GA 2018

School of Engineering Graduate School Travel Grant 2018

Graduate School Travel Grant, *VCU*, Richmond, VA 2015, 2018

World Congress of Biomechanics Diversity Travel Award Recipient, Dublin, Ireland 2018

Board of Visitors Student Representative, *VCU*, Richmond, VA 2018

VAS Best Student Presentation Award (Honorable Mention), Richmond, VA 2017

PROFESSIONAL SOCIETY MEMBERSHIPS

Virginia Biotechnology Association 2016-Present

Virginia Academy of Science 2016-Present

Biomedical Engineering Society 2015-Present

Society for Biomaterials 2015-Present

PEER-REVIEWED PUBLICATIONS

1. **Young, BM,** Shankar, K, Allen, BP, Pouliot, RA, Schneck, MB, Mikhaiel, NS, Heise, RL, "An Electrospun Decellularized Lung Matrix Scaffold for Airway Smooth Muscle Culture", *ACS Biomaterials Science and Engineering*, Nov. 2017. 3(12) DOI: 10.1021/acsbiomaterials.7b00384

2. Trempus, CS, Song, W, Lazrak, A, Yu, Z, Creighton, JR, **Young, BM**, Heise, RL, Yu, YR, Ingram, JL, Tighe, RM, Matalon, S, Garantziotis, S, "A novel role for primary cilia in airway remodeling", American Journal of Physiology-Lung Cellular and Molecular Physiology, August 2017; 313(2). DOI: 10.1152/ajplung.00284.2016

3. Link PA, Pouliot, BP, Mikhaiel, NS, **Young, BM**, Heise, RL, "Tunable Hydrogels from Pulmonary Extracellular Matrix for 3D Cell Culture", *JoVE*, (119), e55094, Jan.2017. DOI:

10.3791/5509

MANUSCRIPTS IN PREPARATION

Young, BM, Shankar, K, Pellegrino, AK, Heise, RL, "Replenishing Lost Matrix Components in Decellularized Lungs to Drive Alveolar Barrier Formation" *Matrix Biology*

BOOK CHAPTERS

Young, BM, Ritchie, A, Golshahi, L, Heise, RL, "3D In vitro/ex vivo systems" Pharmaceutical Inhalation Aerosol Technology 3rd Edition Taylor & Francis Group (In Press)

CONFERENCE PRESENTATIONS

1. **Young, BM**, Shankar, K, Pouliot, RA, Weiss, DJ, Heise, RL, "The Role of Alveolar ECM in Bioengineered Lung Barrier Formation", *Oral Presentation at Society for Biomaterials, Seattle, WA, April 2-6, 2019.*

2. **Young, BM**, Heise, RL, "Replenishing Lost Matrix Components in Decellularized Lungs to Drive Alveolar Barrier Formation", *Oral Presentation at BMES, Atlanta, Georgia, Oct. 12-20,2018.*

3. Shankar, K, **Young, BM**, Pellegrino, AK, Tho, CM, Heise, RL, "Driving Barrier Formation Within Bioengineered Lungs Using a Rotational Seeding System and ECM Coatings", *Oral Presentation at BMES, Atlanta, Georgia, Oct. 12-20,2018.*

4. Pellegrino, AK, **Young, BM**, Shankar, K, Tho, CM, Heise, RL, "The Effects of Fibronectin on Epithelial Barrier Formation and Sustainability in Decellularized Lungs" *Poster Presentation at BMES, Atlanta, Georgia, Oct. 12-20,2018.*

5. **Young, BM,** Heise, RL," Improvement of barrier function in recellularized lung scaffolds with an extracellular matrix hydrogel coating and mechanical conditioning', *Poster presented at WCB, Dublin, Ireland, July 9, 2018.*

6. **Young, BM**, Pouliot, RA, Link, PA, Heise, RL, "Improved Decellularized Lung Scaffold Recellularization with ECM Hydrogel Coating" *Poster Presented at TERMIS, Charlotte, NC, Dec. 3-6, 2017.*

7. Shankar, K, **Young, BM**, Heise, RL, "Novel Small Airway Model Using Electrospun Decellularized Lung Extracellular Matrix", *Poster Presentation at BMES, Phoenix, AZ, Oct. 11-14, 2017.*

8. **Young, BM**, Pouliot, RA, Link, PA, Schneck, MB, Heise, RL, "Modifying Protein Digestion of Lung Derived Extracellular Matrix Hydrogels", *Poster Presented at Vermont Stem Cell Conference, Burlington, VT, July 24-27, 2017.*

9. **Young, BM,** Pouliot, RA, Heise, RL, "Recellularization of Decellularized Lung Scaffolds Improved by Extracellular Matrix Airway Coating and Perfusion Culture", *Poster Presented at Virginia Academy of Science, Richmond, VA, May 17-19, 2017.*

10. **Young, BM,** Allen, BP, Blakeney BA, Pouliot, RA, Schreyack, GE, Heise, RL, "Decellularized Extracellular Matrix Electrospun Scaffold for a Novel Airway Smooth Muscle Model", *Poster Presented at SB3C, National Harbor, MD, June 29, 2016.*

11. **Young, BM,** Allen, BP, Blakeney BA, Pouliot, RA, Schreyack, GE, Heise, RL, "Novel Small Airway Model Using Electrospun Decellularized Lung Extracellular Matrix", *Poster Presented at Virginia Academy of Science, Fredericksburg, VA, May 18-20, 2016.*

12. **Young, BM,** Blakeney, BA, Allen, BP, Schreyack, GE, Pouliot, RA, Heise, RL, "Decellularized Lung Extracellular Matrix Electrospun with Poly-L-Lactic Acid for Tissue Engineering", *Oral Presentation at BMES, Tampa, Fl, Oct. 9, 2015*.

13. Allen, BP, Blakeney, BA, Young, BM, Pouliot, RA, Heise, RL, "Creating a Scaffold for Lung Modeling and Regeneration", 19th Annual Poster's on the Hill, 2015

14. **Young, BM,** Blakeney, BA, Allen, BP, Schreyack, GE, Pouliot, RA, Heise, RL, "Decellularized Lung Extracellular Matrix Electrospun with Poly-L-Lactic Acid for Tissue Engineering", *Poster Presented at Society for Biomaterials, Charlotte, NC, April 15-18, 2015.*

15. Blakeney, BA, Schreyack, GE, Allen, BP, **Young, BM,** Pouliot, RA, Heise, RL, "Decellularized Lung Extracellular Matrix Tissue Scaffold Electrospun with PLLA", *Oral Presentation at Biomedical Engineering Society, San Antonio, TX, October 22-25, 2014.*